Chair of Metal Forming

Department Product Engineering
University of Leoben, Austria

MASTER THESIS

Grain Growth in dependence of different annealing times and temperatures in austenitic stainless steel (Böhler A607) 304L

Supervision

Univ.-Prof. Dipl.-Ing. Dr.techn. Priv.-Doz.
Christof Sommitsch

.

Gerald WINTER

Metallurgy 066 - 424

May, 2009

Affidavit

I hereby declare that myself composed this thesis without any assistance from third parties. Furthermore, I confirm that no sources and resources have been used in the preparation of this thesis other than those indicated in the thesis itself. All references have been cited as appropriate.

Leoben, 15 May 2009 Gerald WINTER BSc

Acknowledgements

My heartfelt thanks must go first to my supervisor, Univ.-Prof. Dr. Christof Sommitsch, without whose expert advice, friendly support and cooperation the writing of this, my MSc thesis, at the Christian Doppler Laboratory for Materials Modelling and Simulation, University of Leoben, Austria, would not have been possible.

I must also thank Dr. Tian Baohui, my industry partner from Böhler Edelstahl, Kapfenberg, Austria, for his encouragement and for his selfless devotion to the task, enabling me to work to very tight deadlines, and thus complete the thesis in a relatively short space of time.

My thanks go, too, to Mirza Candic MSc, my MSc thesis adviser and Phd student at the Christian Doppler Laboratory for Materials Modelling and Simulation, University of Leoben, Austria, for his unfailing support on every occasion that I needed his help.

I would also like to thank Margit Almer, Marco Glettler and Alexander Walzl, members of the metallographic team at the Christian Doppler Laboratory for Materials Modelling and Simulation, University of Leoben, Austria for the effort they put into helping me and for the many pleasant hours we spent together in the basement laboratory.

My gratitude goes also to my parents for affording me the opportunity to study at the University of Leoben and for their unswerving loyalty over the years.

Abstract

The austenitic stainless steel, 304L, is used in the petrochemical, marine, food and nuclear industries, wherever high strength and corrosion resistance is required.

During the annealing process of austenitic stainless steels, abnormal grain growth may occur and its mechanical properties undergo a negative influence. Precipitations may be annihilated during the annealing process and this provides the conditions for grain growth to occur.

For smaller initial grain size, powered by higher driving forces, grain growth occurs faster and further abnormal grain growth may occur depending upon annealing time.

The aim of this work is to locate a process latitude within which abnormal grain growth is disabled. In order to define what exactly launches the process of abnormal grain growth and what factors come into play, cylindrical specimens of austenitic stainless steel 304L (Böhler A607, Fe-18Cr-8Ni) are annealed at different temperatures and for varying periods of time. The process latitude should be defined by different annealing cycles, one and two step, with variable parameters such as 900, 1000, 1100 and 1200°C and annealing times varying between 10 minutes and 40 hours.

Annealing temperatures at 900°C show that precipitations are not annihilated and so no grain growth occurs even over an extended annealing period. At temperatures over 900°C, precipitations are annihilated and so grain growth is possible. At higher temperatures the start of abnormal grain growth occurs earlier. After short annealing times of 10 to 40 minutes at a starting temperature of 1200°C, two step annealing cycles develop a larger initial grain size for the following step. At 1200°C precipitations and faceted grain boundaries are annihilated. So, for the second annealing cycle at 1000°C abnormal grain growth is disabled for annealing times over 24 hours.

The validated cellular automata model shows an excellent correlation between the experimentally determined data and grain growth kinetics based upon considerations of temperature and initial grain size.

The solution heat treatment required to inhibit abnormal grain growth at a precise point for a particular delivery is determined by the data obtained at the experimental stage.

Kurzfassung

Der austenitische Stahl 304L wird in der Wirtschaft vor allem in der Nahrungsmittelindustrie eingesetzt und zeichnet sich besonders durch seine Rost- und Säurebeständigkeit aus.
Bei Wärmebehandlungen von austenitischen Stählen kann abnormales Kornwachstum auftreten und somit die mechanischen Eigenschaften der Stähle negativ beeinflussen. Während der Wärmebehandlung können sich Ausscheidungen teilweise auflösen und somit ein Kornwachstum bewirken. Eine kleinere Anfangskorngröße führt durch eine größere Triebkraft zu einem schnelleren Kornwachstum und es kann in weiterer Folge abnormales Kornwachstum auftreten.

Das Ziel der vorliegenden Arbeit ist die Lokalisierung eines Prozessfensters bei dem abnormales Kornwachstum nicht auftritt. Um den Beginn und die Einflussfaktoren für abnormales Kornwachstum zu bestimmen, wurden zylindrische Proben eines austenitischen Stahls 304L (Böhler A607, Fe-18Cr-8Ni) geglüht. Die Glühungen wurden ein- und zweistufig bei 900, 1000, 1100 und 1200°C durchgeführt, mit Glühzeiten von 10 Minuten bis 40 Stunden.

Die einstufigen Glühungen zeigten, dass bei 900°C die vorhandenen Ausscheidungen nicht gelöst werden konnten und somit das Kornwachstum auch über sehr lange Glühperioden kaum einen Anstieg zeigte. Bei Glühtemperaturen über 900°C konnten die vorhandenen Ausscheidungen gelöst werden und es kam zu einer Kornvergröberung. Mit steigender Temperatur kam es zu einem früheren Beginn des abnormalen Kornwachstums. Die zweistufigen Glühungen führten nach einer kurzen (10 bis 40 Minuten) Lösungsglühbehandlung bei 1200°C zu einer größeren Anfangskorngröße für die zweite Glühung. Bei 1200°C wurden sowohl die facettierten Korngrenzen als auch die Ausscheidungen ausgelöscht und dadurch sind Glühzeiten bis über 24 Stunden bei 1000°C möglich, ohne dass abnormales Kornwachstum auftritt.

Das validierte zweidimensionale zelluläre Automaten Modell zeigt eine gute Übereinstimmung mit den experimentell gewonnenen Daten in Hinsicht auf die Kornwachstumskinetik unter Temperaturabhängigkeit und den Einfluss der Ausgangskorngröße. Die für die Auslieferung vorgeschriebene Lösungsglühbehandlung wurde mit Hilfe der experimentell ermittelten Daten forciert und das abnormale Kornwachstum unterdrückt.

Contents

List of Abbreviations

Abbreviation	Explanation
1SA	One Step Annealing
2SA	Two Step Annealing
AGG	Abnormal Grain Growth
BCC	Body Centered Cubic
CA	Cellular Automata
DRX	Dynamic Recrystallization
EBSD	Electron Back Scatter Diffraction
FCC	Face Centered Cubic
FEM	Finite Element Method
HV	Vikers Hardness
NGG	Normal Grain Growth
OPS	Oxid Polishing Suspension
REF	Reference
REG	Regression
SIC	Silicon Carbide
SRX	Static Recrystallization

1 Introduction

The aim of this thesis is to locate a process latitude in austenitic stainless steel within which abnormal grain growth is disabled. The steel is annealed in order to reduce the internal stresses and to delete the history of the microstructure after the forming process, so as to obtain a new uninfluenced initial grain. The process latitude should be capable of being tapped by different annealing cycles with variable parameters such as annealing times varying between 10 minutes and 40 hours; temperatures ranging from 900 to 1200 degrees Celsius and two step annealing cycles.

The annealing process renders it possible to define the mechanical properties over large areas and thus determine the possibilities for extensive field of application for metallic materials.

Grain boundary energy is important to grain growth during the annealing cycle and allows normal or abnormal grain growth to take place. In spite of the lattice distortion enthalpy, the microstructure strives for a further reduction in energy [1]. In this way it achieves grain growth that, through the annihilation of precipitates, becomes reinforced.

Fundamental, for the Cellular Automata Model of MSc Mirza Candic, is the localisation of the process latitude during the solution annealing process, where abnormal grain growth is disabled. This model will be used to predict both normal and abnormal grain growth during the annealing process for single and multistep treatments.

Depending on the growth behavior of the grains, grain growth can be further classified into two types, shown in Figure 1.1: normal or continuous grain growth and abnormal or discontinuous grain growth. The latter has also been termed exaggerated grain growth, coarsening or secondary recrystallization.

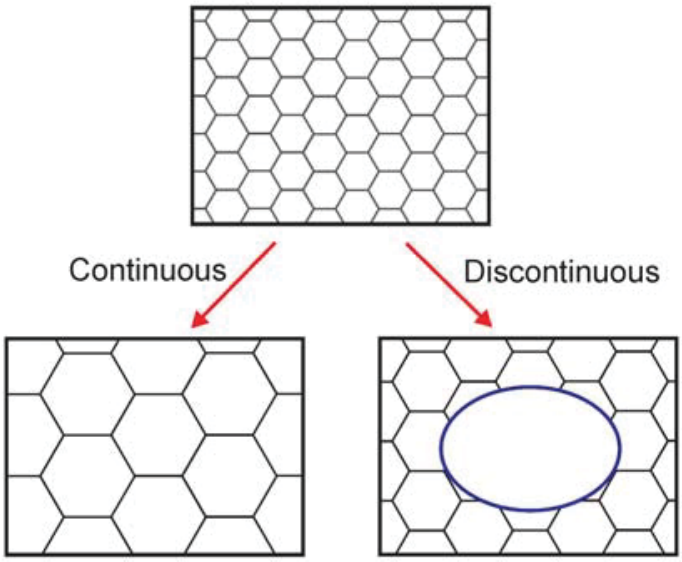

Figure 1.1: The distintion between continuous (normal) grain growth, where all grains grow at roughly the same rate, and discontinuous (abnormal) grain growth, where one grain grows at a much greater rate than its neighbours [2].

Knowledge of the microstructural changes which take place during the annealing process is important to the evolution of the final structural condition of the material.

The primary considerations of the first chapter of this work are: austenitic stainless steel, grain growth (normal and abnormal), precipitations, faceted grain boundary and the underlying structure of the Cellular Automata (CA) model.

In the experimental part, which follows, an exact description of the annealing experiments, preparation of the specimens and evaluation of grain size is provided.

This is followed by the Results chapter, which presents the results obtained from the annealing experiments and the mathematical discussion and comparison of them. The determined process latitude is also presented, and the chapter concludes with a discussion of the validated CA-model accompanied by illustrations and diagrams of the probabilities for grain growth.

A summary of the most important results can be found in the final chapter, entitled Conclusion.

The appendices supply the micrographs and illustrations of the allocations of grain sizes for all annealing specimens.

2 Fundamentals

2.1 Austenitic Stainless Steels

Austenitic stainless steels are used wherever high strength and corrosion resistance is needed. They are widely used in the petrochemical, marine, food and nuclear industries, but may also be used for heat exchangers, pipework, machinery parts and in the manufacture of milder chemicals. The microstructure can be ferritic, martensitic, ferritic-austenitic or austenitic and depends largely on the alloying elements employed.

By altering their chemical composition, different types of austenitic stainless steels have been developed.

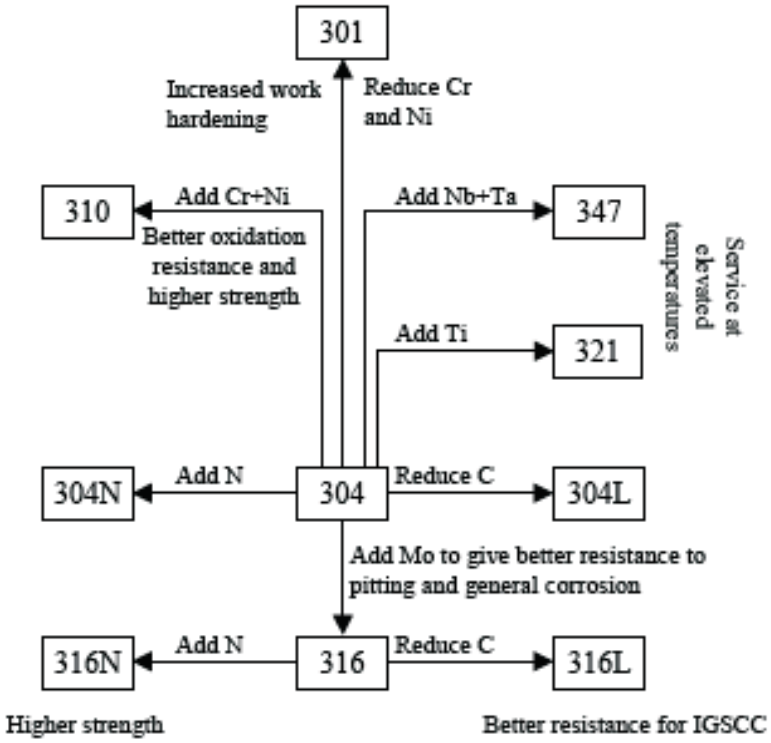

Figure 2.1: Compositional modifications of 18Cr-8Ni steels [3]

Austenitic grades [4] are those alloys which are commonly in use for stainless applications and are shown in figure 2.1 and 2.2 . The austenitic grades are not magnetic. The

most common austenitic alloys are iron chromium- nickel steels and are widely known as the 300 series. The austenitic stainless steels, because of their high chromium and nickel content, are the most corrosion resistant of the stainless group providing unusually fine mechanical properties. They cannot be strengthened by heat treatment, but can be strengthened significantly by cold-working.

Further, the so called L-grades are used to provide extra corrosion resistance after welding. The letter L after a stainless steel type indicates low carbon (as in 304L). The carbon is kept to .03% or before to avoid carbide precipitations. Carbon [5] in steel when heated to temperatures in what is called the critical range precipitates out, combines with the chromium and gathers on the grain boundaries. This deprives the steel of the chromium in solution and promotes corrosion adjacent to the grain boundaries. By controlling the amount of carbon, this corrosion is minimized. In addition, carbon, at high temperatures imparts great physical strength.

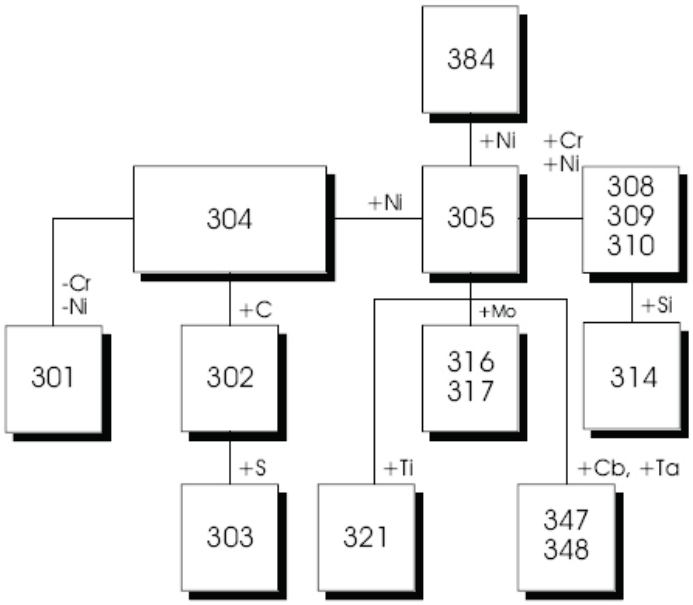

Figure 2.2: Austenitic Group [4]

Exclusively for the austenitic stainless steel 304L (X2CrNiMo17-12-2 or 1.4404) the chemical composition is given in Table 2.1.

Elements:	C	Si	Mn	P	S	Cr	Mo	Ni
Percent:	max. 0,03	max. 1,00	max. 2,00	max. 0,045	max. 0,030	16,50-18,50	2,00-2,50	11,00-14,00

Table 2.1: Chemical composition of the stainless steel 304L in weight percent [6]

The alloy composition [3] is often characterized by use of Cr- and Ni-equivalents. The first group stabilises the α phase and the second one the γ phase. The ferritic α phase has a body centred cubic (bcc) and the austenitic γ phase has a face centred cubic crystal (fcc) structure. The low carbon content affects the flow behavior by modifying the stacking fault energy [7].

Diffusion-Controlled Precipitation

In the absence of stabilizing elements, $M_{23}C_6$ is the predominant carbide formed in austenitic stainless steel and is mainly composed of chromium carbide [3][8]. The principal practical consequences of precipitation are degradation of intergranular corrosion resistance and reduction in tensile properties, especially ductility and toughness. Precipitation occurs very rapidly on the ferrite-austenite interfaces, followed by precipitation on other non-coherent boundaries including inclusions, grain and twin boundaries.
The intragranular precipitation occurs on dislocations as many evenly spaced angular blocks. The dislocations are generally straight and form a cube-like body, bounded by a pair of {111} and two pairs of {110} planes.
Carbide precipitation then occurs on the partial dislocation with growth inwards along the stacking fault to the boundary. The interface between the carbide and the parallel matrix grain is generally in line with that of the gamma - gamma interface, that between the carbide and the other grain generally being jagged. Most grain boundaries have all the carbides in a parallel orientation with one grain only, although mixtures have been observed.
Other types of precipitation are MC, M_6C, M_7C_3, i.e. carbonitrides and other intermetallic phases.

They are solution annealed between 1000-1150°C and thereafter quenched quickly to avoid carbide formation. The austenitic structure is for some steel types metastable at room temperature and can form martensite by deep cooling and/or plastic forming operations.

2.2 Development of Microstructure During Annealing

Grain growth is the term used to describe the increase in grain size which occurs upon annealing a polycrystalline aggregate after primary recrystallization is completed. Two different types of grain growth phenomena, namely normal grain growth and abnormal grain growth are distinguished [9] and constitute in figure 2.3. The main driving force is the decrease in free energy which accompanies reduction in total grain boundary area.

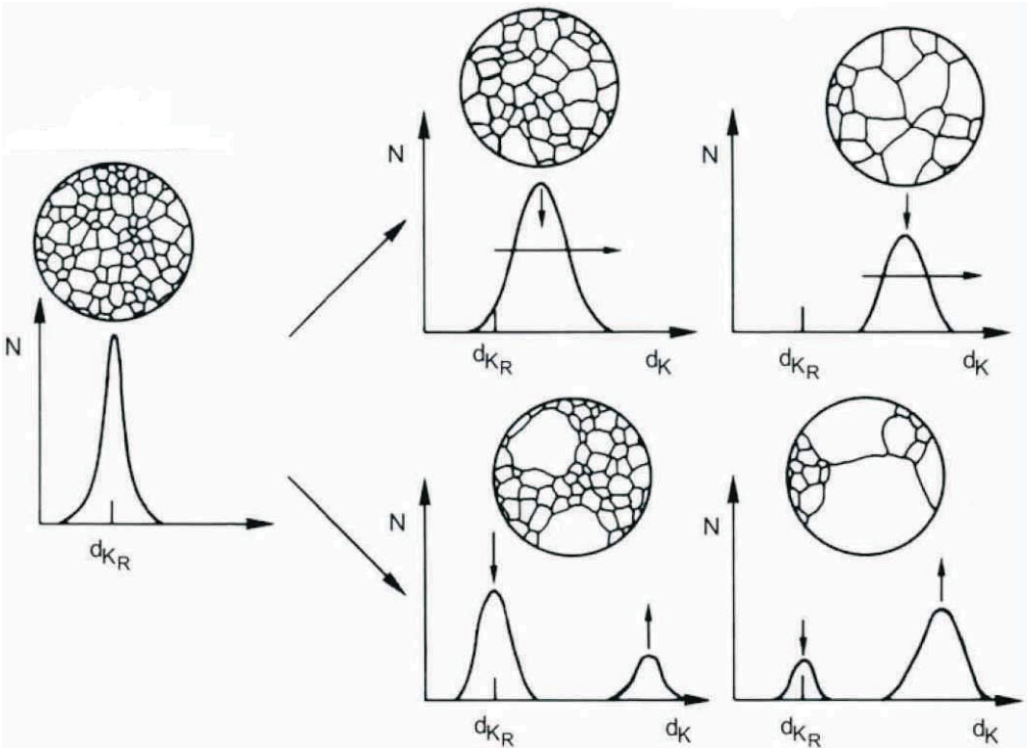

Figure 2.3: Demonstrate the difference between normal (top) and abnormal (bottom) grain growth. N = probability and d_{KR} = average initial grain size diameter; [10]

2.2.1 Normal Grain Growth

One of the structural characteristics during normal grain growth is that the grain-size and grain-shape distributions are essentially invariant [11]; that is, during normal grain-growth, the average grain size increases, but the size and shape distributions of the grains remain essentially the same before and after the growth, differing only by a scale factor. During the normal grain growth, the change in texture is small and gradual. Assuming

the initial grains are nearly randomly oriented, after extensive normal grain growth, some weak preferred orientations may be developed among the final grains, depending on such a factor as the energies of the free surfaces of the grains. If the initial grains are strongly textured, normal grain growth may be inhibited as a consequence of low mobility of the matrix grain boundaries. The size and shape distributions of these grains are essentially the same as those of the much finer grains before growth.

Normal grain growth occurs [12][13] when the microstructure exhibits a uniform increase in grain size. This type of growth is a steady state kinetic process characterized by time invariance of grain size distribution. In this case the mean grain size d increases with time as:

$$d = kt^n \tag{2.1}$$

with isothermal annealing, where k is a constant, which is a function of temperature and $n \leq 0.5$.

Driven by the grain boundary energy reduction, the local grain boundary movement during grain growth is governed by surface tension forces, grain boundary mobility and the second phase particles.

The velocity of the grain boundary depends on the net pressure acting on the grain boundary:

$$P = \frac{2\gamma}{R} \tag{2.2}$$

where γ is the grain boundary energy and R is the local radius of curvature of the grain boundary. The pressure on the grain boundaries acts in such a way that it forces the grain boundary to move towards the center of the curvature, where a grain with a convex grain boundary grows and a grain with a concave grain boundary shrinks.

The grain boundary displacement, ΔX, in a single time increment, Δt, is a function of the pressure, P, and the mobility M of the grain boundary, is given by:

$$\Delta X = MP\Delta t \tag{2.3}$$

The grain boundary mobility, M, is a function of temperature T and activation energy for the grain coarsening Q.

$$M = M_0 exp\left(\frac{-Q}{R_{gas}T}\right) \tag{2.4}$$

where R_{gas} is the gas constant and M_0 is a material constant.

Due to second phase particles the normal grain growth can be impeded. Therefore the maximum grain size of each grain d_{max} can be defined by using the following equation:

$$d_{max} = \frac{2d_p}{f} \tag{2.5}$$

where f is the fraction of the particles decreasing with annealing time and d_p is the diameter of the particles, which increases due to Ostwald ripening:

$$d_p(t) = 2\left\{\left[kt^{\frac{1}{3}}\right]^3 + \left(\frac{d_p^0}{2}\right)^3\right\}^{\frac{1}{3}} \tag{2.6}$$

where k is a constant and d_p^0 is the diameter of the particles at the beginning of annealing.

2.2.2 Abnormal Grain Growth

A second type of grain growth phenomenon which can occur after recrystallization is abnormal grain growth [12] [13]. In general, it is defined as a rapid increase in size of a few grains in the recrystallized microstructure such that topology is not time invariant and the maximum grain size increases at a rate much faster than the arithmetic mean.

It is commonly observed, that secondary recrystallization requires normal grain growth to be strongly impeded, with the exception of a few grains which act as a nuclei for secondary recrystallization. Inhibition of normal grain growth is attributed to a number of mechanisms:

- Grain boundary grooving in the case of thin films and sheet materials
- Particle pinning of boundaries
- Texture inhibition in a material with strong preferred orientation

- Impurity inhibition

The driving force is generally assumed to be provided by associated reduction in total grain boundary energy, as for normal grain growth. However, an additional driving force has been experimentally demonstrated in thin films and sheet materials, which arises from orientation dependance of the gas-metal surface energies [14].

The start of secondary recrystallization [15] has some common characteristics:

- The grains that grow large are not newly nucleated but of the primary structure.
- The very large grains initially grow slowly, followed by rapid growth to sizes of the order of centimeters in some cases.
- The grains that coarsen possess many sides.
- The explanation for the growth of the favored grains is the least understood part of the process, but it has been observed that these grains have orientations which are different from the primary texture of the material.
- Normal grain growth must be impeded. The commonly known conditions for inhibiting grain growth are a fine dispersion of second-phase particles, a discrete grain-boundary precipitate, a strong single-orientation texture, and a stabilized two-dimensional grain structure imposed by sheet thickness. The conditions for inhibiting grain growth are readily understandable, because the fine particles exert a pinning force on the boundary motion, the matrix grain boundaries are predominantly low-angle boundaries, and therefore, both low mobilities and the boundary grooving at the sheet surfaces retard boundary motion.
- The large grains of the secondary structure frequently exhibit a unique texture always different from the texture of the former primary structure.

2.2.2.1 The Starting Microstructure

For 316L stainless steel [16] it is observed that during heat treatment by 1150 $°C$, abnormal grain size develops depending strongly on the initial grain size after the primary recrystallization (figure 2.4). When decreasing the initial grain size, abnormal grain growth begins earlier during the heat treatment, and if the initial grain size is large only slow grain growth occurs without any distinct abnormal grain growth. The extremely slow grain

growth with initially large average grain size is attributed to the low grain boundary velocity limited by the boundary step nucleation or growth (figure 2.5).

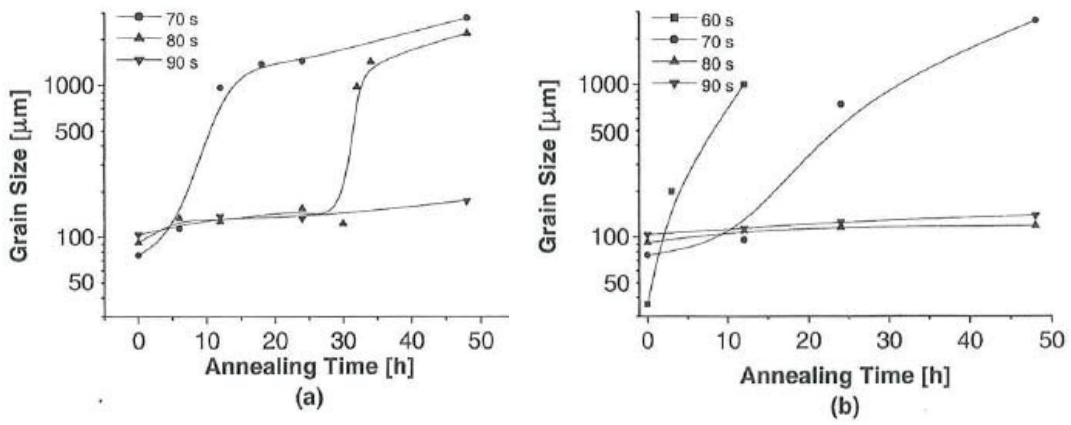

Figure 2.4: Lee produced at 1300°C different initial grain sizes and annealed at (a) 1150°C and (b) 1100°C [16]

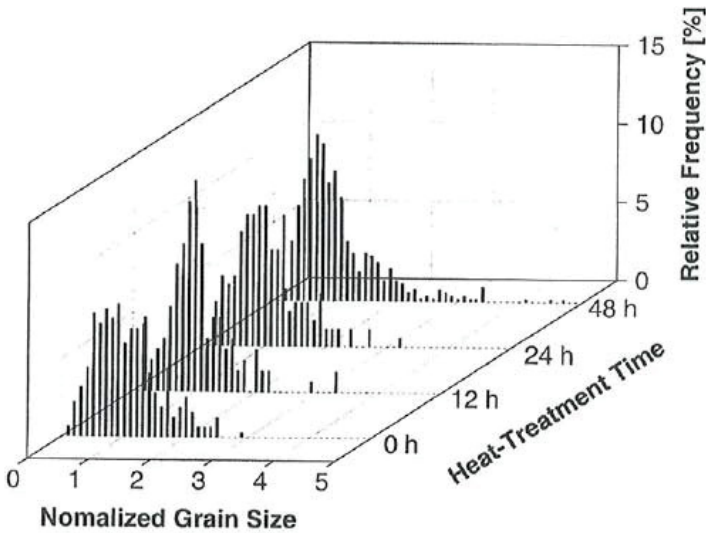

Figure 2.5: Grain size frequency for heat treatment at: 1300°C for 90 seconds and annealing at 1150°C for 48h [16]

2.2.2.2 Faceted Grain Boundary

Grain boundary phase transformations based on the observation of an apparently discontinous change of the energies of grain boundaries are often made during the annealing

process at different annealing temperatures (e.g. $0.73T_m$ for Pb) [17]. This defaceting transition are marked by slope changes of the log of the grain boundary migration rates against the reciprocal temperatures. This roughening transition is often related to the so-called roughening transitions of grain boundaries.

The faceting of grain boundaries have been observed in many metals and oxides, and such impurities and additives as O in Ni or Ag, Bi in Cu, Te in Fe, and CaO or SiO_2 in Al_2O_3 have been observed to induce the grain boundary faceting [18][19]. It has also been observed that at high temperatures close to the melting point in a carburizing atmosphere, the grain boundaries of a Nickel based alloy become defaceted, producing curved shapes that have an atomically rough structure. In contrast, the normal grain growth occurs at low temperatures. At high annealing temperatures faceted grain boundaries take shape and abnormal grain growth occurs.

The dependence of abnormal grain growth, also termed secondary recrystallization, on annealing temperature in the range between $600°C$ and $1050°C$ has been observed in pure bulk Cu specimens [20]. The average grain size after primary recrystallization represents the initial grain size for secondary recrystallization during further annealing. The incubation time for AGG decreases and the number of density of abnormally large grains increases with decreasing initial grain size and increasing annealing temperature. At low temperatures, most of the grain boundaries are faceted, with some facet planes probably of singular structures corresponding to cusps in the polar plots of the grain boundary energy vs the grain boundary normal. With increasing temperatures, the grain boundaries become defaceted and atomically rough. The observed grain-growth behavior appears to be qualitatively consistent with the movement of faceted grain boundaries by two dimensional nucleation of boundary steps. The temperature dependence appears to be consistent with roughening of grain boundaries. Before the onset of AGG, stagnant growth of the grains occurs at low rates, probably limited by slow two-dimensional nucleation of boundary steps. The specimens with relatively small initial grain sizes show double AGG when annealed at high temperatures [20].

In experimental series for the stainless steel 316L, by Choi et al. [21], the first heat treatment at $1100°C$ leads to an AGG structure but afterwards heat-treated again at $1300°C$ a NGG structure appeared. This time the fine matrix grains coarsened but the large grains did not grow abnormally, and a normal grain size distribution was reached. It is shown that with changing the growth mechanism due to producing rough grain bound-

aries, the abnormally grains did not continue to grow.

Both general grain boundaries in polycrystalline materials and grain boundaries with well-defined geometrical characteristics such as the coincidence site lattice (CSL) relations were observed to have faceted grain structures, which are often associated with impurities and additives [18] are shown in figures 2.6, 2.7 and 2.8.

The stagnant, abnormal and normal growth are critically dependent on the thermodynamic and kinetic roughening of the grain boundaries [18][20].

There is a correlation between the faceted grain boundaries and abnormal grain growth [21]. Examplarilly, the heat-treated 316L stainless steel in a single phase state at 1100 $°C$ leads to abnormal grain growth and some grain boundaries are observed to be faceted with the so-called hill-and-valley structures.

A heat treatment at 1300 $°C$ produces normal grain growth with all grain boundaries smoothly curved. These grain boundaries would be expected to be atomically rough (figure 2.6).

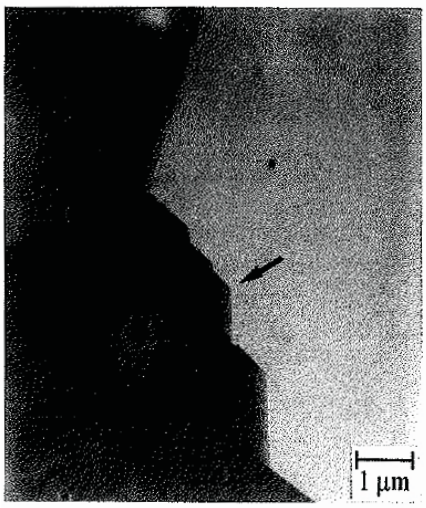

Figure 2.6: The arrow shows two apparently defaceted grain boundaries at a triple junction in the specimen. Heat Treatment: 1300$°C$ for 80 seconds and annealed at 1100$°C$ for 6 hours; [21]

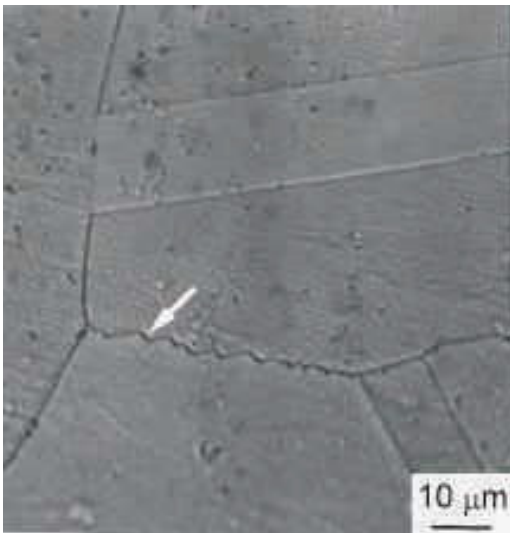

Figure 2.7: A faceted grain boundary in silver [19]

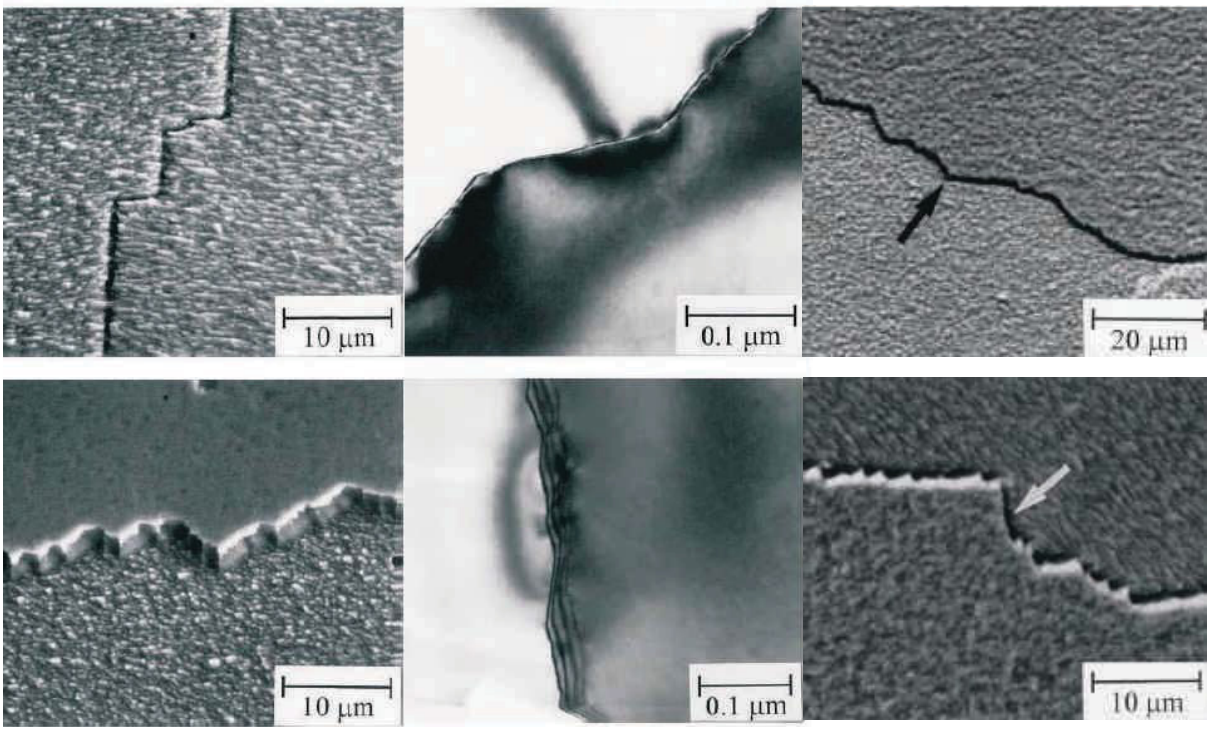

Figure 2.8: A faceted grain boundary in copper [20]

The occurrence of abnormal grain growth with faceted grain boundaries is attributed to grain boundary movement with boundary steps either produced by two-dimensional nucleation or existing at the junction with dislocations. As the grain boundaries become

rough at 1300 $^{\circ}C$ normal growth occurs because the grain boundaries migrate continuously with their rate expected to increase linearly with the driving force arising from the size difference.

These faceted grain boundaries can move by two-dimensional nucleation of steps or on existing steps produced by dislocation (figure 2.9), as proposed by Gleiter [17][22]. The grain-boundary migration rate will then increase nonlinearly with the driving force, causing rapid growth of only large grains and, hence, AGG [8]. If the grain boundaries have an atomically rough structure, the migration rate will increase linearly with the driving force, thus normal grain growth will occur [20].

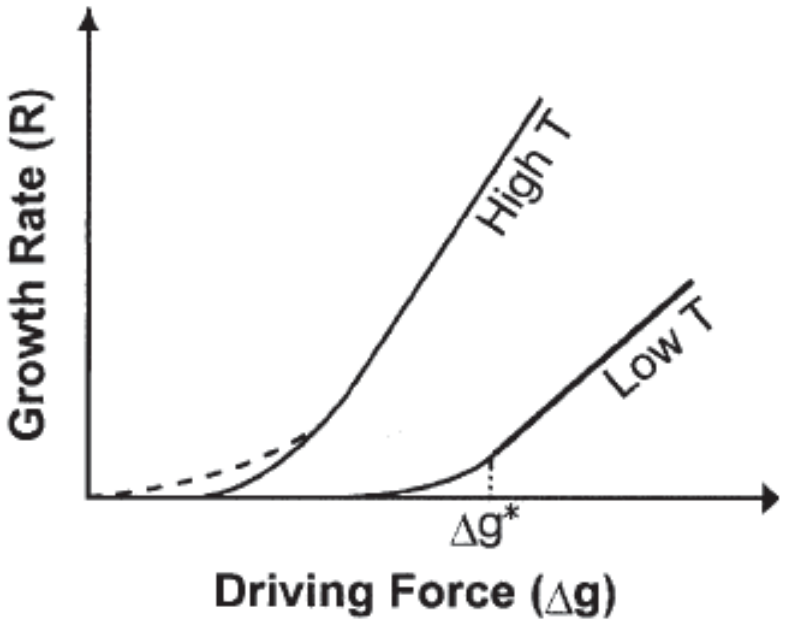

Figure 2.9: Schematic variation of the rate of grain growth by two-dimensional nucleation with the driving force at high and low temperatures with the dashed curve for the dislocation growth mechanism at high temperatures [20]

If the faceted grain boundaries migrate by growth on the steps produced by dislocations, the migration at low driving force will be substantionally higher than that by two-dimensional nucleation, as shown by dashed curve at figure 2.9. But at high driving forces, the growth can still occur by two-dimensional nucleation, and, with either type of non-linear migration behavior with driving force, AGG can occur in the system of many grains [20].

The growth by two-dimensional nucleation of boundary steps, the growth rate (R) depends on the step-edge free energy ($\sigma(T)$) and the driving force (Δg) as

$$R \propto exp\left(\frac{-\pi V_m \sigma(T)^2}{h\Delta g k T}\right) \tag{2.7}$$

where V_m is the molar volume, h is the step height, k is the Boltzman constant, and T is the temperature. As in most of the grain-growth theories, it may be assumed that (Δg) is approximately given as

$$\Delta g\left(\overline{r}, r_i\right) = \beta V_m \gamma \left(\frac{1}{\overline{r}} - \frac{1}{r_i}\right) \tag{2.8}$$

where β is a geometric factor, γ is the grain boundary energy, r_i is the size of the growing grain, and $\overline{r}$ is the average size of the grains sourrounding it, which may be assumed to be the average size of all grains. For a large grain growing abnormally in the matrix of fine grains, $\overline{r}$ will represent the average size of the matrix grains. Writing $r_i = \overline{r}\alpha_i$

$$\Delta g_i\left(\overline{r}, r_i\right) = \frac{\beta V_m \gamma}{r}\left(\frac{\alpha_i - 1}{\alpha_i}\right) \tag{2.9}$$

Therefore a grain must be large enough to exceed the critical driving force.

The equation 2.7 for R as a function of (Δg) is shown schematically in figure 2.9 at two temperatures. Because this equation describes the growth by mononucleation, it is expected to be valid for relatively low driving forces. As the driving forces increases, polynucleation is expected to occur with slightly different dependence on (Δg), and above (Δg^*), R is expected to increase linearly with (Δg), because the growth will be limited by the rate of the atom jump across the boundary [20].

If initially none of the grains are large enough to exceed Δg^*, which is required for AGG, then all the grains will grow at very low rates in the very low-driving-force range shown in figure 2.9. Such a slow growth limited by nucleation of steps is known as stagnant growth. During stagnant growth, large grains can grow relatively faster than the increase of the average size because of the nonlinear variation of the growth rate with the driving force, and when the large grains attain the critical sizes required to exceed Δg^*, they will undergo accelerated growth to produce AGG. If the initial $\overline{r}$ value is smaller, the time required for the large grains to exceed Δg^* will be shorter, thus the incubation time for AGG will be shorter which is in agreement with experimental results [20].

2.3 Cellular Automata

Due to [23] the difficulty of directly incorporating the topological features into the empirical models of grain coarsening, together with the difficulty of giving a space-time description of grain distributions, there has been increasing interest in using computer simulations to study the grain coarsening in single phase materials. A variety of models have therefore been put forward, including the continuum field model, the Monte Carlo model, the Vertex model and the cellular automaton model (CA).

In cellular automata, the space, time and state of the physical system are discretized. Subsequently, using a rule set of incremental time steps, the state of dependent variables is determined at each of these discrete spatial locations. The rule sets that govern the transition of the state of the cell are critical in determining the final microstructure and the degree to which these rules correspond to physical reality determines the accuracy of the CA model.

In the deterministic CA models the equations relating the grain boundary velocity to the misorientations, boundary energy and the temperature are solved to calculate the net displacement of the boundary. For the probabilistic CA models, the moving of a boundary bases on the stochastic majority rules.

2.3.1 Probabilistic Model

In order to simulate normal grain coarsening, a network of cells is laid out according to a regular lattice arrangement and the distance between two neighboring cells is assumed to be 1 unit. In general, the lattice is divided into a regular network of cells with a periodic boundary condition. Every lattice cell represents one part of a grain and is marked with a grain identification number. Lattice cells which are adjacent to neighboring cells with different grain identifications are regarded as being part of the grain boundary, while the cells surrounded by cells with the same grain identification are in the grain interior. The unit of time is defined as 1 cellular automaton step (CAS), which corresponds to one loop re-identification attempt, which means that for all cells, at every CAS, the state index of each step is updated simultanously.

In the probabilistic model, at each step, every cell is scanned, and its state will change according to the following integrated rules (figure 2.10):

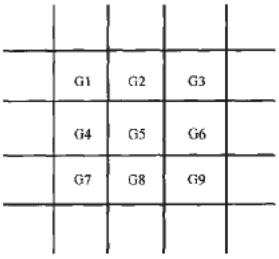

Figure 2.10: Moores Neighbourhood

1. If all 8 cells around the $G5$ have the same state as $G5$, then $G5$ will keep its state at the next time step.

2. (a) If any three of the states $G2$, $G4$, $G6$, $G8$ are the same integer (grain identification), for example equal to A, then $G5$ is A. Similarily, if this does not hold, then (b) if any three of the states $G1$, $G3$, $G7$, $G9$ are the same integer, for example equal to an integer B, then $G5$ is B.

3. The distribution of grain boundary energy is homogenous. A cell must overcome an energy barrier to change its state: if any of the eight surrounding cells have different state from $G5$, then $G5$ has the possibility to change its state. In this case, the probability is the same for all grains and is set to be P_{low}.

If the state of a cell can meet any of these conditions, then the following condition will be ignored. For example, the condition (1) is actually to judge if this cell is in the interior or on the boundary. If it is in the interior, it must maintain its state and the following conditions do not need considerations any more and the next cell will be checked subsequently. If not, the cell must be on the boundary and then the computer will check if its state can meet condition (2a) and so on.

On the integrated rules given above, the second rule simulates the grain curvature effect, where the grain boundary would tend to form a straight line due to the surface tension requirement. The reason to use the Moore configuration considering both the nearest and next-nearest neighbours is to make a boundary move in any direction.

The third rule simulates the effect of grain boundary energy, which is vital to keep the boundaries move and make small grains vanish. It reflects the effect of mobility on the grain growth, which includes the temperature dependance.

3 Experimental Work

3.1 Specimen Geometry

For the annealing tests cylindric specimens of 304L with a diameter of 10 mm and a height of 5 mm were used with an initial grain size of 14.7 μm. The geometry of the specimen was finished at Böhler Edelstahl, Kapfenberg, Austria.

For the pretests, quadratic specimens 304L from Böhler with the dimensions 15 x 15 x 5 mm were used. The initial grain size of this material was lower with 10.7 μm.

3.2 Annealing and Quenching

In the present thesis the heat transfer in the specimen at different annealing temperatures was simulated in order to calculate the exact charging time for each sample in the furnace. The simulations are made for 900°C, 1000°C, 1100°C and 1200°C by the commercial finite element software DEFORM.

Furnace
The specimen was heated in a laboratory furnace RHF 14/35 from Carbo light shown in figure 3.1. The simulated time for the temperature to raise the specimen core added to the furnace temperature stabilization time, from door opening and closing, provide the total time for charge.
For the lower temperatures 900°C and 1000°C a charge time of 4.5 minutes and for 1100°C and 1200°C a charge time of 3 minutes was fixed from the simulation output and the experimental values from the furnace behavior. That means for example if the annealing time is 20 minutes at 1200°C the specimen would be in the furnace for 23 minutes. So the 20 minutes are an absolute time value for the temperature without heating and cooling.

In the middle of the furnace chamber 3.1 the temperature is taken from the oven software to control the user fixed temperature. The temperature element is the ceramic tube. The specimen needs a fireclay base to get near to the center area of the chamber.

Figure 3.1: Left: Carbo light furnace RHF 14/35; Right: Magnification of the heating chamber

Quenching
After annealing, the microstructure of the specimen had to be fixed so that subsequent evaluations could be carried out. The small scale of the specimen meant that on removal from the furnace it could be immediately quenched in cold (≈10°C) water. A steel box placed directly in front of the furnace and containing about 3 liters of cold water was used to maintain the charge times at a low level.

During the two step annealing process the specimen was handled in the same way as for the one step annealing experiments.

Two step annealing example - 20 minutes at 1200°C and 12 hours at 1000°C:
The specimen was charged twice within the furnace. First, for 23 minutes at 1200°C, then quenched to water temperature, the second time for 12 hours and 4.5 minutes at 1000°C and again quenched to water temperature.

3.2.1 One Step Annealing Specimen

One step annealing means, that the specimen was charged only once to a specific temperature inside the furnace, then quenched. The charging temperatures used were: 900°C, 1000°C, 1100°C and 1200°C. The REF specimens are the reference material without any annealing. These were used to classify the initial grain sizes. The x in table 3.1 shows the annealing temperatures and times for the specimens. In the REF column at the annealing time zero seconds double x is used to represent the two different specimens employed. 3.1.

Time [s]	*REF*	*900˚C*	*1000˚C*	*1100˚C*	*1200˚C*
0	xx				
1200					x
2400					x
3600					x
4800					x
7200					x
10800					x
14400		x	x	x	
18000					x
28800		x	x	x	
36000					x
43200		x	x	x	
57600		x	x	x	
72000		x		x	
86400		x	x	x	
115200		x	x		
144000		x	x		

Table 3.1: One step annealing specimen table

3.2.2 Two Step Annealing Specimen

In two step annealing two heat treatment cycles were applied to a cylindric specimen (section 3.1) with a diameter of 10 mm and a hight of 5 mm. The charging temperatures and times for the specimen series *1200˚C and 1000˚C*, *1000˚C and 1200˚C* and *900˚C and 1200˚C* are shown in the following tables 3.2, 3.3 and 3.4. The ”x” and ”o” in the tables represent respectively the annealing temperatures and times for the specimens. Table 3.2 is divided into two parts. The upper part shows the annealing time and temperature for the first annealing step (name of column) and the lower part for the second step. Table 3.3 for 1000°C and 1200°C annealing series and table 3.4 for the 900°C and 1200°C series are not split because the timesteps are too large. The ”x” in the tables in each column stands for the first annealing temperature and time and the ”o” stands for the second annealing temperatures and times.

Time [s]	*1200˚C10min*	*1200˚C20min*	*1200˚C40min*	*1200˚C80min*	*1200˚C180min*
600	x				
1200		x			
2400			x		
4800				x	
10800					x
43800	o				
44400		o			
45600			o		
48000				o	
54000					o
58200	o				
58800		o			
60000			o		
62400				o	
68400					o
87000	o				
87600		o			
88800			o		
97200				o	
115800	o				
116400		o			
117600			o		
144600	o				
145200		o			
146400			o		
148800				o	
154800					o

Table 3.2: Two step annealing 1200°C and 1000°C specimen table

Time [s]	*1000˚C 2h*	*1000˚C 8h*	*1000˚C 24h*
7200	x		
10800	o		
15600	o		
22800	o		
28800		x	
32400		o	
37200		o	
40800	o		
44400		o	
62400		o	
86400			x
90000			o
94800			o
102000			o
120000			o

Table 3.3: Two step annealing 1000°C and 1200°C specimen table

Time [s]	*900˚C 4h*	*900˚C 40h*
14400	x	
21600	o	
144000		x
151200		o

Table 3.4: Two step annealing 900°C and 1200°C specimen table

3.3 Metallography

Metallography [24] is the science of preparing a metal surface for analysis by grinding, polishing, and etching to reveal microstructural constituents. Mechanical preparation [25] is the most common method of preparing the samples for examination. Abrasive particles are used in successively finer steps to remove material from the sample surface until the required result is achieved.

3.3.1 Embedding

Once the annealing cycle is complete the specimen is descaled. For the success of the electrolytic etching process which is to follow, it is essential that no particles of any kind be allowed to interfere with conductivity [11].
The sample is placed in a hot mounting press, resin is added, and the sample is processed under heat and high pressure, see figure 3.2.

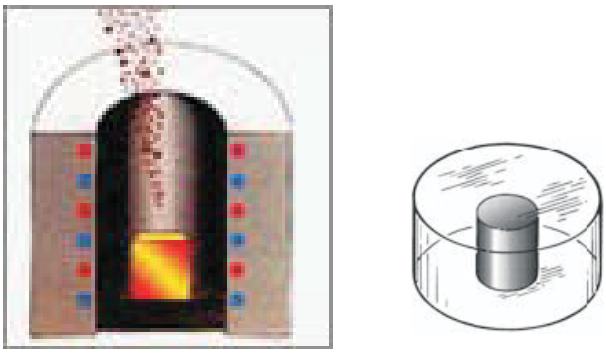

Figure 3.2: Hot Mounting Press [26]

Hot Mounting Press and Resins

For hot mounting a Struers Cito Press 10 [25] was used with two different resins. For the polishing side a Struers MultiFast Black (Phenolic resin with wood flour filler) and on the top side Struers ConduFast (Acrylic conductive resin with iron powder filler) was used.

Process Parameters:
Diameter: 40 mm
Quantity MultiFast: 15 ml
Quantity ConduFast: 30 ml
Pressure: 250 bar
Temperature: 180 °C
Heating Time: 4,5 min
Cooling Time: 3,0 min
Cooling Rate: High (Full Flow)

3.3.2 Grinding and Polishing

The purpose of the grinding is to planarise the specimen and to remove material approaching the area of interest. It is important to note that it is possible to create more damage by grinding than by sectioning.

Silicon Carbide [27] is a manufactured abrasive produced by a high temperature reaction between silica and carbon. It has a hexagonal-rhombohedral crystal structure and has a hardness of approximately 2500 HV. It is an ideal abrasive for cutting and grinding because of its hardness and sharp edges. It is also somewhat brittle, and therefore it cleaves easily to produce sharp new edges (self sharpening). SiC is an excellent abrasive for maximizing cutting rates while minimizing surface and subsurface damage.
Soft ferrous metals like 304L are relatively easy to grind with the depth of deformation being a major consideration. 180 grit SiC abrasives provide a good initial start with subsequent use of 320, 600, 800, 1200 and 2500 grit SiC.

Polishing is the most important step in preparing a specimen for microstructural analysis. It is the step which is required to completely eliminate previous damage. Ideally, the amount of damage produced during cutting and grinding should be minimized through proper blade and abrasive grinding so that polishing can be kept to a minimum.
For the 304L only a 3μm step with Struers monocrystalin diamondsuspension on a MD-NAP was necessary. The fine polishing was done with OPS (0,05μm) and a Struers MD-Chem towel.

Cleaning and drying is perhaps the most underrated processing step in specimen preparation and has to be carried out at every single change in the process. Cleaning with ethanol and an ultrasonic cleaning system is required to remove polishing residue as well as particles on the surface.
For Grinding and Polishing a single wheel ATM - Saphir 550 was used. Working wheel: Ø300 mm; Single pressure: 5 - 100 N; Motor: 1,2 kW; Speed: 50 - 600 rpm;

3.3.3 Etching

Electrolytic etching modifies the pH-value of the acid or base. The potential can be controlled electrically by varying the voltage and or current. Electrolytic etching is often used for harder to etch specimens that do not respond well to basic chemical etching

techniques.
The Struers LectroPol 5 uses a two-electrode design (anode and cathode) with acids or bases for the electrolyte and it is an apparatus [25] for automatic, micro-processor controlled electrolytical polishing and etching of metallographic specimens. With a scanning function for easy determinations of parameters, built-in safety features, and a database with methods for various materials, short polishing times and maximum reproducibility are achieved.

Setup:
Acid Temperature: 22°C
Flow Rate: 10
Voltage: 1,0V
Time: 30 - 400 sec (depends on the annealing time)

Electrolyte:
60% nitric acid

3.4 Grain Size Evaluation

The etched specimens were recorded with an Olympus light microscope in different magnifications. The microstructure pictures were printed on A3 or A4 for editing. The traced grain boundaries were digitized and evaluated with a Software Package from Digital Imaging Solution.

3.4.1 Microscopy

Inverted Metallographs GX51

The GX51 [28] is Olympus's most advanced inverted metallurgical microscope system. With the addition of complete integration to all digital imaging subsystems, it is possible to provide advanced solutions for cutting edge research. Its digital imaging system seeks to provide pictures of high quality and simplicity, which increase observation efficiency, and offer other beneficial features. High quality images are obtained for every observation method, and the performance of the digital camera is maximized for ultimate flexibility. Digital images transferred to a PC can easily be viewed and/or prepared with advanced

image analysis software.

The grain boundaries are recorded in different magnifications from 5x (50 fold extension), 10x, 20x, 50x and 100x. From each sample a 5x and a 10x picture was taken and if the magnification was too small for evaluation, pictures with better extensions were taken.

For example, figures 3.3 and 3.4 show the pictures taken in 5x and 10x magnification of the two step annealed specimen: 1200°C 20min and 1000°C 12h

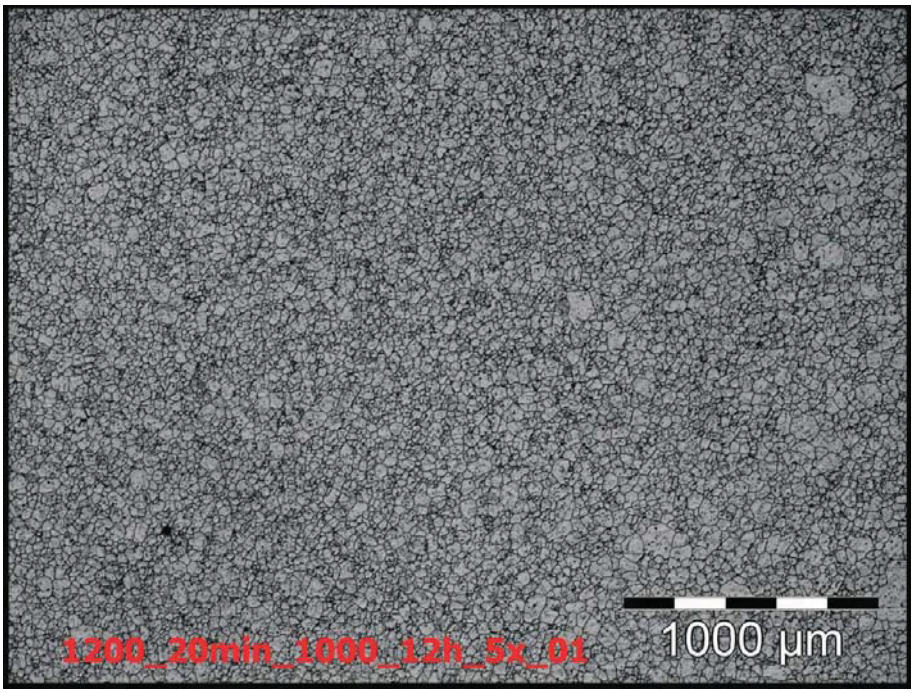

Figure 3.3: 1200°C 20min 1000°C 12h 5x

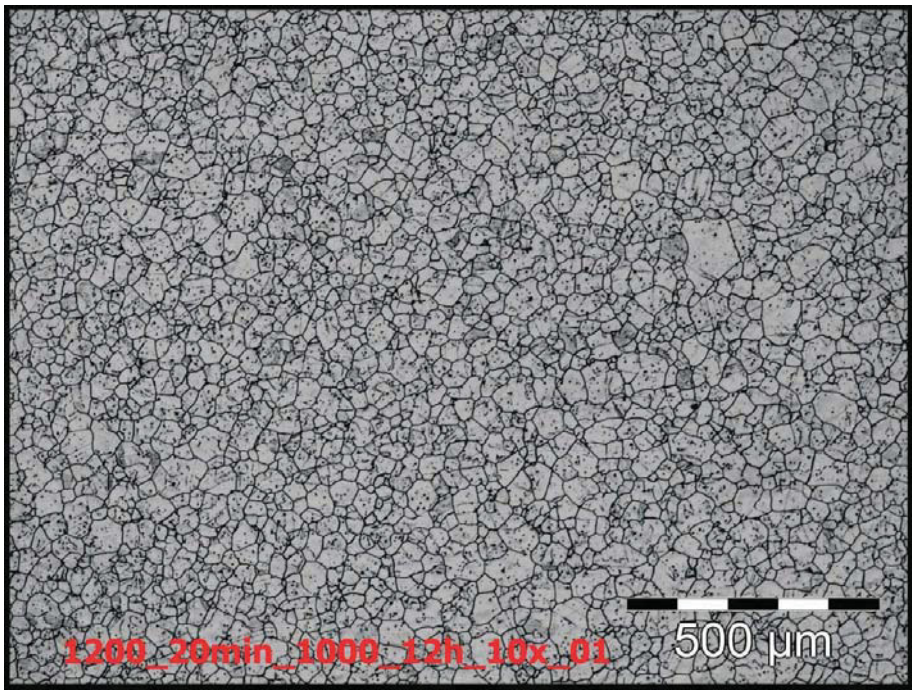

Figure 3.4: 1200°C 20min 1000°C 12h 10x

3.4.2 Data Edit

Evaluation of the grain size is naturally extremely difficult to realize because of etching artefacts, twin boundaries and other irregularities. It would have taken longer to check and correct the detected grain boundaries than to trace them to a transparency film, so all pictures of the annealed specimen were printed to paper format A4 and traced onto transparency films. For a correct evaluation of the grain size of each sample a minimum of 300 grains had to be detected. If there were fewer grains on a micrograph, a second picture or more had to be taken and traced. For correct transmission of small grains some of the micrographs were printed on A3 paper format. In figure 3.5 the traced micrograph of figure 3.4 is shown.

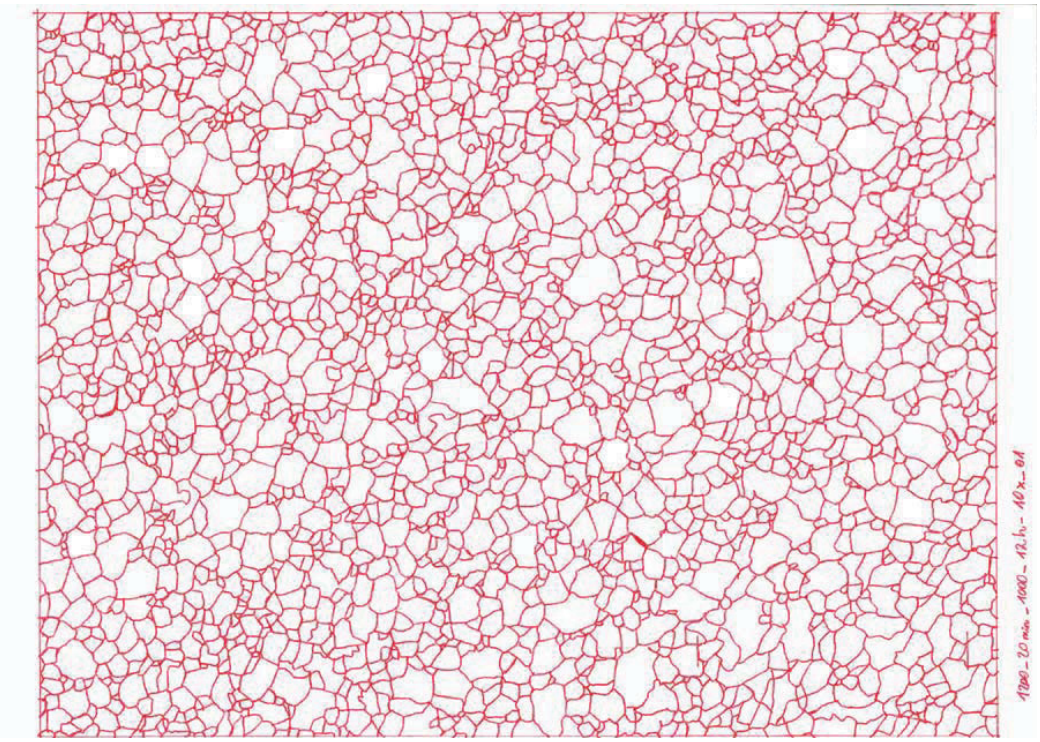

Figure 3.5: Traced micrograph 1200°C 20min 1000°C 12h 10x scan

3.4.3 Grain Evaluation with Olympus AnalySIS® FIVE

Preparatory work

The traced and scanned digital micrographs were converted into a gray scale picture. During this converting process a lot of detailed information was lost, but to restore the information an intensity adjustment was made. The adjustment gave greater accuracy to the various gray lines and thus provided a more detailed outline of the grain boundaries. An additional problem was to detect the intersection points of the grain boundaries. This problem was minimized through using the software tool NxN-filter. The filter produced a relatively blurred image, but one which enabled more precise detection of the intersection points. The prepared micrograph for the evaluation is shown in figure 3.6.

Grain Evaluation

After the preparatory work the real evaluation starts. The first step is to produce a decollator picture. The decollator is a contour detection software tool to find all traced grain boundaries. This tool detects the different grey scales and defines the boundaries.

Once this process was complete the boundaries which had been discovered were edited again to correct any mistakes and the picture geometry was trimmed and calibrated. The result is shown in figure 3.7. For every single grain, the software's grain module calculates the surface area, diameter, elongation and any other user-defined parameters. For this work the quantity, diameter and the surface of all grains were detected. The grains in the border area were excluded from the evaluation.

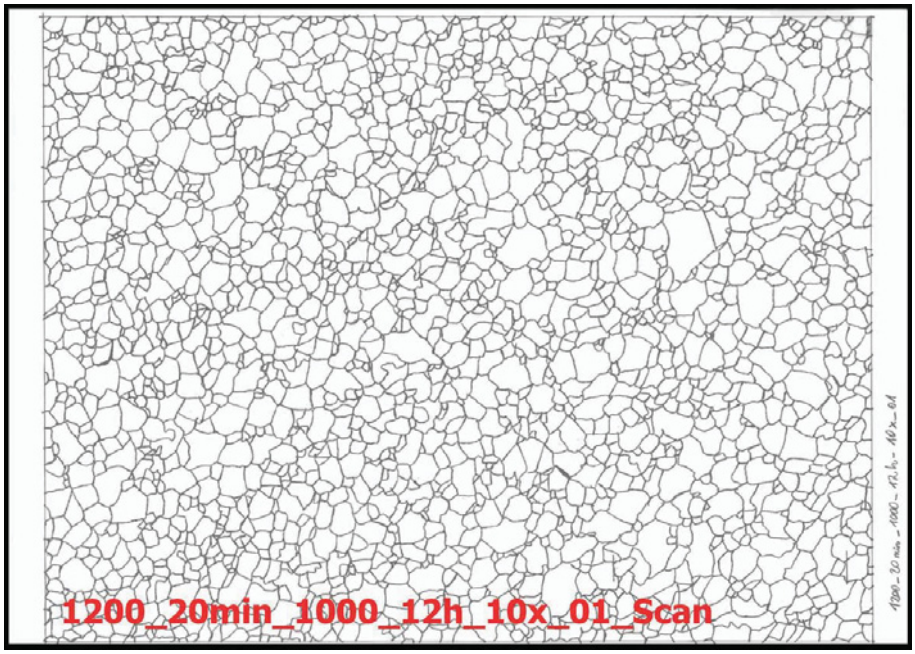

Figure 3.6: 1200°C 20min 1000°C 12h 10x scan

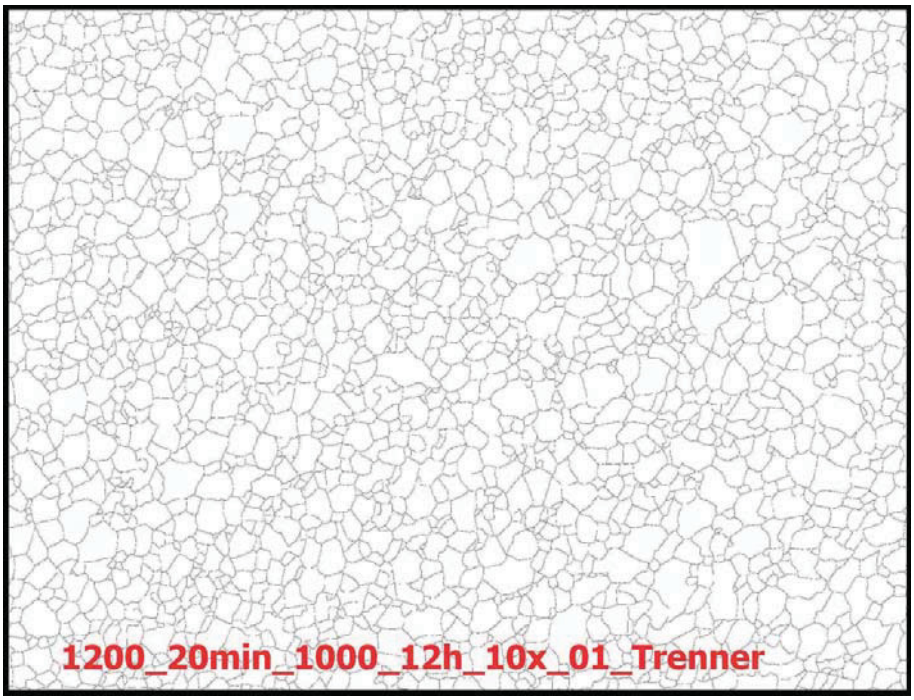

Figure 3.7: 1200°C 20min 1000°C 12h 10x decollator

3.4.4 Definition of the Limit Grain Size between Normal and Abnormal Grain Growth

In the literature many different methods are used to define the limit grain size diameter between normal and abnormal grain growth. In this thesis the limit was defined after an optical method. The smallest abnormal grains were measured and the average grain size was defined as the limit grain size between normal and abnormal grain growth. For example in figure 3.8 there are two pictures of the annealed specimen at 1200°C for 300min in 5x. The measured grains have approximately 200 μm, so the limit grain size for this sample was defined as 200 μm. With the aim of increasing the accuracy of the defined value a second definition was employed: the sizes of all single grains belonging to a particular specimen were sorted and graded from the smallest to the largest. To find a step between consecutive grains the actual value over the preceding value was calculated. The expected factor normally takes values from 1.00 to 1.02. In the area of the optical defined grain diameter the value may rise to 1.20 or more. For the last grains on the list, in the area of abnormal grain growth, values of up to 1.50 are possible.

With the limit grain size and the tables of grain surface and diameter the area frac-

tions of the normal and abnormal grains can be evaluated and also the average grain size diameter of the normal and abnormal grains of a specimen.

Small abnormalities may bastardize the calculated vales for the abnormal grain size area fraction. If the area fraction is less than 10%, in the evaluation there is no abnormal grain size and the values over the limit grain size would not account for the average normal grain size diameter.

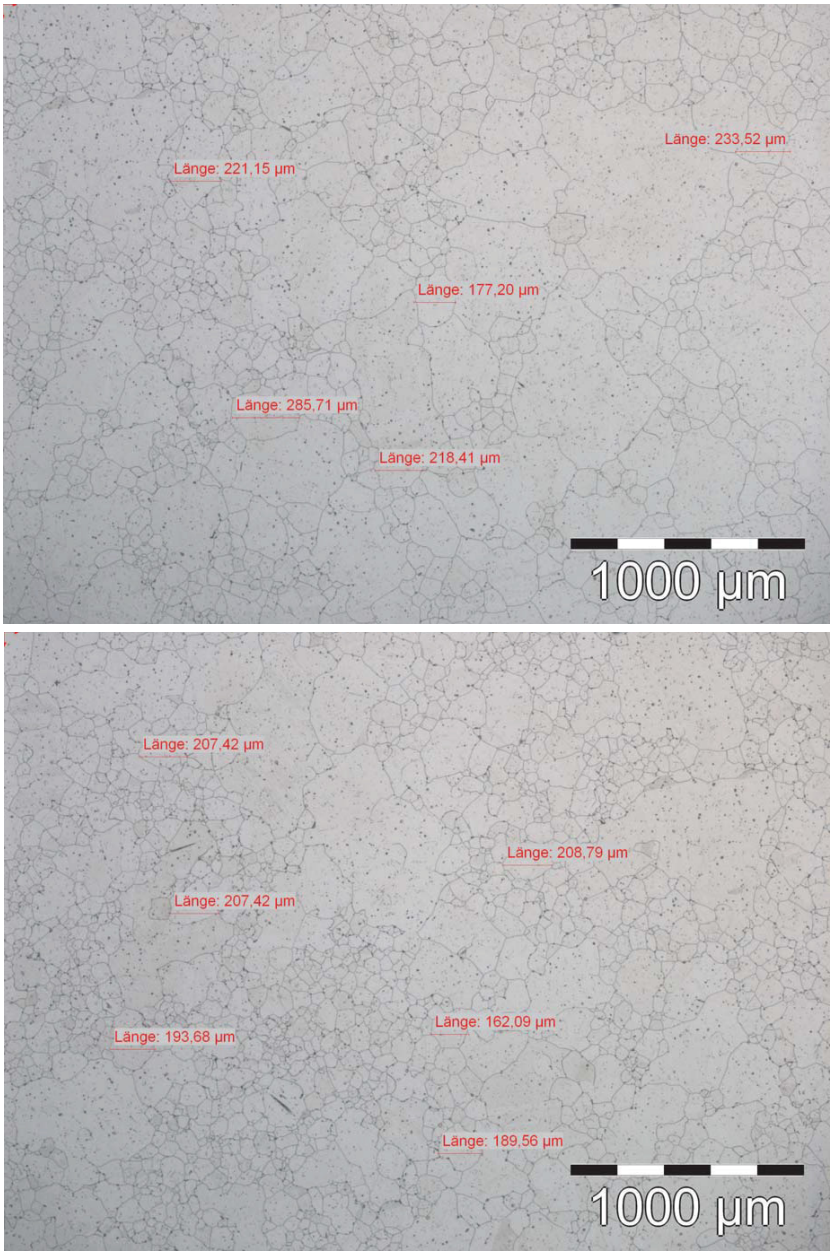

Figure 3.8: Limit 1200°C 300min annealed 5x

3.5 Evaluation of Determined Grain Size

The determined grain sizes of the annealed specimen had to be evaluated according to the grain growth law from [5], see equations 3.1 - 3.4. The parameters A,Q and m are calculated by non linear regression with the Software Statistica.

$$d = K * t^n \tag{3.1}$$

$$d = [K^m * t + do^m]^{(\frac{1}{m})} \tag{3.2}$$

$$K = A * exp^{\frac{-Q}{RT}} \tag{3.3}$$

$$d = [(A * exp^{\frac{-Q}{RT}})^m * t + do^m]^{(\frac{1}{m})} \tag{3.4}$$

Symbol explanation:

- d = grain diameter after a particular annealing time
- do= initial grain diameter
- K = mobility
- A = prefactor
- Q = activation energy for grain growth
- RT= ambient temperature
- m = 1 over n
- n = grain growth exponent - n values are below 0,5

3.6 Cellular Automata Modeling

Modeling and control of microstructure and grain size during annealing process are essential for tailoring the properties of materials. The fundamentals of cellular automaton model was tested at the shrinking of a circular grain and for its behavior at triple junctions.

3.6.1 Shrinkage of a Circular Grain in a Matrix

For the validation of the model, a simple case of circular grain embedded in a matrix ($100x71$ cells) was used to validate the present cellular automaton model, depicted in the figure 3.9.

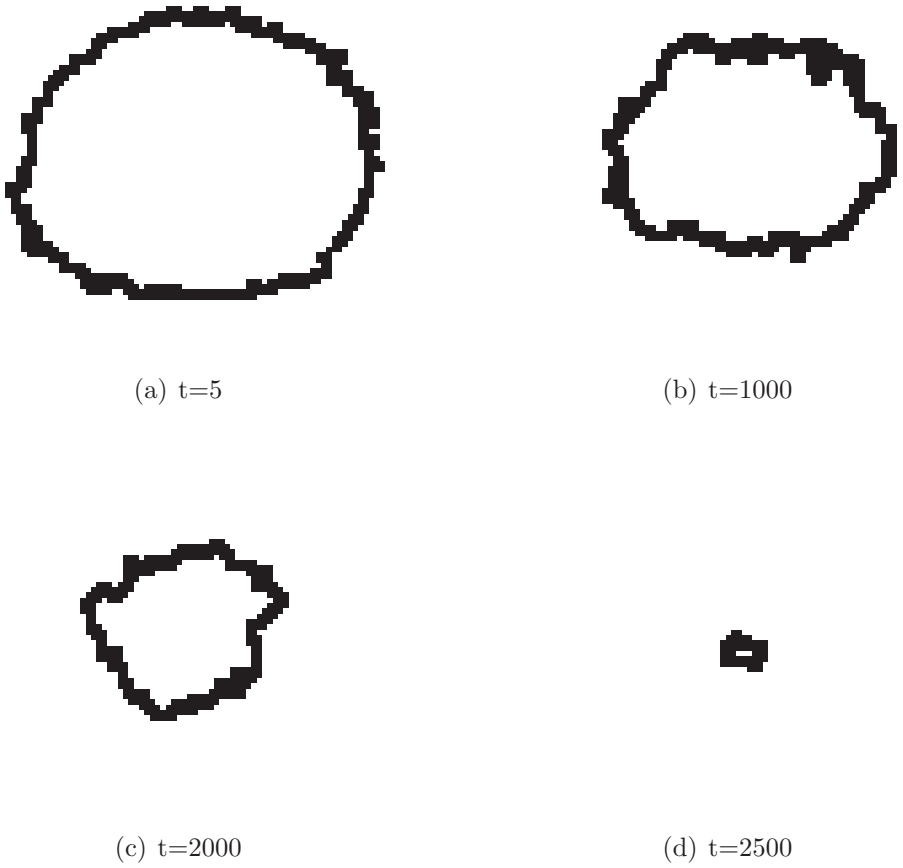

(a) t=5 (b) t=1000

(c) t=2000 (d) t=2500

Figure 3.9: Circle evolution

The circle evolution at a reorientation probability of 50% shows that the circle briefly maintains the circle shape, shrinking towards the center under its own curvature. The reason for the fluctuation of a grain boundary is due to statistical perturbations. Therefore, this cellular automaton model couples the grain boundary migration driven by both curvature and energy.

3.6.2 Effect of Triple Junctions

The effect of a triple junction is an important part of the microstructure. The reason is that the investigations of triple junctions is difficult and thus only few experimental data on well characterized samples are available.

Among fundamental mechanisms of microstructure formation, the grain boundary migration has to be investigated on well defined simple samples containing a small number of microstructure elements.

The samples containing two inclined grain boundaries and a connecting segment parallel to the free surfaces have been chosen as starting configurations depicted in the figure 3.10. They will be called open-H and slant-H after distorted letters H.

Figure 3.10: Initial a.) open-H and b.) slant-H configurations. The grid size is $100x78$ cells.

This method provides the opportunity to study details of grain shape change in addition to the kinetics of the grain boundary movement. The reorientation occur with the probability of 50% in order to prevent non-physical anisotropic growth reflecting the symmetry of the square grid. The grid size is $100x78$ cells and no periodic boundaries are used. In every time step the entire grid of automata cells is updated simultaneously according to the local transition rule. Therefore, the time is also a discrete quantity similar to the space divided into discrete cells. Since a straight grain boundary segment represents a stable configuration, the process of grain boundary migration is triggered by the fluctuations of cell reorientation at the ends of the straight segment.

The angles at the intersections of the grain boundaries with the free surfaces in the initial configurations are 45°. The equilibrium intersection is attained when this angle reaches 90°. The angles between grain boundary planes at triple junctions are 45°, 135° and 180° while at equilibrium they should be 120° as no anisotropy of grain boundary energy is considered.

Morphological changes of the quadriccrystals are illustrated in figure 3.11 and 3.12 for the chosen open-H and slant-H starting configurations, respectively. The migration begins at free surfaces where the straight boundary segments start to curve. This behavior is a consequence of the non-equilibrium inclined intersection of the grain boundary with the sample surface. Simultaneously, the triple junctions start to move to equilibrate the dihedral angles between the boundary planes. A rotation of the boundary about the triple junction leads to curvature of the boundary surface, too. When curved segments are established they move towards their centers of curvature.

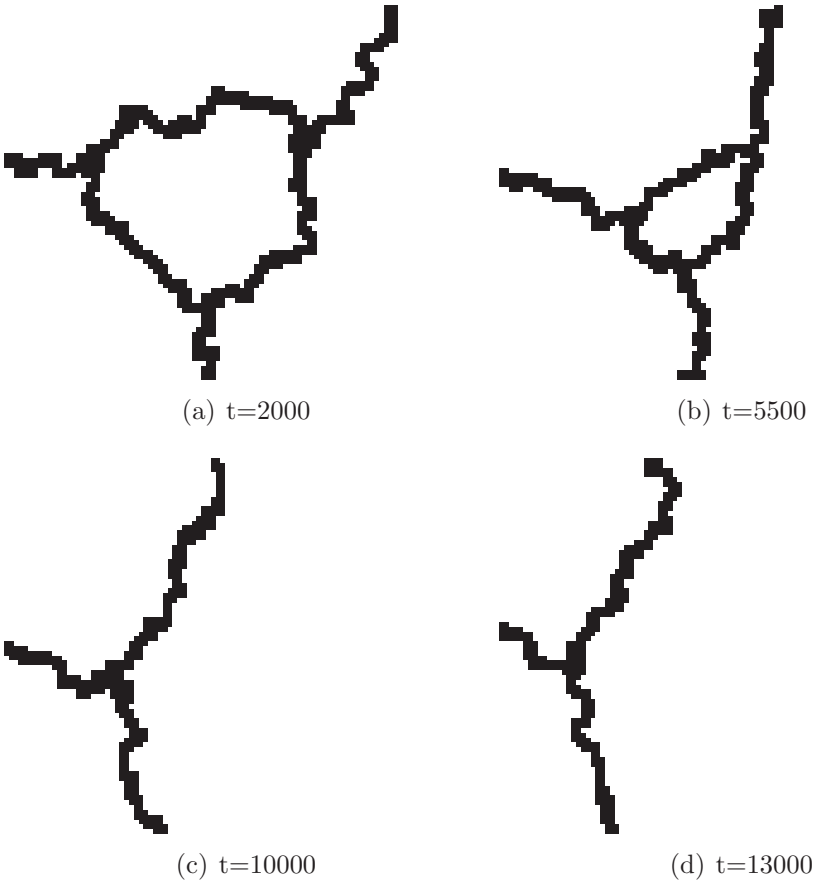

(a) t=2000 (b) t=5500

(c) t=10000 (d) t=13000

Figure 3.11: Development of microstructure for open-H configurations

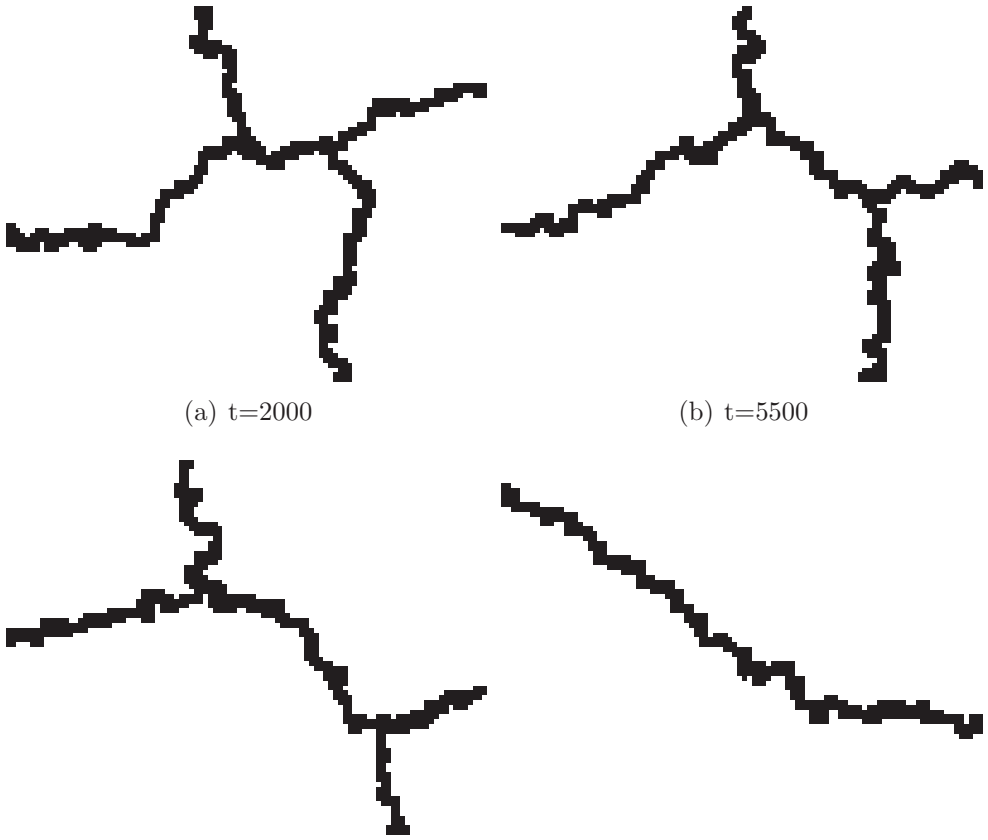

(a) t=2000 (b) t=5500

(c) t=10000 (d) t=13000

Figure 3.12: Development of microstructure for slant-H configurations

This is an elementary topological event happening during the grain growth in polycrystalline materials, which comes out naturally in the used method of simulation.

4 Results and Discussion

4.1 The Simulation of the Heating Up Process

The results of the heating up simulation by DEFORM FEM software are shown in figure 4.1 and table 4.1. The results demonstrate the time needed to reach an annealing temperature which is distributed homogenously throughout the whole specimen in the furnace.

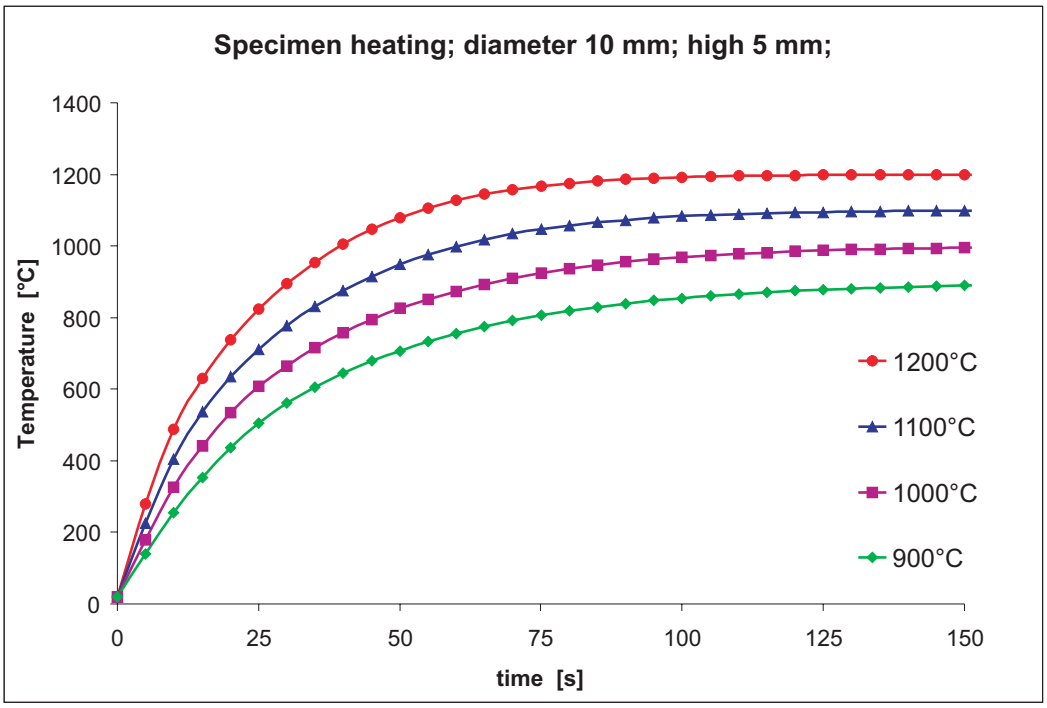

Figure 4.1: Simulation of the heating up process time over temperature

temperature [°C]	*time [s]*
900	300
1000	250
1100	200
1200	175

Table 4.1: Simulation of the heating up process results

Further, in exemplary fashion the figures 4.2 and 4.3 show the axisymmetric specimens at different time steps during the heating up process.

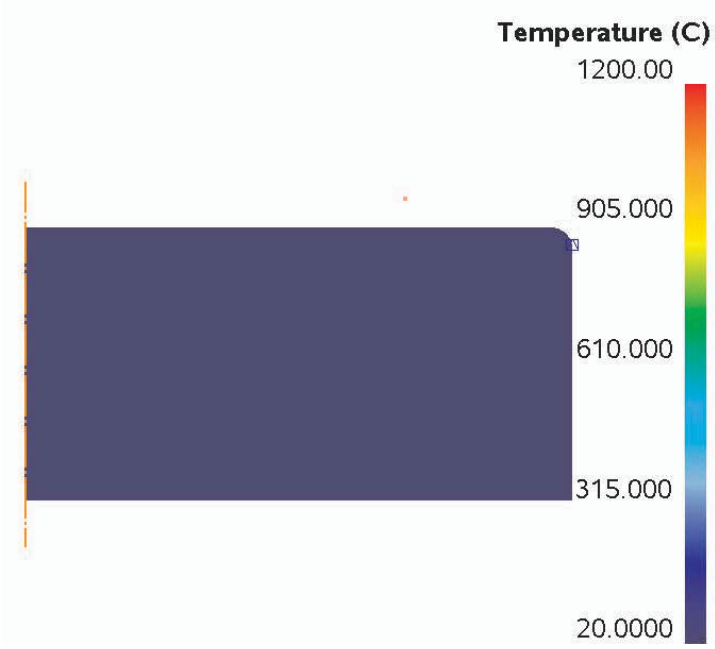

Figure 4.2: Simulation results for 1200°C time: 0 seconds; axisymmetric-lower left corner is the core of specimen

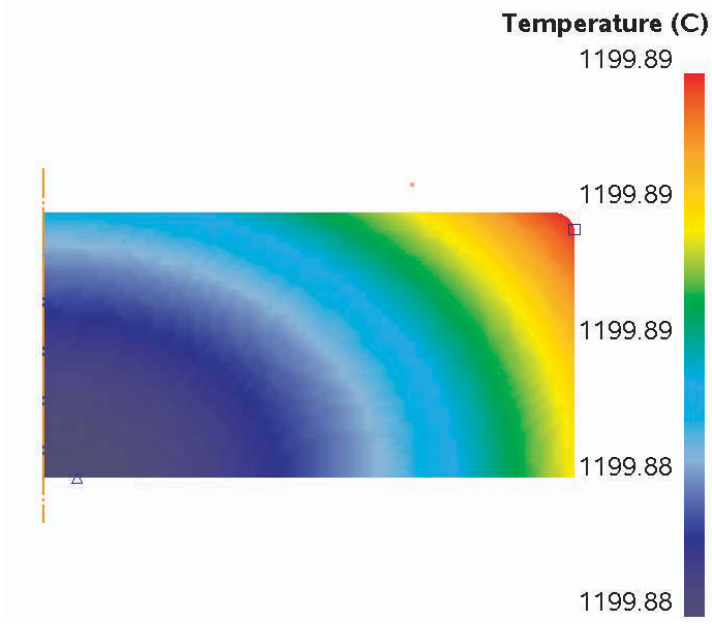

Figure 4.3: Simulation results for 1200°C time: 175 seconds; axisymmetric- lower left corner is the core of specimen

4.2 Results of One-Step-Annealing Process

In this section the evaluated grain sizes for the one step annealing process are given. The limit grain sizes distinguishing normal and abnormal grains and the area fractions of abnormal grains are evaluated.

In the following section, all diagrams and tables are sequenced as follows:

- Firstly, the results of normal grain growth for all temperatures are shown (figure 4.4). Further, table 4.2 displays the values of the normal grain sizes.
- Secondly, the results of abnormal grain growth are shown (figure 4.5) where the following table 4.3 gives the values of the evaluated abnormal grain sizes.
- Thirdly, the fixed limit grain sizes (section 3.4.4) are illustrated in figure 4.6.
- Fourthly, the figure 4.7 shows the part of surface of abnormal grains over the annealing time. Further, table 4.5 displays the evaluated fraction values.

Figure 4.4 displays the normal grain sizes over the annealing time for the one-step annealing process. The diagram clearly illustrates the high influence of annealing temperature on the development of grain size.

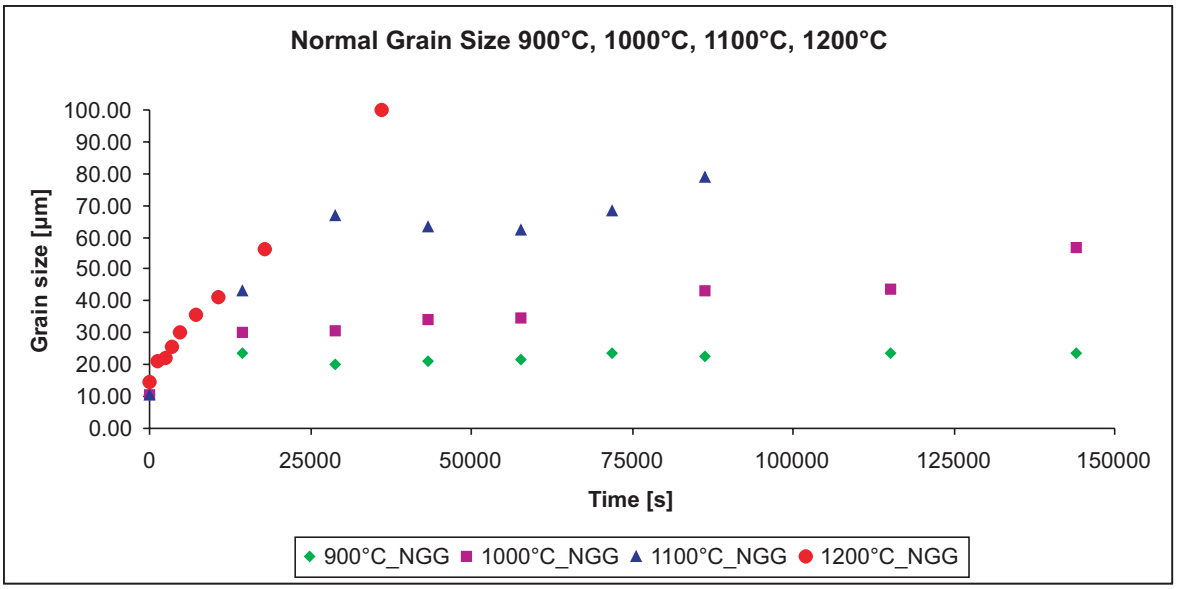

Figure 4.4: Normal grain growth for different annealing temperatures one-step annealing process

For the annealing temperature of 900°C, the grain size doubles at 14400 seconds and then remains constant for 36 annealing hours. The small variation of 4 μm is not significant, because there was only one specimen at each annealing time evaluated. The annealing temperatures of 1000°C and 1100°C lead to a higher grain growth gradient. The 1200°C samples show a huge increase in grain size during a short annealing period. The evaluated normal grain size values are displayed in table 4.2.

Time [s]	*900C*	*1000C*	*1100C*	*1200C*
0	11 μm	11 μm	11 μm	15 μm
1200				21 μm
2400				22 μm
3600				26 μm
4800				30 μm
7200				36 μm
10800				41 μm
14400	24 μm	30 μm	43 μm	
18000				56 μm
28800	20 μm	31 μm	67 μm	
36000				100 μm
43200	21 μm	34 μm	63 μm	
57600	22 μm	35 μm	62 μm	
72000	24 μm		69 μm	
86400	23 μm	43 μm	79 μm	
115200	24 μm	44 μm		
144000	24 μm	57 μm		

Table 4.2: One-step annealing process normal grain growth

The huge increase in grain size at high temperatures and short annealing times stimulate the development of abnormal grain growth. Figure 4.5 and table 4.3 show the abnormal grain sizes at different annealing temperatures. For the 900°C the forces for abnormal grain growth are too weak due to low temperature and precipitations, thus no abnormal grain growth occurs. At higher annealing temperatures the forces for secondary recrystallization are high enough for exaggerated grain growth to develop. With higher temperatures abnormal grain growth starts earlier, displayed in table 4.3. For 900°C there is no abnormal grain growth even after 40 hours of annealing time, but for 1200°C abnormal grain growth is evident after just 7200 seconds. At 1100°C abnormal grain

growth needs 28800 seconds (three times that of 1200°C) and the 1000°C specimen needs 43200 seconds, which is almost double that at 1100°C and six times that at 1200°C.

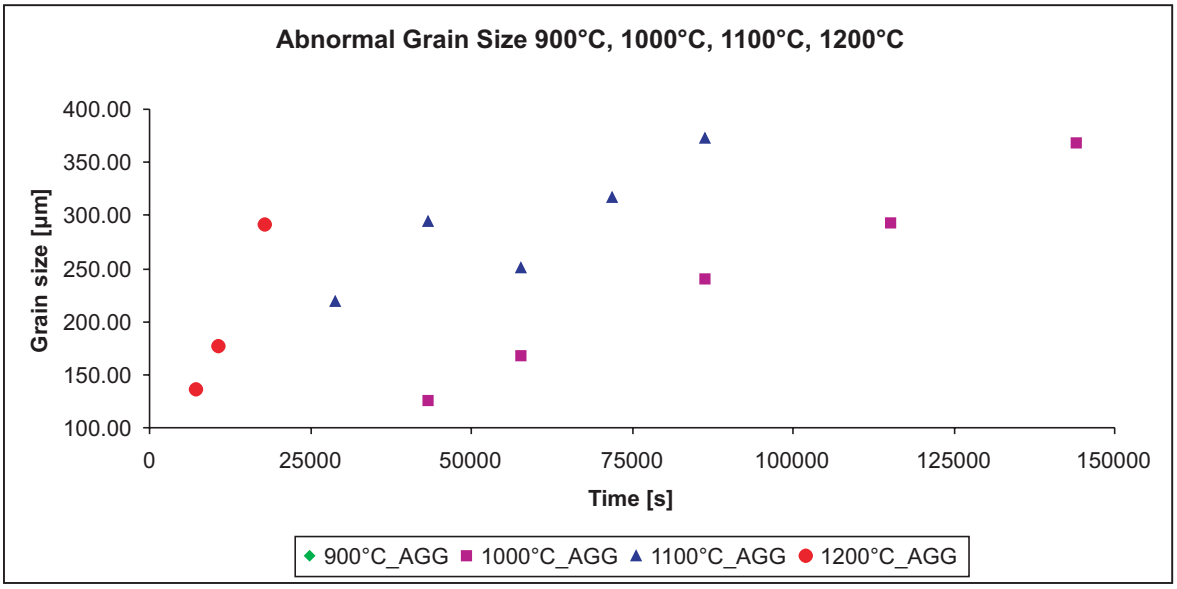

Figure 4.5: Abnormal grain size vs. annealing time for one-step annealing process

Time [s]	*900C*	*1000C*	*1100C*	*1200C*
7200				137 μm
10800				177 μm
18000				292 μm
28800			219 μm	
36000				473 μm
43200		126 μm	294 μm	
57600		168 μm	257 μm	
72000			317 μm	
86400		240 μm	372 μm	
115200		293 μm		
144000		368 μm		

Table 4.3: One-step annealing abnormal grain size

The limit grain sizes to distinguish between normal and abnormal grain size after 3.4.4 are shown in figure 4.6 and the values are given in table 4.4.

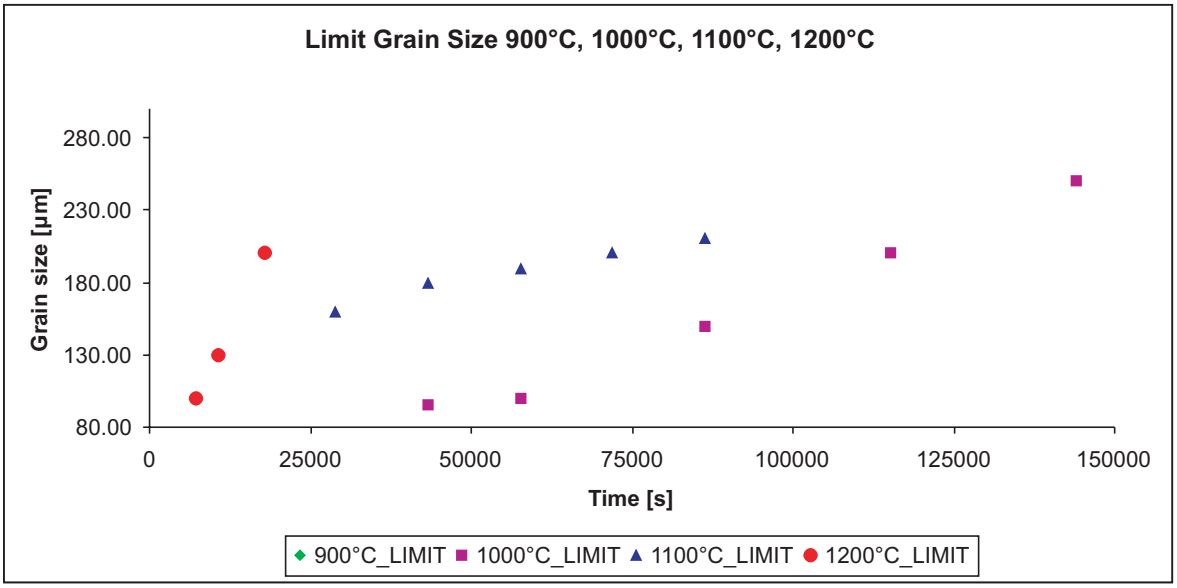

Figure 4.6: Defined limiting grain size between normal and abnormal grain growth vs. annealing time for one-step annealing process

Time [s]	*900C*	*1000C*	*1100C*	*1200C*
7200				100 μm
10800				130 μm
18000				200 μm
28800			160 μm	
36000				350 μm
43200		95 μm	180 μm	
57600		100 μm	190 μm	
72000			200 μm	
86400		150 μm	210 μm	
115200		200 μm		
144000		250 μm		

Table 4.4: One step annealing limit grain size

In order to complete the one-step annealing series at different temperatures and times the evaluated results (figure 4.7) *and/or* the values (table 4.5) of the abnormal grain area fraction are displayed.

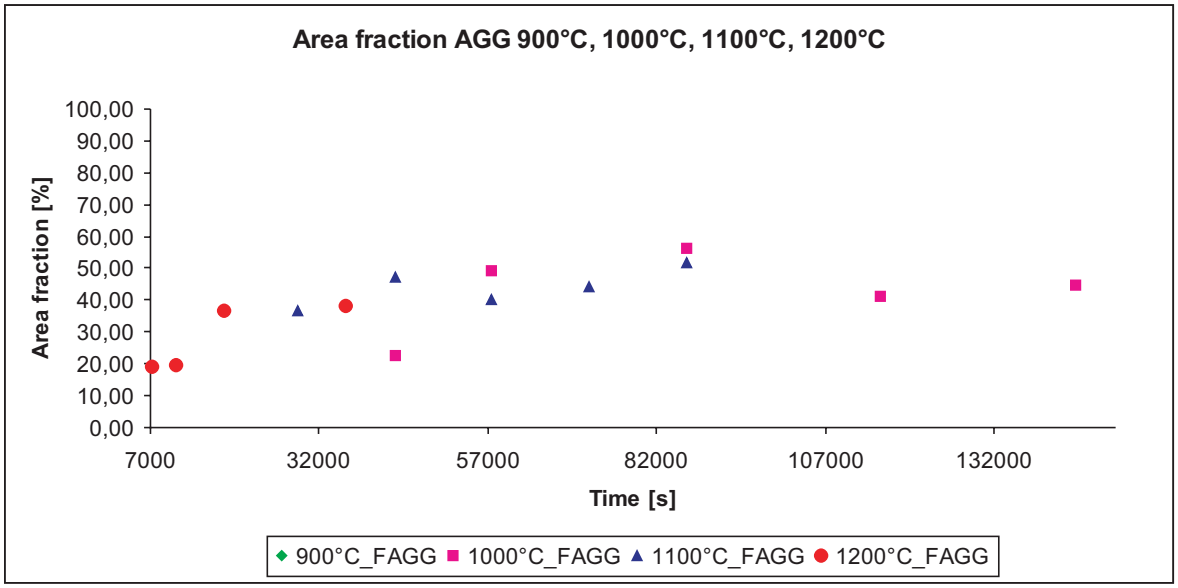

Figure 4.7: Area fraction for abnormal grain growth vs. annealing time for one-step annealing process

Time [s]	*900C*	*1000C*	*1100C*	*1200C*
7200				19 %
10800				20 %
18000				37 %
28800			37 %	
36000				38 %
43200		22 %	47 %	
57600		49 %	40 %	
72000			44 %	
86400		56 %	52 %	
115200		41 %		
144000		45 %		

Table 4.5: One step annealing abnormal grain growth area fraction

The area fraction values in table 4.5 for the 1000°C annealing specimen decline after 115200 seconds. A possible reason for this phenomenon is the evaluated limiting grain size between the allocation of abnormal and normal grains. At long annealing times over 24 hours and high temperatures the allocations of the grains overlap and the limit grain size reduces and so the fraction rises. At 1000°C and 115200 seconds annealing time the

limit grain size was fixed at 200 μm and the result of the fraction of abnormal grains was 41 %. At 144000 seconds the limit grain size was 250 μm and the fraction 45 %. The fraction of abnormal grains rises to 55 and 69 % when the limit grain sizes are reduced to 100 and 120 μm. When the allocation overlaps and develops more than one peak the limit grain sizes are difficult to define after this schema (see chapter 3.4.4). For the future, the limit grain size for annealed specimens over a protracted period will be evaluated by developed Cellular Automata model.

4.3 The Grain Growth Kinetics for the One-Step Annealing Process

In the following section the kinetic results of the normal and abnormal grain sizes explained in section 3.5 are demonstrated.

The well known equation $d = [(A * exp^{\frac{-Q}{RT}})^m * t + do^m]^{(\frac{1}{m})}$ was used and regressed (Software Statistica and TableCurve) in order to calculate: n, A and Q for the different annealing temperatures.

For a useful regression at least three measurement points of the same annealing temperature are required. Figure 4.8 shows the measurement points of the normal grain sizes of all one step annealing specimens and the regressed curves for the same.

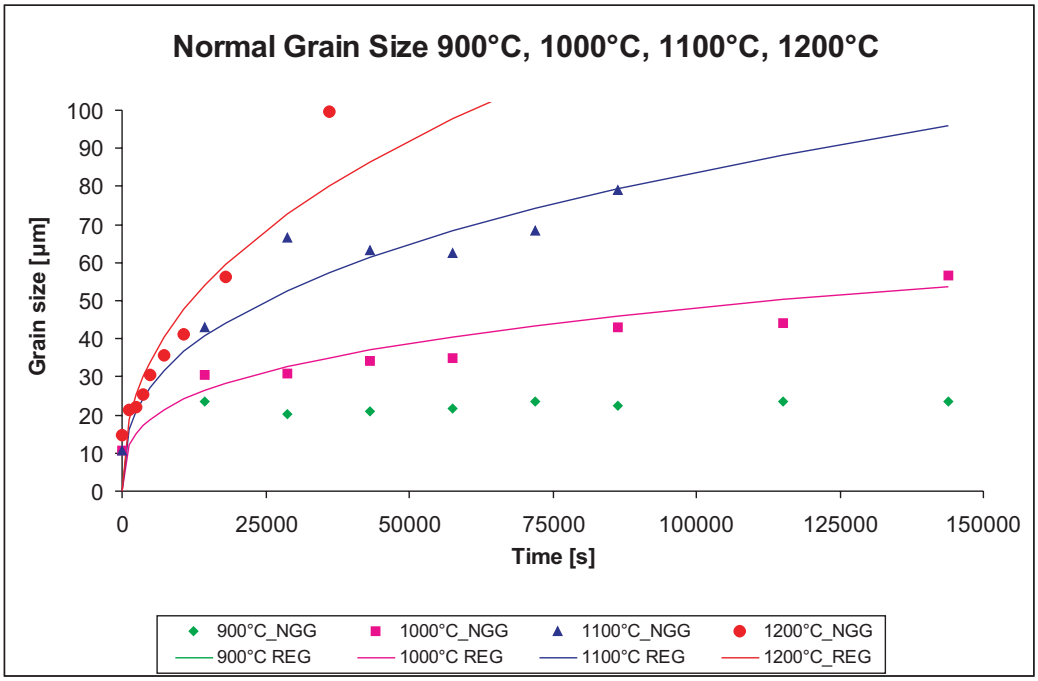

Figure 4.8: Regression curves ($d = [(A * exp^{\frac{-Q}{RT}})^m * t + do^m]^{(\frac{1}{m})}$) for normal grain growth at 900°C, 1000°C, 1100°C and 1200°C

The received n values, illustrated in table 4.6, for the regression of the one-step annealed specimens are below 0.5, which corresponds to the literature after [29] and [30]. The activation energy Q_{NGG} is constant for normal grain growth at 62314.6 J/Kmol. So the influence of high temperature during the annealing process is confirmed by the growth exponent n.

Temperature	*n [-]*	*A [-]*	*Q_{NGG} [J/Kmol]*
1000C	0.31	0.00376	62314.6
1100C	0.37	0.00494	62314.6
1200C	0.43	0.00569	62314.6

Table 4.6: n, A and Q values for normal grain growth regression

The regressions for the one step annealing abnormal grain growth are shown in figure 4.9 and table 4.7. The calculated results for the grain growth exponent n are higher than the values evaluated for normal grain growth due to a higher growth gradient. The activation

energies for normal and abnormal grain growth are constant, but the value of Q_{AGG} is lower at 33682.7 J/Kmol.

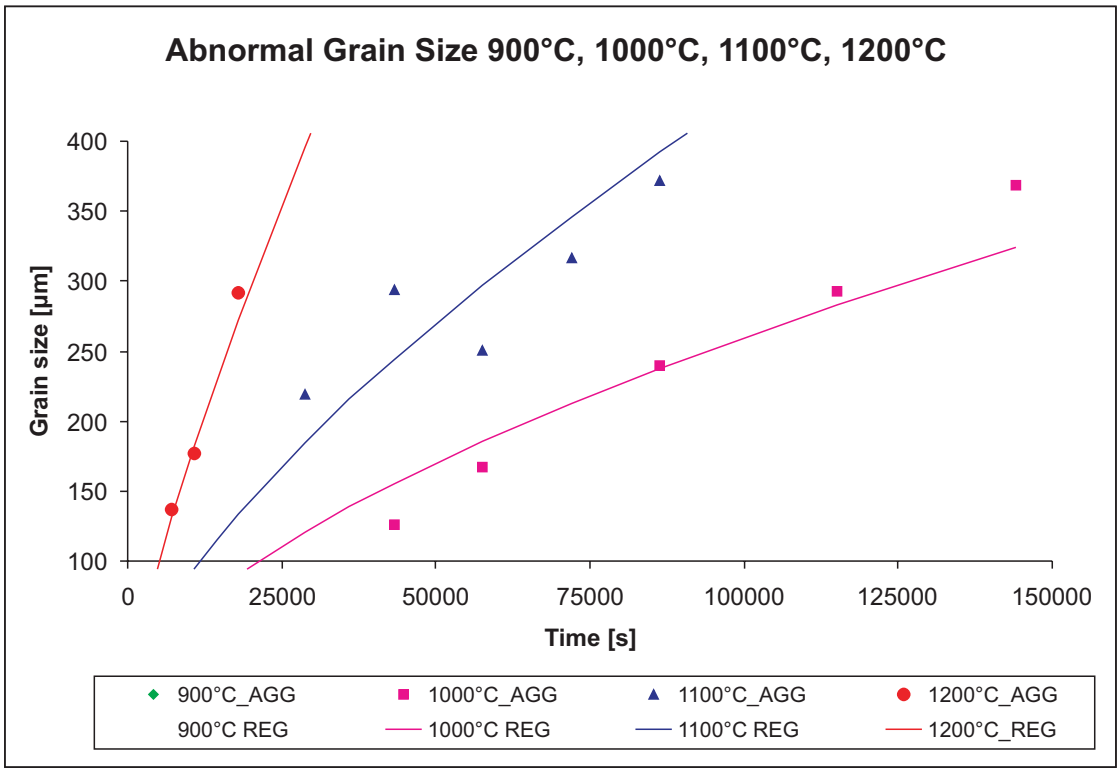

Figure 4.9: Regression curves ($d = [(A * exp^{\frac{-Q_{AGG}}{RT}})^m * t + do^m]^{(\frac{1}{m})}$) for abnormal grain growth 900°C, 1000°C, 1100°C and 1200°C

Temperature	*n [-]*	*A [-]*	Q_{AGG} *[J/Kmol]*
1000C	0.75	0.00217	33682.7
1100C	0.80	0.00242	33682.7
1200C	0.89	0.00297	33682.7

Table 4.7: n, A and Q values for abnormal grain growth regression

In order to validate the regressed results, results of grain coarsening treatments for type 304L steel of [5] are regressed in the same way. The grain growth sizes of literature are shown in table 4.8 and the n, A and Q values of the regression curves are shown in table 4.9. The magnitude of the regressed values of the EU Commission report match the regression values of the annealing experiments.

Time [s]	*1000C*	*1050C*	*1100C*
0	7 μm	7 μm	7 μm
60	9 μm	14 μm	28 μm
120	13 μm	19 μm	31 μm
240	17 μm	30 μm	40 μm
600	25 μm	40 μm	49 μm
1200	31 μm	48 μm	62 μm

Table 4.8: EU Commission paper [5] grain sizes

Temperature	*n [-]*	*A [-]*	Q_{NGG} *[J/Kmol]*
1000C	0.36	0.0105	58329,6
1050C	0.39	0.0152	58329,6
1100C	0.42	0.0203	58329,6

Table 4.9: n, A and Q values for normal grain growth regression

As a summary of all results evaluated, the figure 4.10 shows the complete regression values of the one-step annealing process.

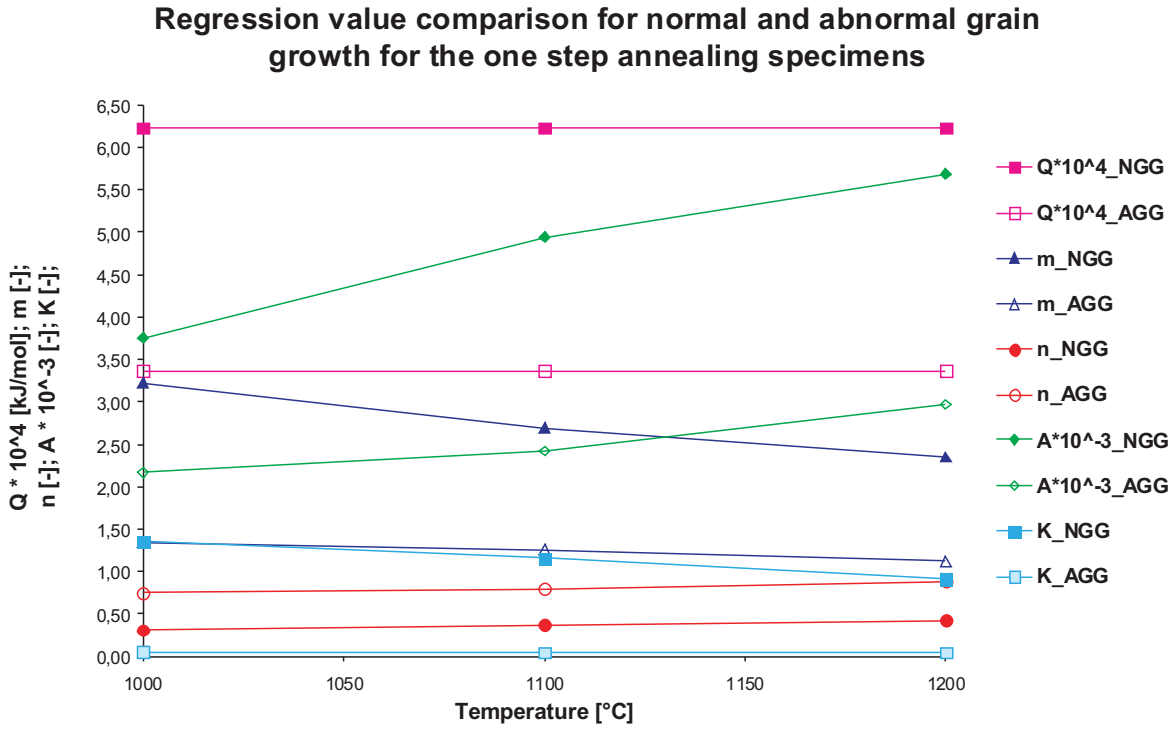

Figure 4.10: The comparison of all regression values for the one-step annealing process normal and abnormal grain growth

4.4 Results of the Two-Step Annealing Process

In this section the results for the two-step annealed process are given according to the scheme explained in section 4.2.

4.4.1 Two-Step Annealing Process 1200°C and 1000°C

Figure 4.11 illustrates the development of normal grain sizes vs. the annealing time for the two-step annealing process of preheating at 1200°C and subsequently annealing at 1000°C. Preheating at 1200°C (10 to 180 minutes) leads to higher grain sizes after the second annealing period at 1000°C (12, 16, 24, 32 and 40 hours). The grain growth rate after preheating is not as steep as the slope for the one step annealing specimens. Thus the initial grain size and the preheating temperature is significant for the grain growth at second annealing procedure. The grain sizes (table 4.10) for the second annealing step at

1000°C show minimal rise over a time period of 40 hours for low time periods of preheating at 1200°C.

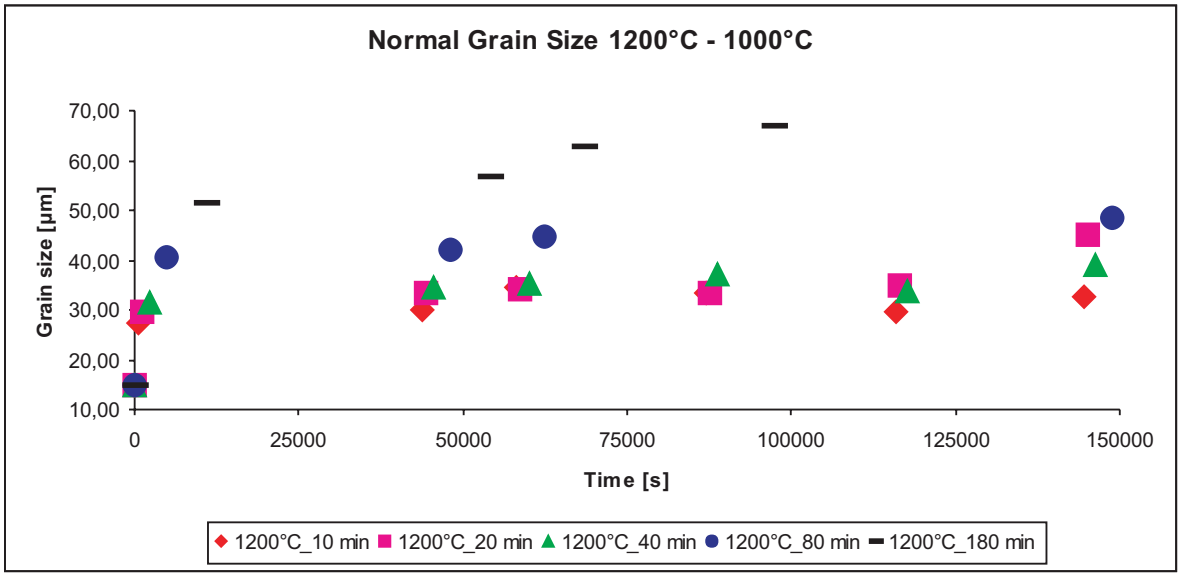

Figure 4.11: Normal grain growth vs. annealing time for two-step annealing firstly at 1200°C and afterwards at 1000°C

Time [s]	*1200C10min*	*1200C20min*	*1200C40min*	*1200C80min*	*1200C180min*
0	15μm	15μm	15μm	15μm	15 μm
600	27 μm				
1200		30 μm			
2400			32 μm		
4800				41 μm	
10800					51 μm
43800	30 μm				
44400		33 μm			
45600			35 μm		
48000				42 μm	
54000					57 μm
58200	35 μm				
58800		34 μm			
60000			35 μm		
62400				45 μm	
68400					63 μm
87000	34 μm				
87600		33 μm			
88800			37 μm		
97200				67 μm	
115800	30 μm				
116400		35 μm			
117600			34 μm		
144600	33 μm				
145200		45 μm			
146400			39 μm		
148800				49 μm	
154800					62 μm

Table 4.10: Two-step annealing process firstly at 1200°C and afterwards at 1000°C for normal grain growth; The upper part of the table shows the initial grain sizes after 1200°C heat treatment. The lower part shows the grain sizes after a subsequent 1000°C annealing process

The corresponding abnormal grain sizes in figure 4.12 and values are illustrated in table 4.11. The specimens preheated at 1200°C after 20 and 180 minutes showed a reduction of abnormal grain size, influenced by the fixing of the limit grain sizes, which corresponds to the multiple peaks in the grain size distribution.

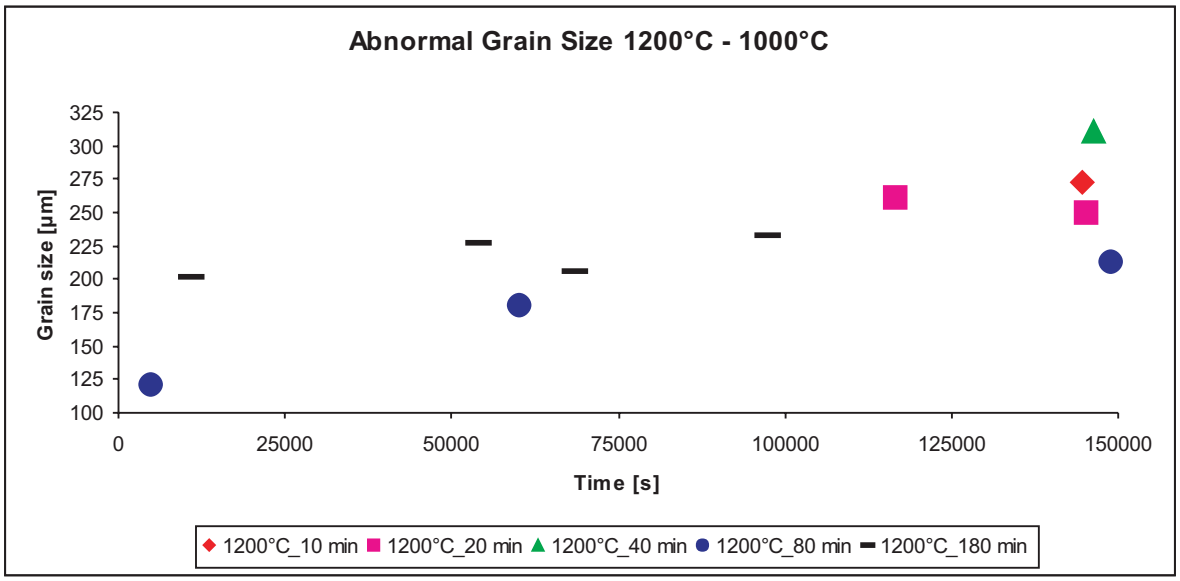

Figure 4.12: Abnormal grain growth vs. annealing time for the two-step annealing process firstly at 1200°C and secondly at 1000°C

Time [s]	*1200C10min*	*1200C20min*	*1200C40min*	*1200C80min*	*1200C180min*
4800				122 μm	
10800					201 μm
54000					227 μm
60000				181 μm	
68400					206 μm
97200					232 μm
116400		261 μm			
144600	273 μm				
145200		250 μm			
146400			311 μm		
148800				213 μm	
154800					221 μm

Table 4.11: Two-step annealing process for two-step annealing process firstly at 1200°C and secondly at 1000°C abnormal grain growth

The limit grain sizes to distinguish between normal and abnormal grain size (described in section 3.4.4) are shown in figure 4.13 and the corresponding values are given in table 4.12.

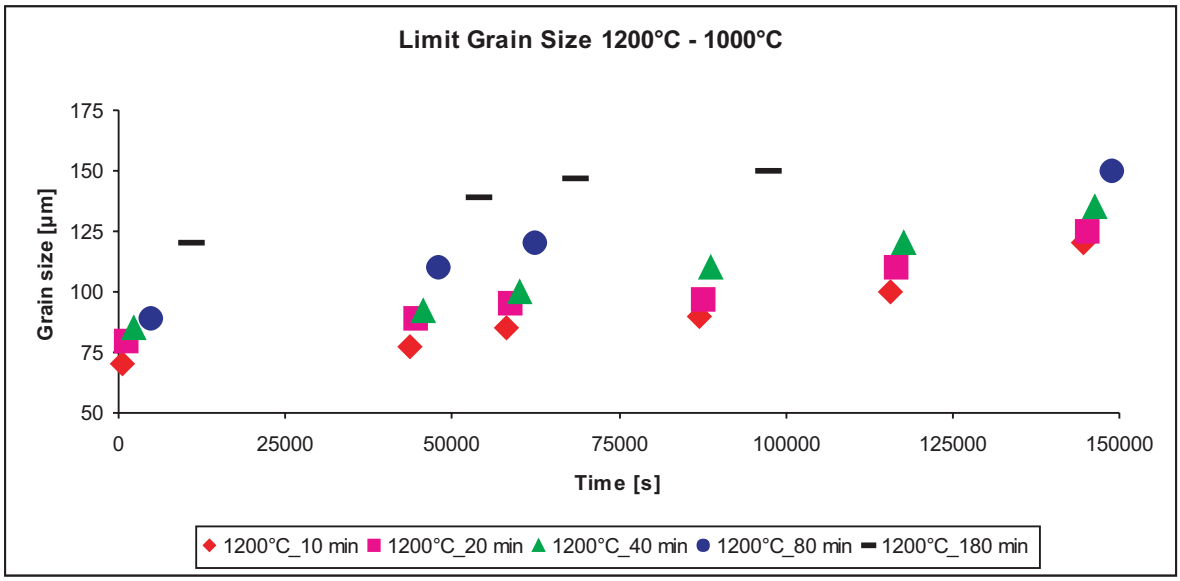

Figure 4.13: Defined grain size limits between normal and abnormal grain growth vs. annealing time for the two-step annealing process firstly at 1200°C and secondly at 1000°C

Time [s]	*1200C10min*	*1200C20min*	*1200C40min*	*1200C80min*	*1200C180min*
600	70 μm				
1200		80 μm			
2400			85 μm		
4800				89 μm	
10800					120μm
43800	77 μm				
44400		89 μm			
45600			92 μm		
48000				110 μm	
54000					139 μm
58200	85 μm				
58800		95 μm			
60000			100 μm		
62400				120 μm	
68400					147 μm
87000	90 μm				
87600		97 μm			
88800			110 μm		
97200				150 μm	
115800	100 μm				
116400		110 μm			
117600			120 μm		
144600	120 μm				
145200		125 μm			
146400			135 μm		
148800				150 μm	
154800					155 μm

Table 4.12: Two-step annealing firstly at 1200°C and secondly at 1000°C limiting grain sizes

In order to complete results of the two-step annealing process, figure 4.14 and table 4.13 show the abnormal grain fractions. The fraction values decline after long annealing durations. The reason could be the evaluated limiting grain sizes (4.2).

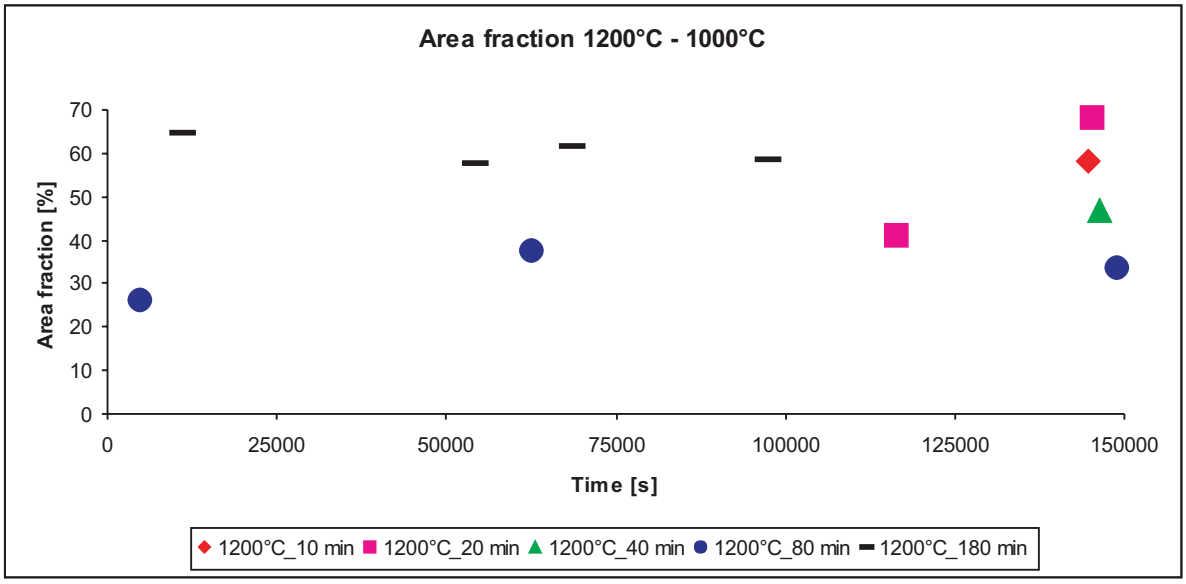

Figure 4.14: Area fraction for abnormal grain growth vs. annealing time two step annealing firstly at 1200°C and secondly at 1000°C

Time [s]	*1200C10min*	*1200C20min*	*1200C40min*	*1200C80min*	*1200C180min*
4800				26 %	
10800					65 %
54000					58 %
60000				38 %	
68400					62 %
97200					59 %
116400		41 %			
144600	58 %				
145200		68 %			
146400			47 %		
148800				34 %	
154800					44 %

Table 4.13: Two-step annealing process firstly at 1200°C and secondly at 1000°C abnormal grain growth area fraction

4.4.2 Two-Step Annealing Process 1000°C and 1200°C

Figure 4.15 illustrates the results of normal grain growth of the two-step annealing process of preheating at 1000°C (2, 8 and 24 hours) and annealing at 1200°C (60, 80, 120 and 300 minutes). Further, the grain sizes are listed in table 4.14. The grain sizes show a continuous rise starting at different initial grain sizes at the second treatment step of about 55μm. The first annealing step at 1000°C does not show any significant influence due to grain development.

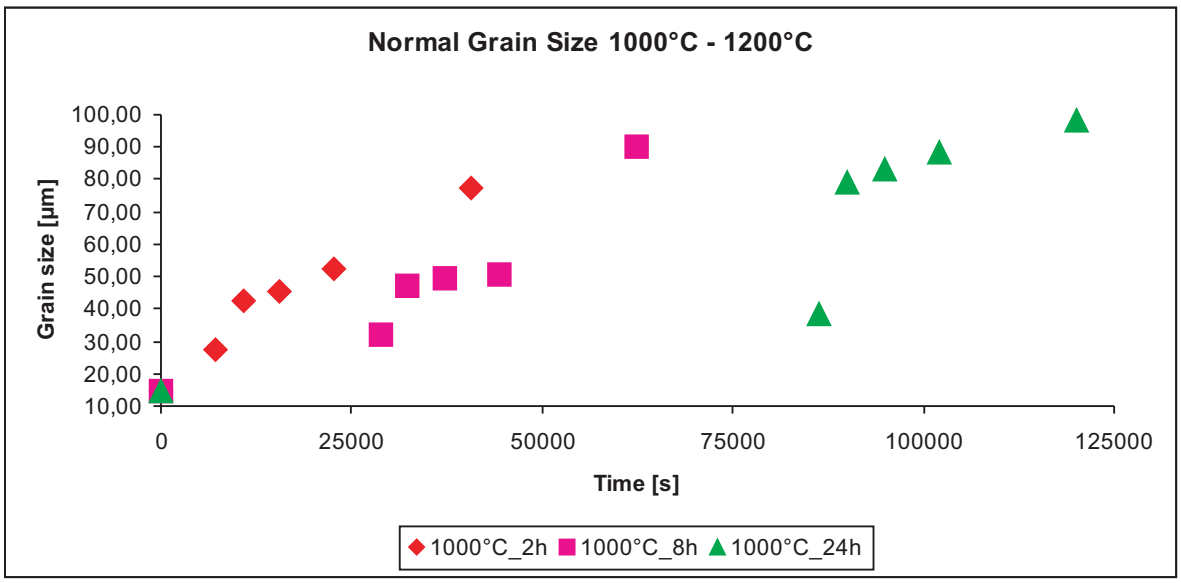

Figure 4.15: Normal grain growth vs. annealing time for a two-step annealing process, firstly at 1000°C and afterwards at 1200°C

Time [s]	*1000C 2h*	*1000C 8h*	*1000C 24h*
0	15 μm	15 μm	15 μm
7200	28 μm		
10800	43 μm		
15600	45 μm		
22800	52 μm		
28800		32 μm	
32400		47 μm	
37200		50 μm	
40800	77 μm		
44400		51 μm	
62400		90 μm	
86400			38 μm
90000			79 μm
94800			83 μm
102000			88 μm
120000			98 μm

Table 4.14: Two-step annealing process firstly at 1000°C and afterwards at 1200°C normal grain growth

Preheating for two and eight hours at 1000°C leads to a moderate increase in the abnormal grain size after annealing at 1200°C. Further preheating for 24 hours at 1000°C leads to abnormal grains even before the second treatment step starts. Thus the slope representing growth of the abnormal grain size is more gentle by comparison with the other specimens.

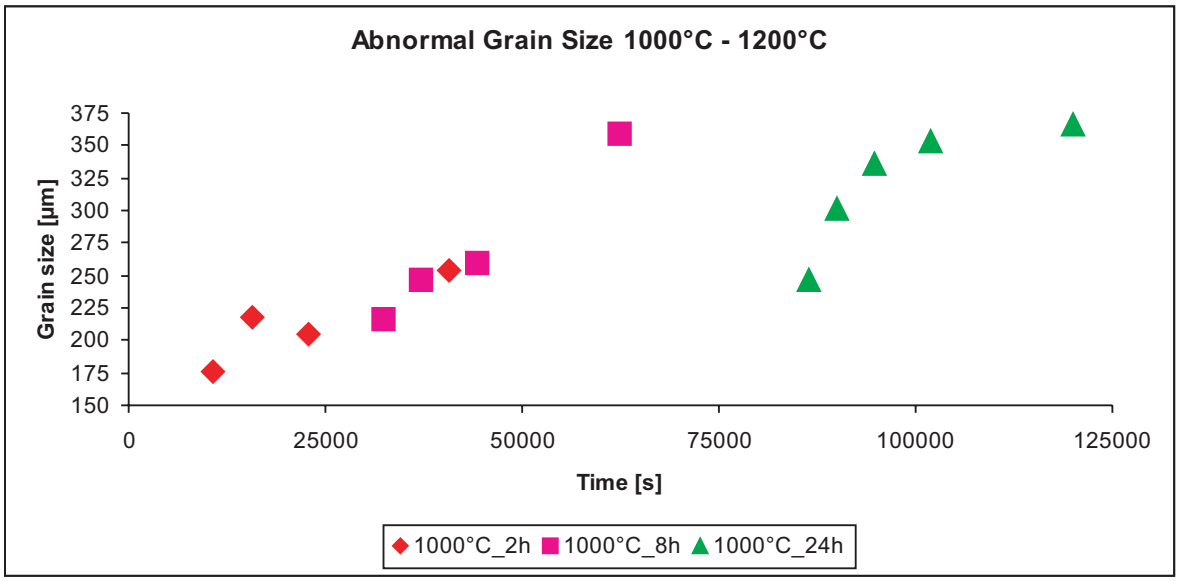

Figure 4.16: Abnormal grain growth vs. annealing time for a two-step annealing process firstly at 1000°C and secondly at 1200°C

Time [s]	*1000C 2h*	*1000C 8h*	*1000C 24h*
10800	177 μm		
15600	218 μm		
22800	205 μm		
32400		217 μm	
37200		246 μm	
40800	253 μm		
44400		260 μm	
62400		359 μm	
86400			247 μm
90000			302 μm
94800			336 μm
102000			353 μm
120000			366 μm

Table 4.15: Two-step annealing process at firstly 1000°C and secondly at 1200°C abnormal grain growth

The limiting grain sizes which define the difference between normal and abnormal grains (section 3.4.4) are shown in figure 4.17 and table 4.16.

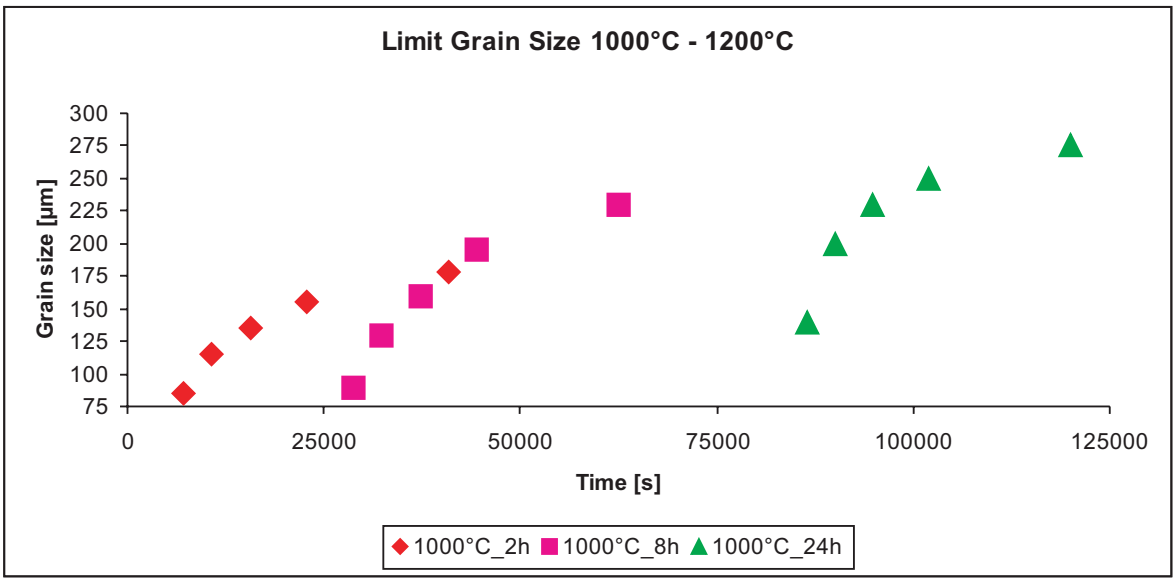

Figure 4.17: Defined grain size limiting between normal and abnormal grain growth vs. annealing time two step annealing process, firstly at 1000°C and secondly at 1200°C

Time [s]	*1000C 2h*	*1000C 8h*	*1000C 24h*
7200	85 μm		
10800	115 μm		
15600	135 μm		
22800	155 μm		
28800		90 μm	
32400		130 μm	
37200		160 μm	
40800	178 μm		
44400		195 μm	
62400		230 μm	
86400			140 μm
90000			200 μm
94800			230 μm
102000			250 μm
120000			275 μm

Table 4.16: Two-step annealing process firstly at 1000°C and secondly at 1200°C limit grain size

In order to complete the results of the two-step annealing process, figure 4.18 and table 4.17 show the abnormal grain fractions. The fraction values decline after long annealing durations. The reason could be the evaluated limiting grain sizes (4.2).

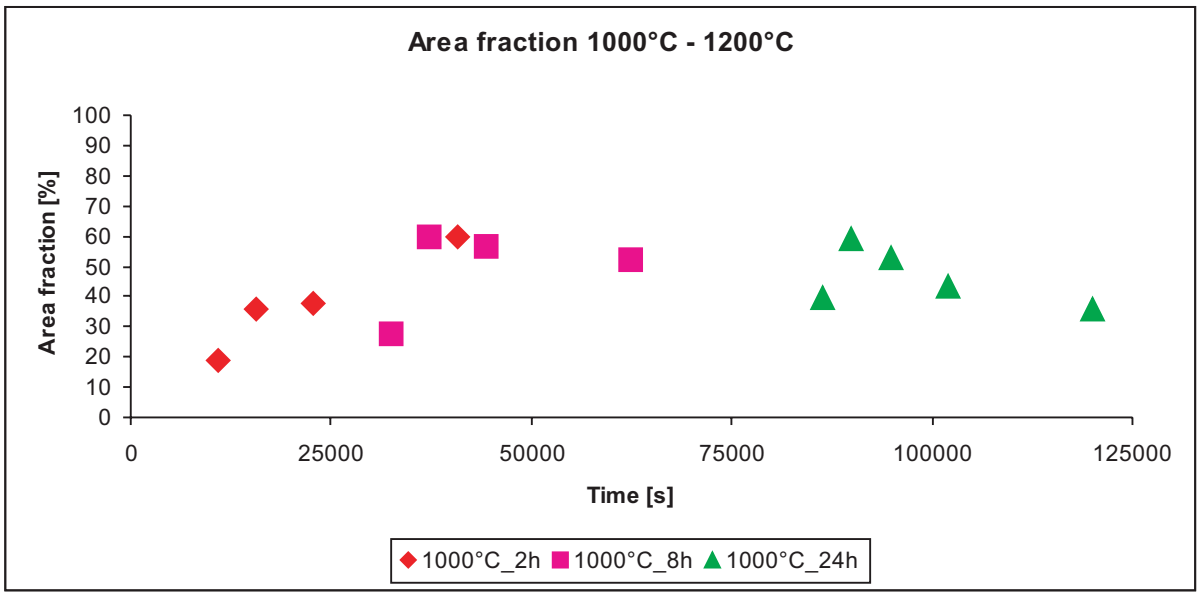

Figure 4.18: Area fraction for abnormal grain growth vs. annealing time

Time [s]	*1000C 2h*	*1000C 8h*	*1000C 24h*
10800	19 %		
15600	36 %		
22800	38 %		
32400		28 %	
37200		60 %	
40800	60 %		
44400		57 %	
62400		52 %	
86400			40 %
90000			59 %
94800			53 %
102000			43 %
120000			36 %

Table 4.17: Two step annealing process firstly at 1000°C and secondly 1200°C abnormal grain growth area fraction

4.4.3 Two-Step Annealing Process 900°C and 1200°C

Figure 4.19 illustrates the development of normal grain sizes vs. the annealing time for the two-step annealing process of preheating at 900°C and subsequently annealing at 1200°C. The grain sizes (table 4.18) for the second annealing step at 1200°C show minimal growth over a short period of preheating at 900°C.

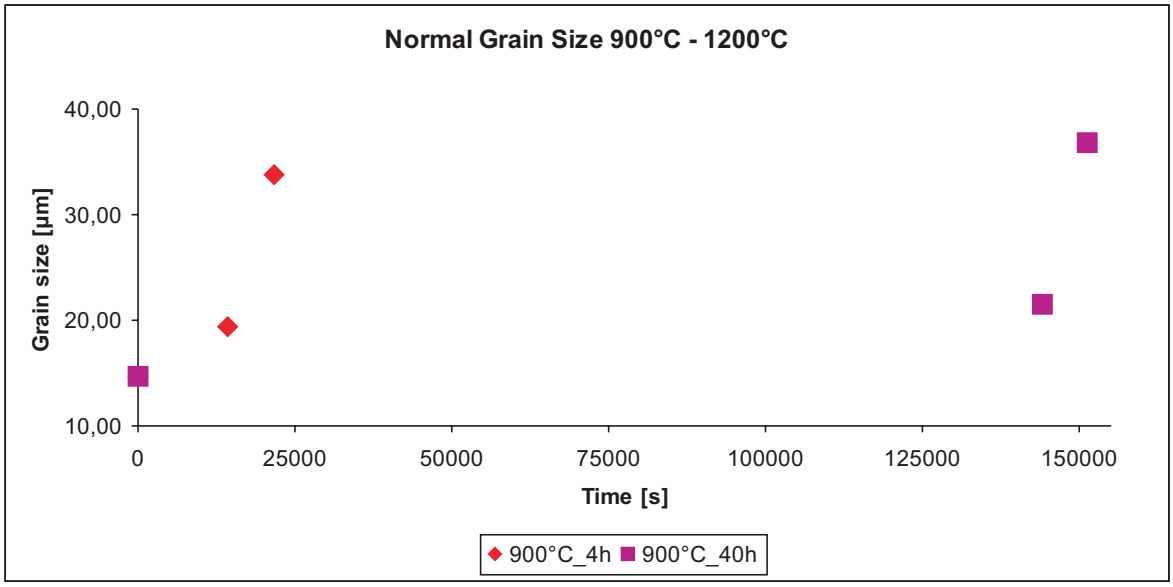

Figure 4.19: Normal grain growth vs. annealing time for two-step annealing process firstly at 900°C and afterwards at 1200°C

Time [s]	*900C 4h*	*900C 40h*
0	15 μm	15 μm
14400	19 μm	
21600	34 μm	
144000		22 μm
151200		37 μm

Table 4.18: Two-step annealing process firstly at 900°C and afterwards at 1200°C normal grain growth; (top to bottom): initial grain size, grain size after 900°C annealing and grain size after 2 hours at 1200°C heat treatment

Figure 4.20 illustrates the development of abnormal grain sizes vs. the annealing time for the two-step annealing process of preheating at 900°C and subsequently annealing at 1200°C. The grain sizes are listed in table 4.19.

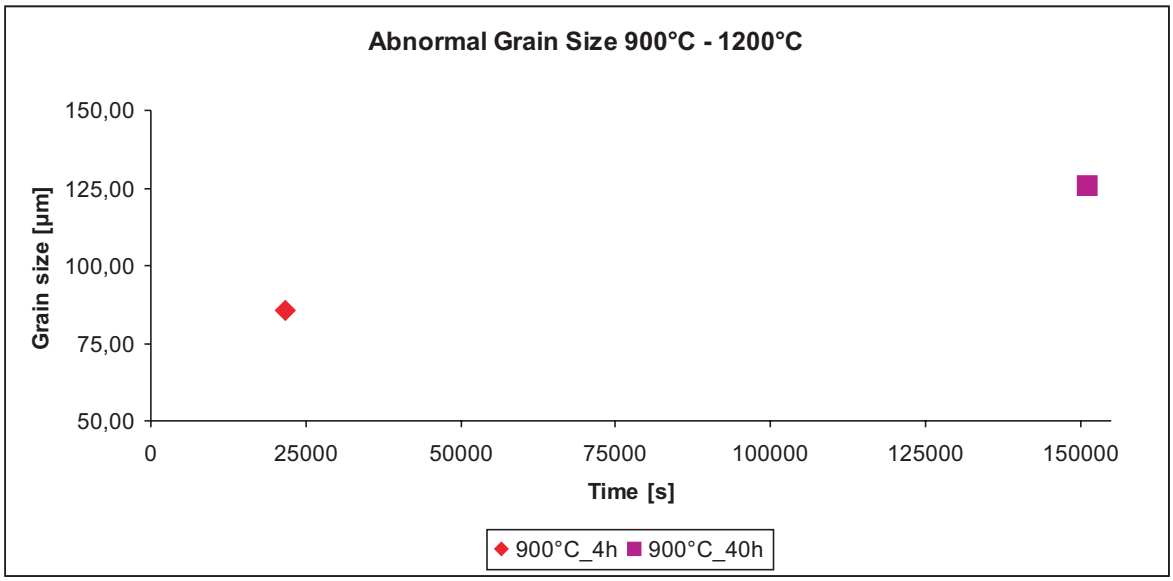

Figure 4.20: Abnormal grain growth vs. annealing time for a two-step annealing at firstly 900°C and secondly at 1200°C

Time [s]	*900C 4h*	*900C 40h*
21600	85 μm	
151200		126 μm

Table 4.19: Two step annealing process firstly at 900°C and secondly at 1200°C abnormal grain growth

The limiting grain sizes between normal and abnormal grain size (section 3.4.4) are shown in figure 4.21 and listed in table 4.20.

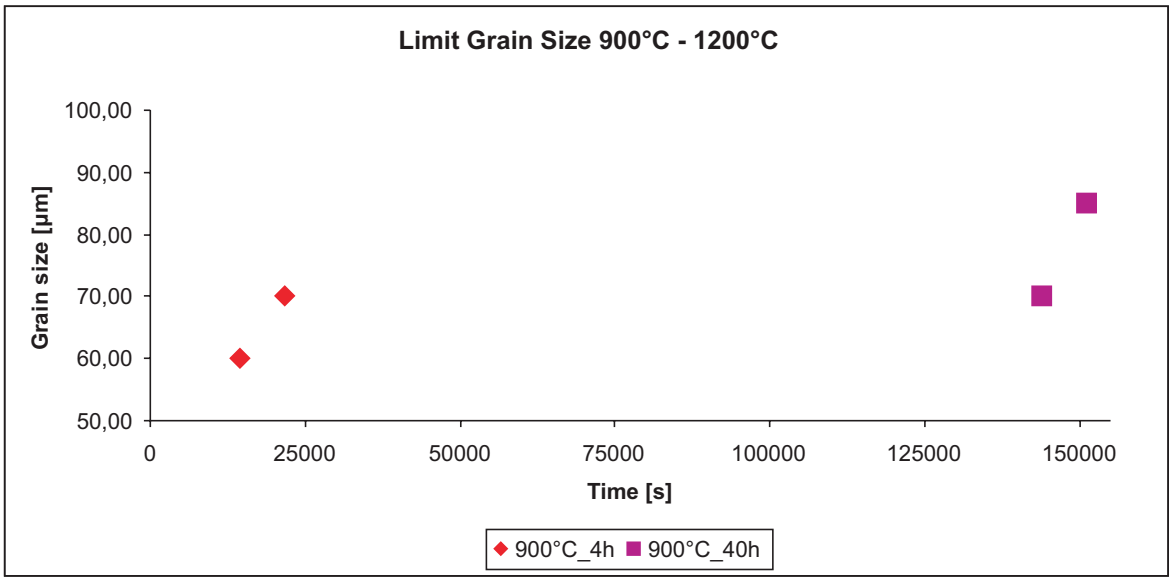

Figure 4.21: Defined grain size limiting between normal and abnormal grain growth vs. annealing time two step annealing 900°C and 1200°C

Time [s]	*900C 4h*	*900C 40h*
14400	60 μm	
21600	70 μm	
144000		70 μm
151200		85 μm

Table 4.20: Two-step annealing process firstly at 900°C and secondly at 1200°C limit grain size

In order to complete the results of the two-step annealing process, figure 4.22 and table 4.21 show the abnormal grain fractions.

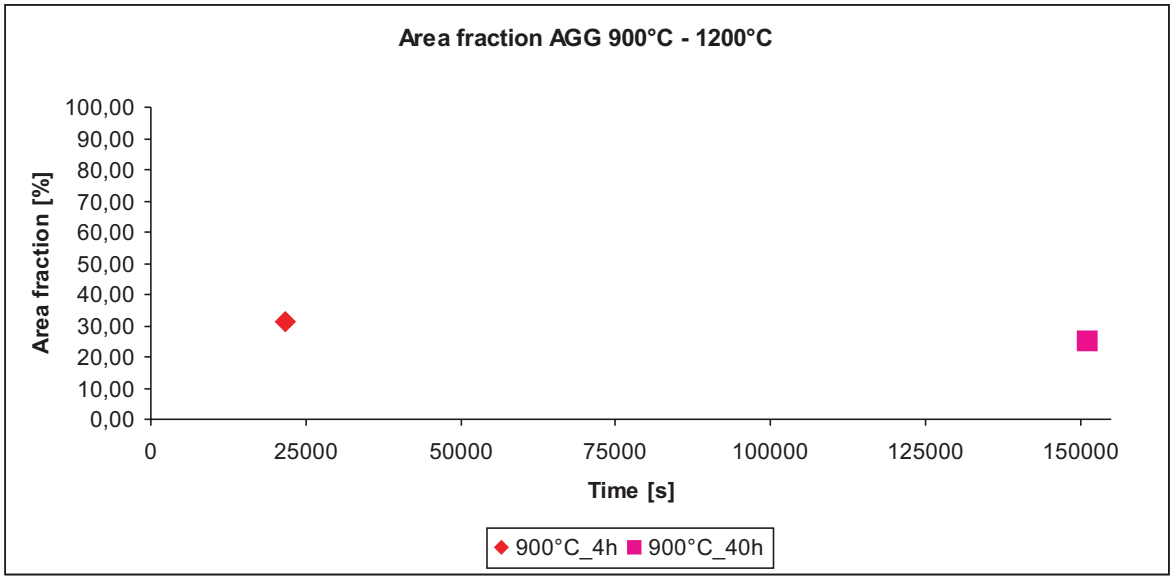

Figure 4.22: Area fraction for abnormal grain growth vs. annealing time

Time [s]	*900C 4h*	*900C 40h*
21600	32 %	
151200		26 %

Table 4.21: Two step annealing process firstly at 900°C and secondly 1200°C abnormal grain growth area fraction

4.5 The Regression Curves for Two-Step Annealing Processes

Two step annealed specimens show a more gentle slope of the grain growth rates because the initial grain sizes for the second treatment steps are higher than for the one step samples. Preheating for short times at high temperatures like 1200°C annihilates facetted grain boundaries and so the grains are not prevented from growing normally. This annihilation allows for the second heat treatment long annealing times until abnormal grains occur.

The diagrams (4.23 to 4.26) show the adapted regression curves after $d = [(A * exp^{\frac{-Q}{RT}})^m *$

$t + do^m]^{(\frac{1}{m})}$ for the two-step annealing series. The slope of the growth gradient for the two-step annealing processes are so gentle, that the received regression values are not representative and are therefore not illustrated. The initial grain size for the second treatment step and the temperature and time of the annealing process is the basis for the behavior of the grains during annealing.

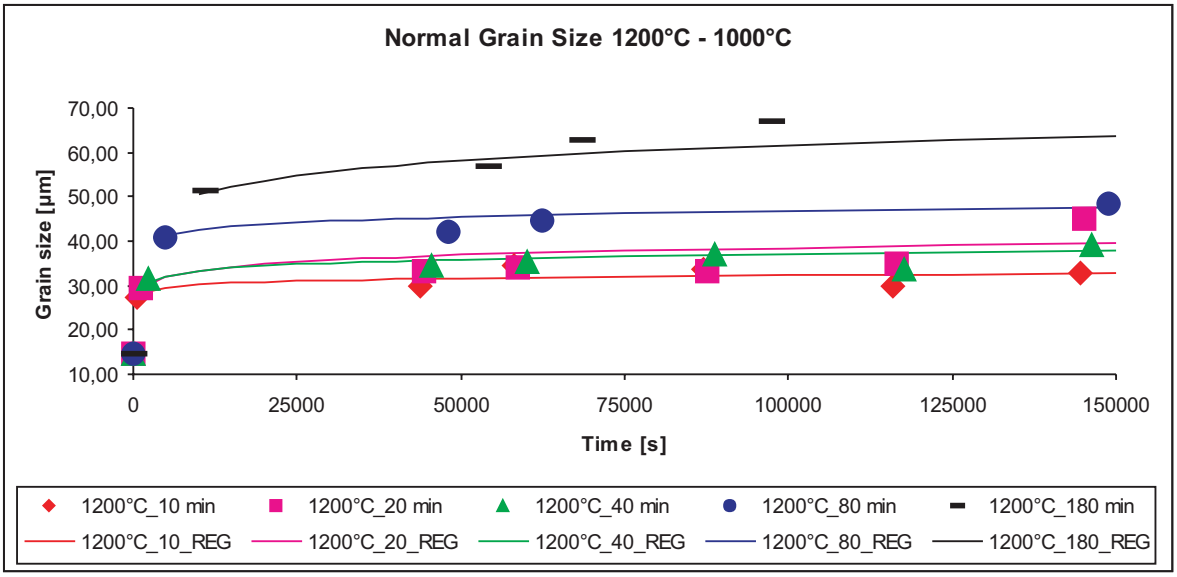

Figure 4.23: Line fit normal grain growth firstly at 1200°C and secondly at 1000°C

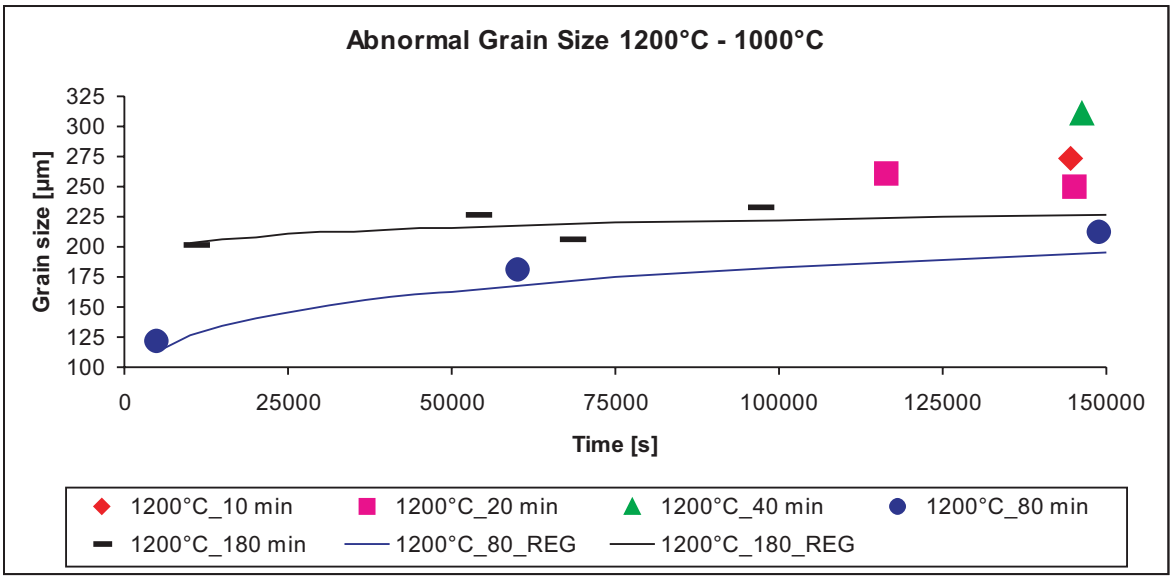

Figure 4.24: Line fit abnormal grain growth firstly at 1200°C and secondly at 1000°C

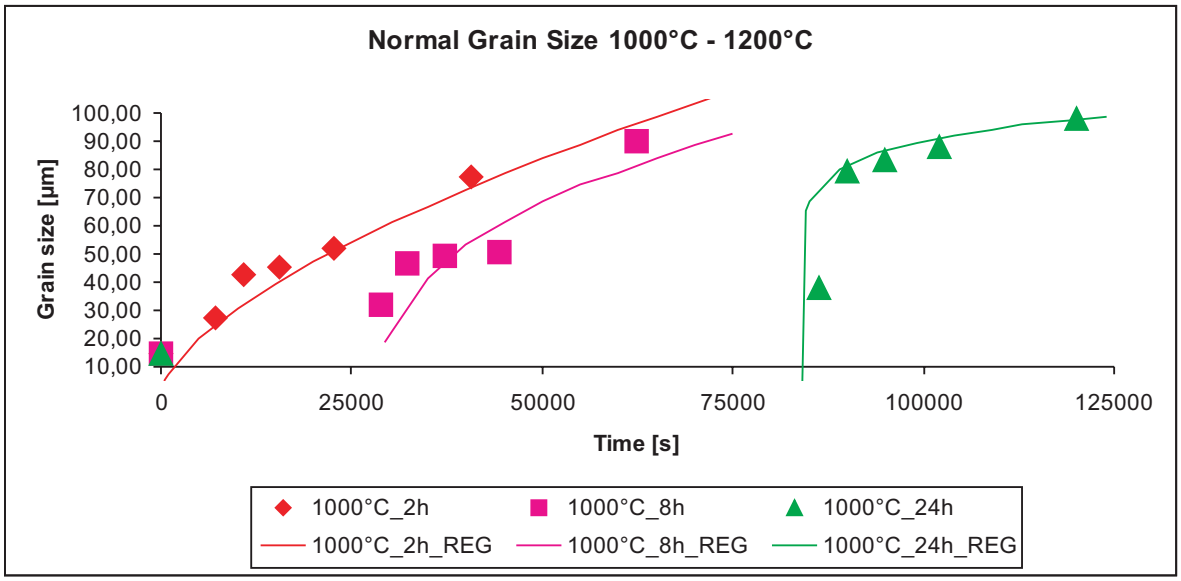

Figure 4.25: Line fit normal grain growth firstly at 1000°C and secondly at 1200°C

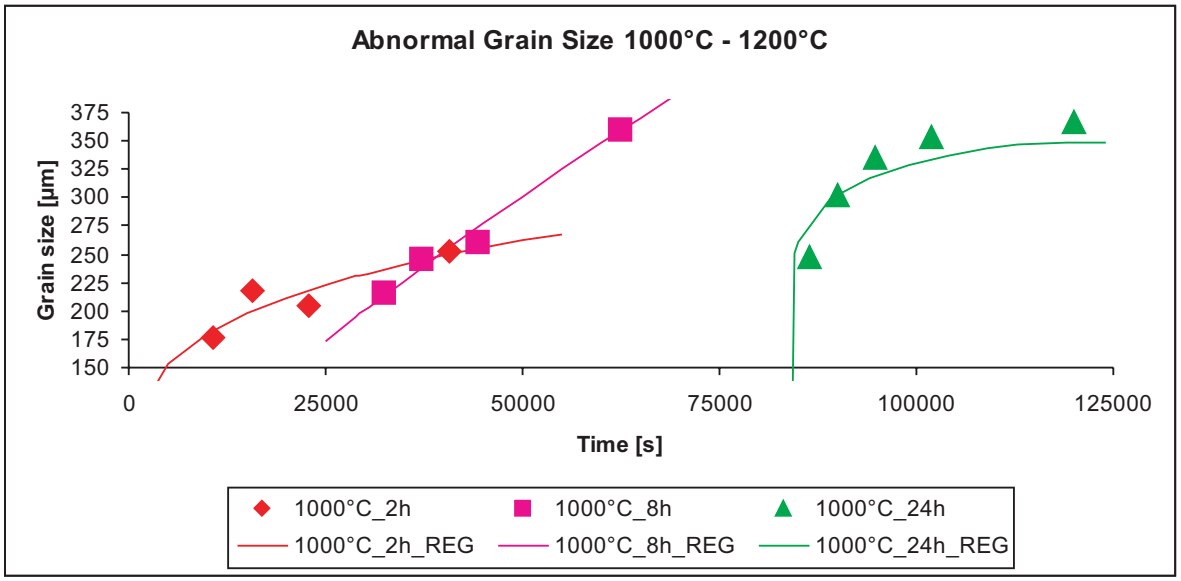

Figure 4.26: Line fit abnormal grain growth firstly at 1000°C and secondly at 1200°C

4.6 Comparison of the Grain Growth Rates for One- and Two-Step Annealing Process

To enable comparison of grain growth rates for both normal and abnormal grain growth during the annealing process the results are shown in figure 4.27 - 4.30.

The red line always indicates the one step annealing cycle. The main information presented in these diagrams is that the acclivity for the one step annealing specimens always shows a steeper gradient than for the two step annealed specimens.

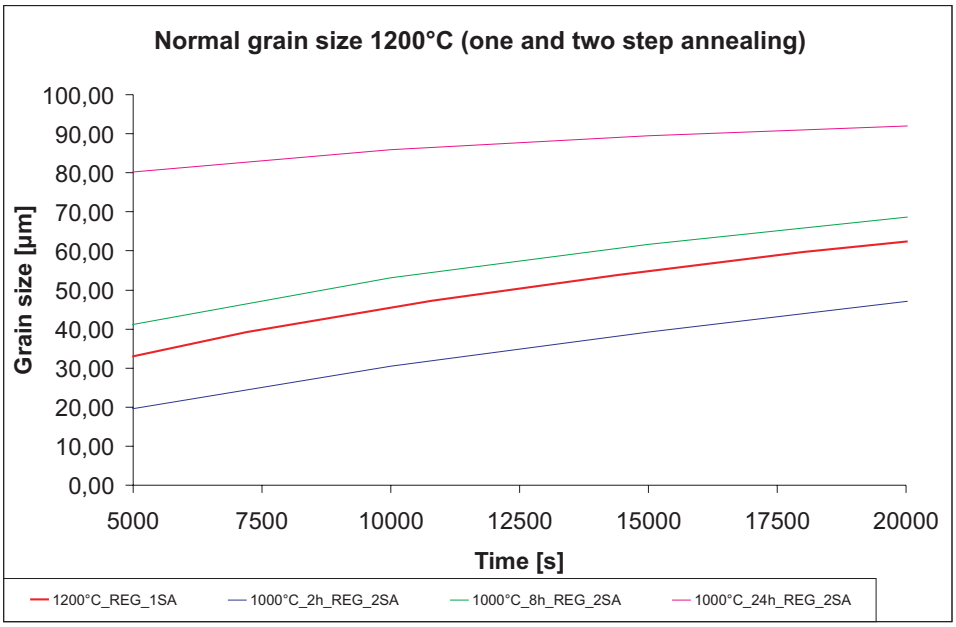

Figure 4.27: Annealing series at 1200°C normal grain growth one- and two-step annealing process

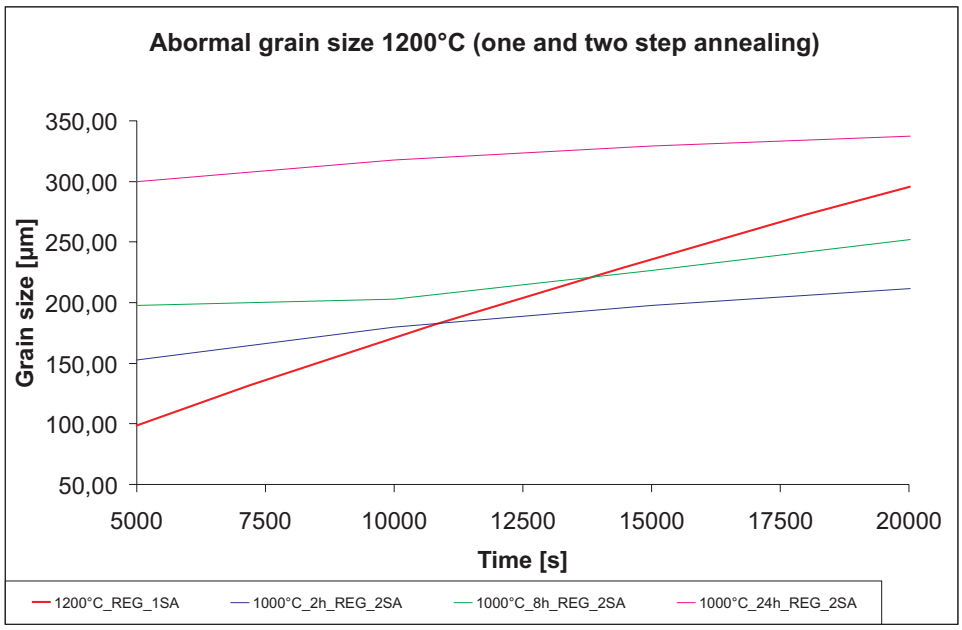

Figure 4.28: Annealing series at 1200°C abnormal grain growth one- and two- step annealing process

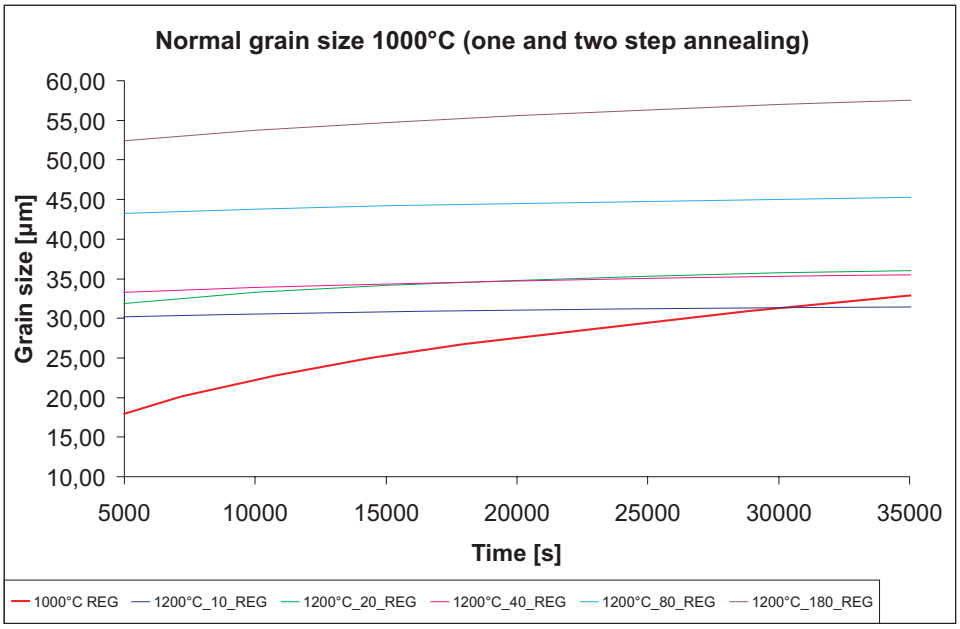

Figure 4.29: Annealing series at 1000°C normal grain growth one- and two-step annealing process

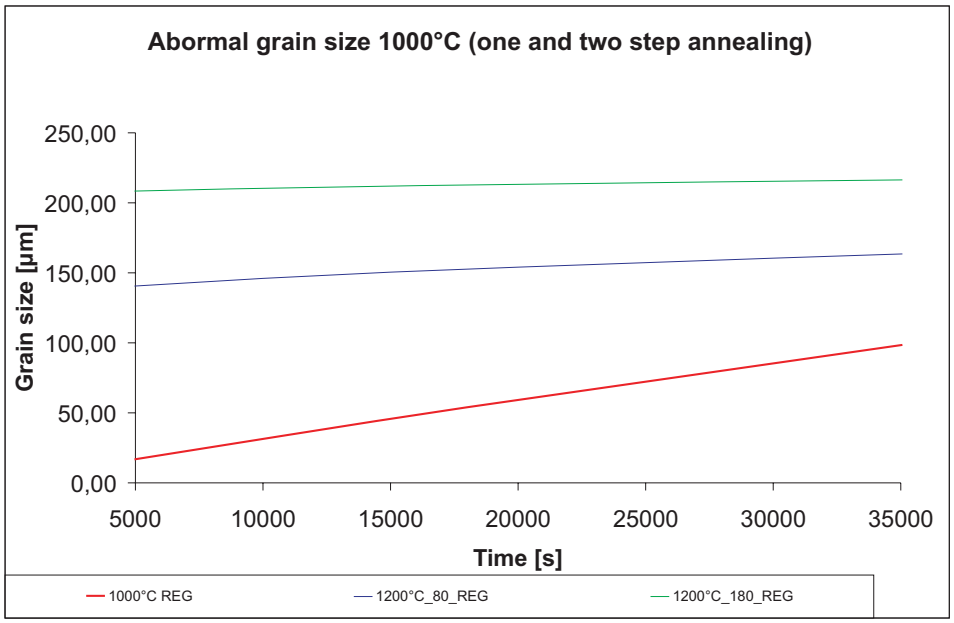

Figure 4.30: Annealing series at 1000°C abnormal grain growth one- and two -step annealing process

4.7 Process Latitude

The aim of this work was to find an annealing process latitude where abnormal grain growth is disabled. In figure 4.31 the micrographs of the 1000C specimens with annealing times of two, four, eight, 12, 16 and 24 hours are illustrated. Abnormal grain growth starts at an annealing time of eight hours at 1000C. The following figures (4.32 - 4.34) show the two step annealed specimens with 10 to 40 minutes at 1200C and 0 to 40 hours at 1000C.

Unlike the 1000C specimens the short preheating time of 10, 20 and 40 minutes at 1200C abnormal grain growth disabled up to 24 hours. The reason for this phenomena is that the grain boundaries are not disabled to move at temperatures of about 1200C. At the second annealing step of 1000C the grain growth is very slow, see figure 4.23, and so there are long annealing times possible till abnormal grain growth occurs.

Preheating at 1200C the initial grain sizes for the second annealing step at 1000C are after 10 minutes 27 μm, 20 minutes 30 μm and after 40 minutes 32 μm. After 24 hours in the furnace at 1000C the grain size only climbs to 34, 33 and 37 μm. For the one step annealing specimens at 1000C the initial grain size is 15 μm and in 24 hours climbs to

43μm. The big drawback of the one step annealing is, that in the 24 hours annealing time the fraction of abnormal grains as opposed to normal grains increases to 56 percent. However, in the two step annealing no abnormal grains were found. In the specimen with 10 and 40 minutes preheating at 1200C the abnormal grain growth was disabled at close to 32 hours.

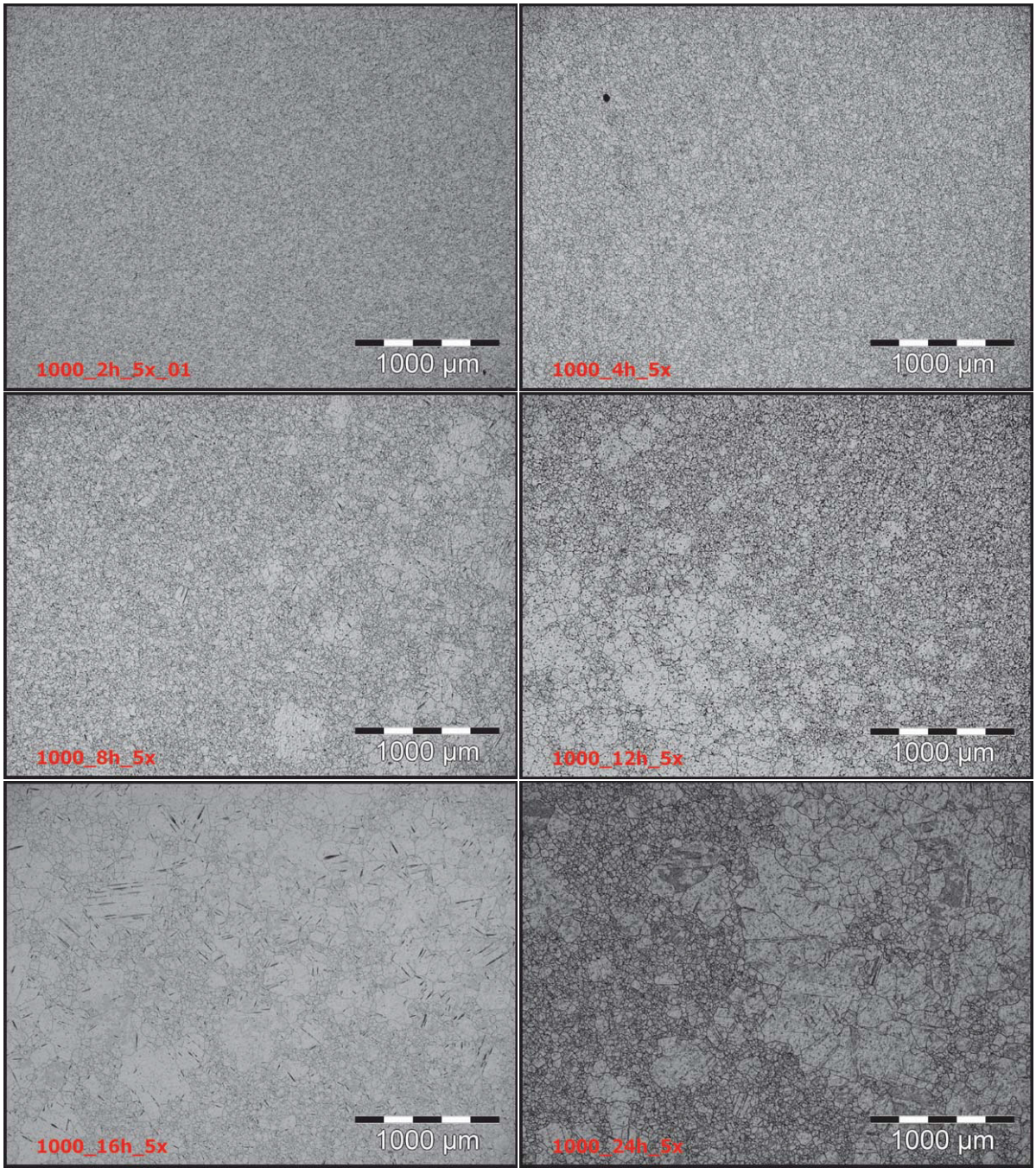

Figure 4.31: Annealing series 1000C from 2 to 24 hours

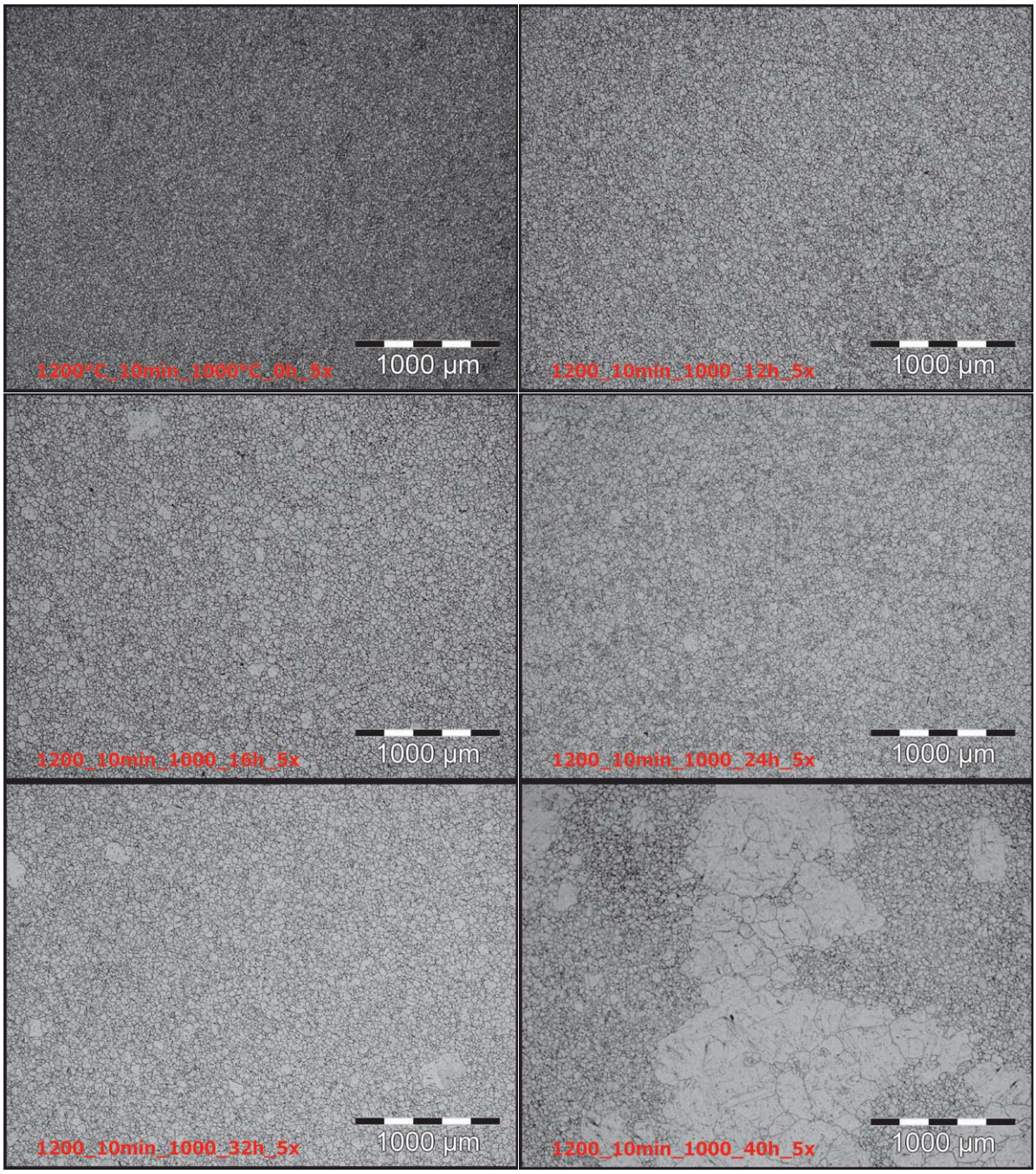

Figure 4.32: Annealing series 1200C for 10 minutes and 1000C from 0 to 40 hours

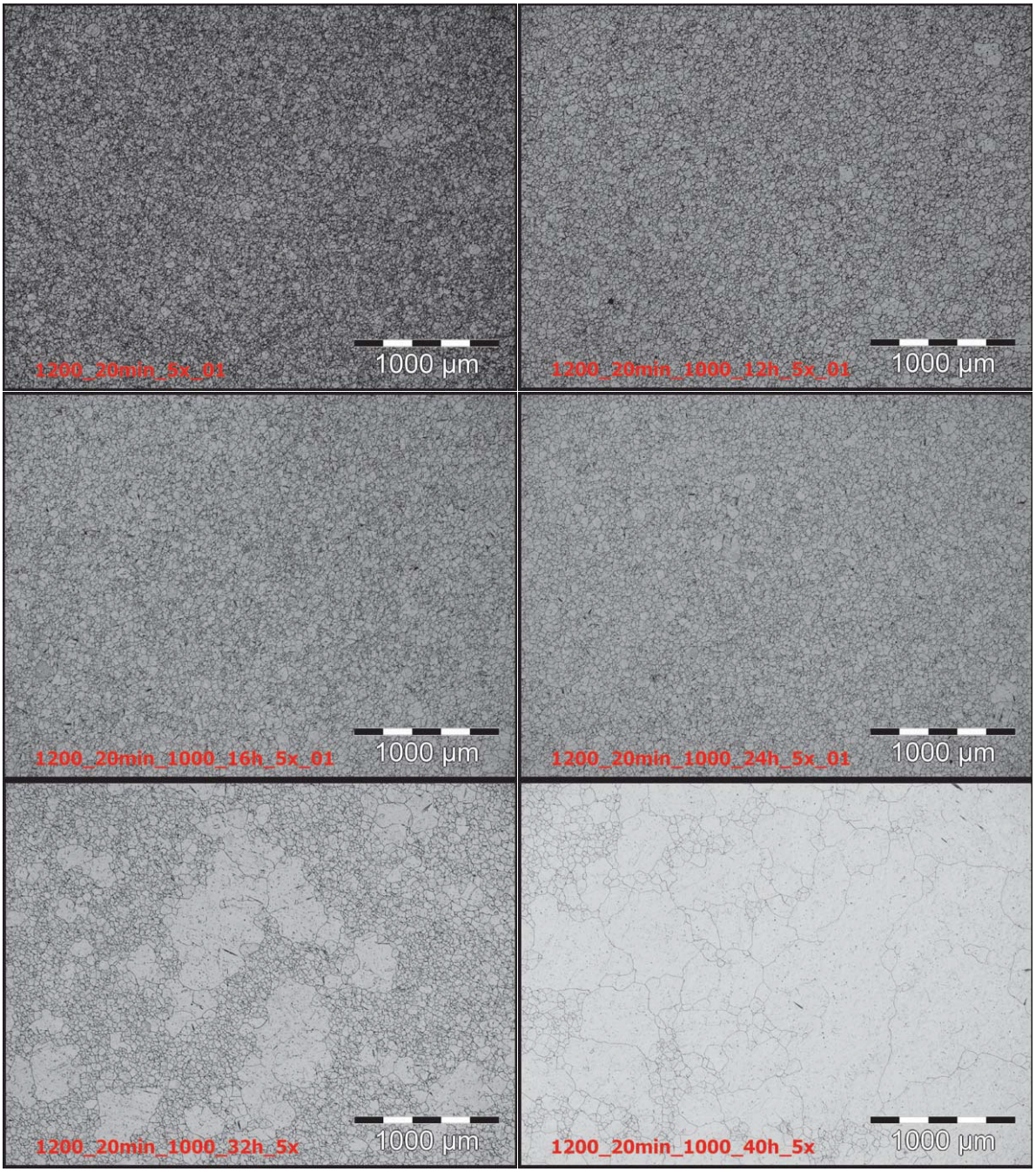

Figure 4.33: Annealing series 1200C for 20 minutes and 1000C from 0 to 40 hours

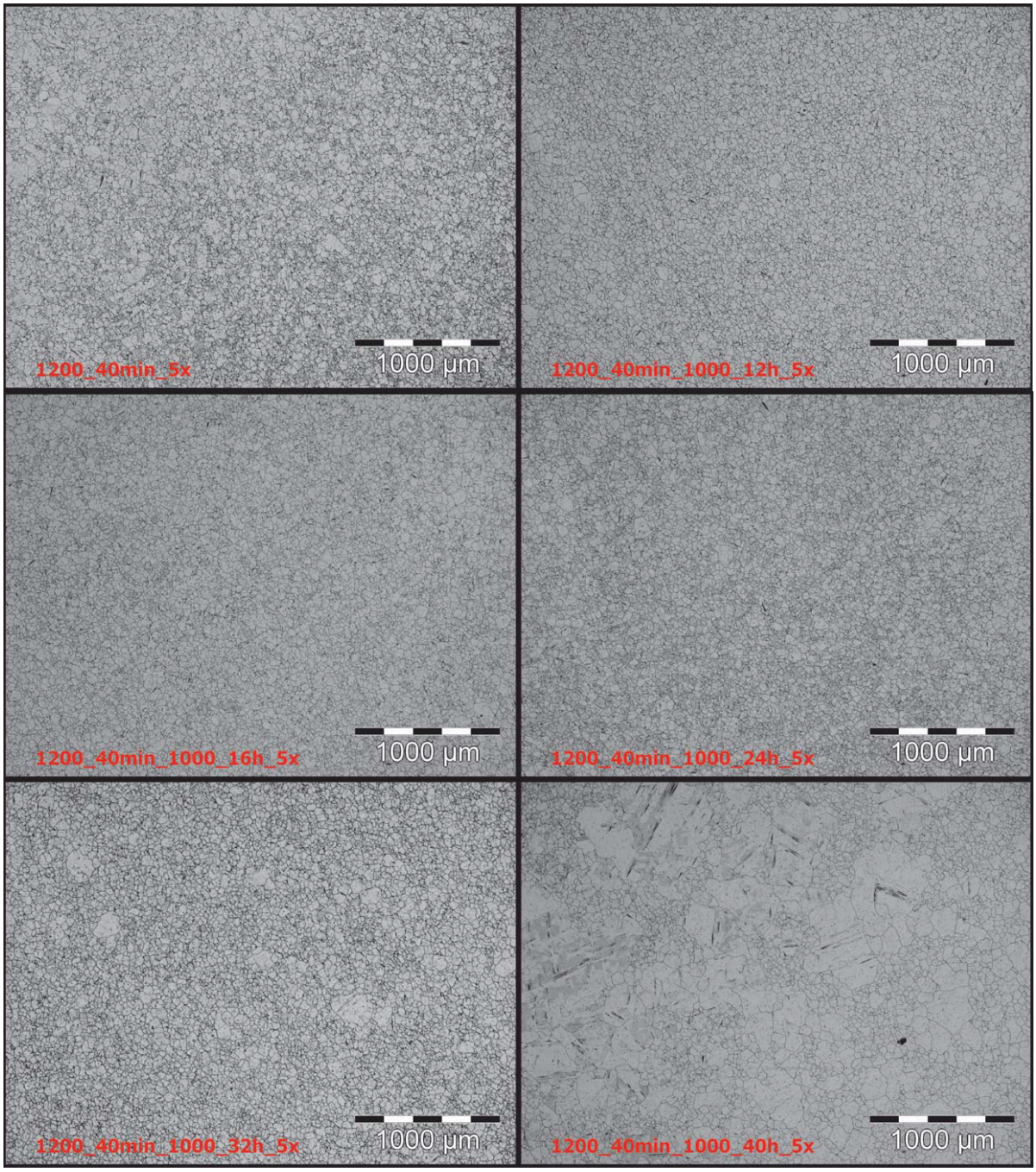

Figure 4.34: Annealing series 1200C for 40 minutes and 1000C from 0 to 40 hours

4.8 SEM Results

There is a correlation between the faceted grain boundaries and abnormal grain growth [21]. For example the 304L specimen annealed at 1000C for 24 hours leads to abnormal

grain growth and some grain boundaries are observed to be faceted with the so called hill-and-valley structures shown in figure 4.35 and 4.36. The micrograph of this specimen is illustrated in figure 4.31.

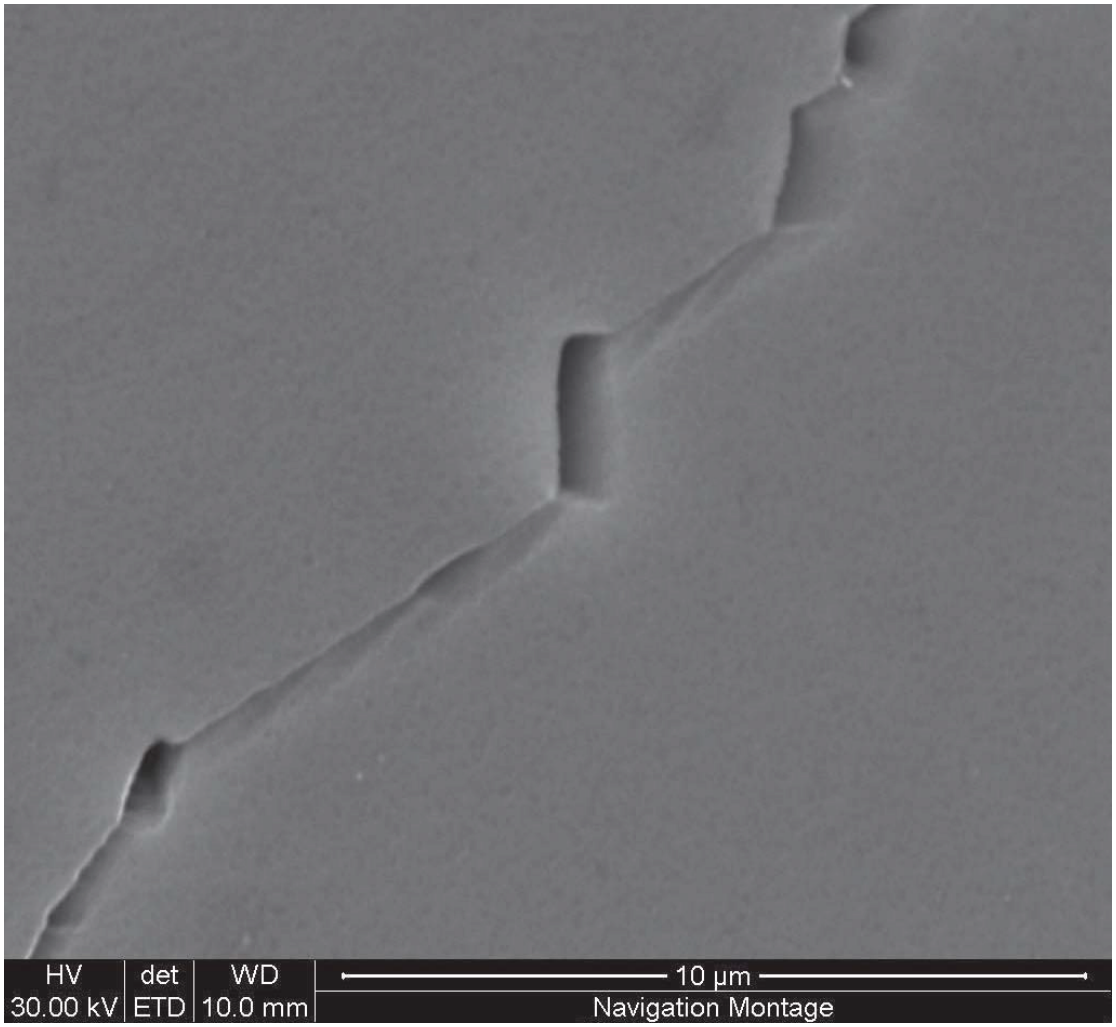

Figure 4.35: SEM image facetted grain boundary in 304L annealed at 1000C for 24 hours;

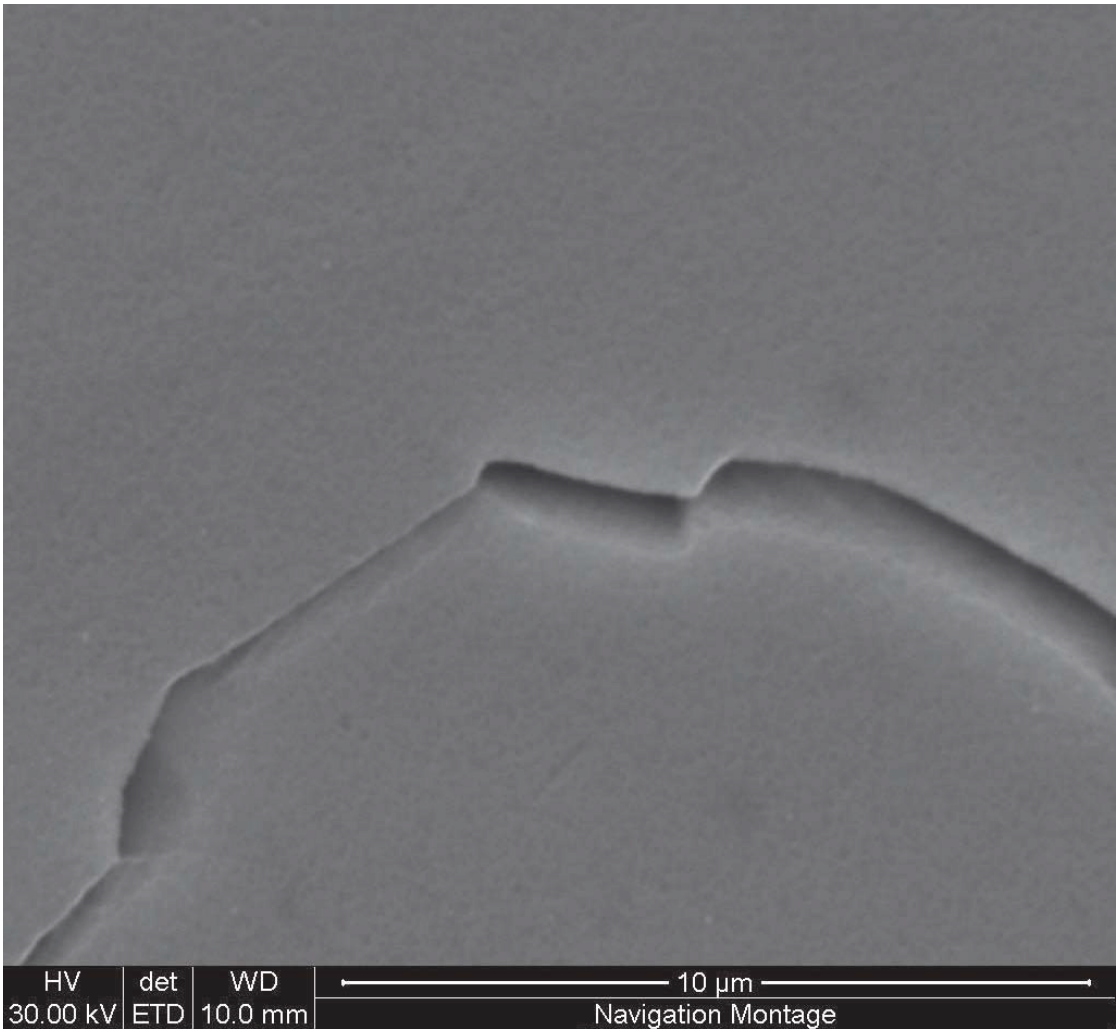

Figure 4.36: SEM image facetted grain boundary in 304L annealed at 1000C for 24 hours;

4.9 The Results of Cellular Automaton Modeling

Modeling and control of microstructure and grain size during annealing process are essential for tailoring the properties of materials. The developed cellular automaton model was validated for normal grain growth of austenitic stainless steel at different annealing temperatures and times.

4.9.1 The Effect of Grain Structure Resolution on Grain Growth Kinetics

As with all models, the CA approach has limitations, especially with regard to the length and time scale. The cellular automaton modeling strictly depends on the resolution of the microstructure, especially a model based on probabilistic transition rules (figure 4.37).

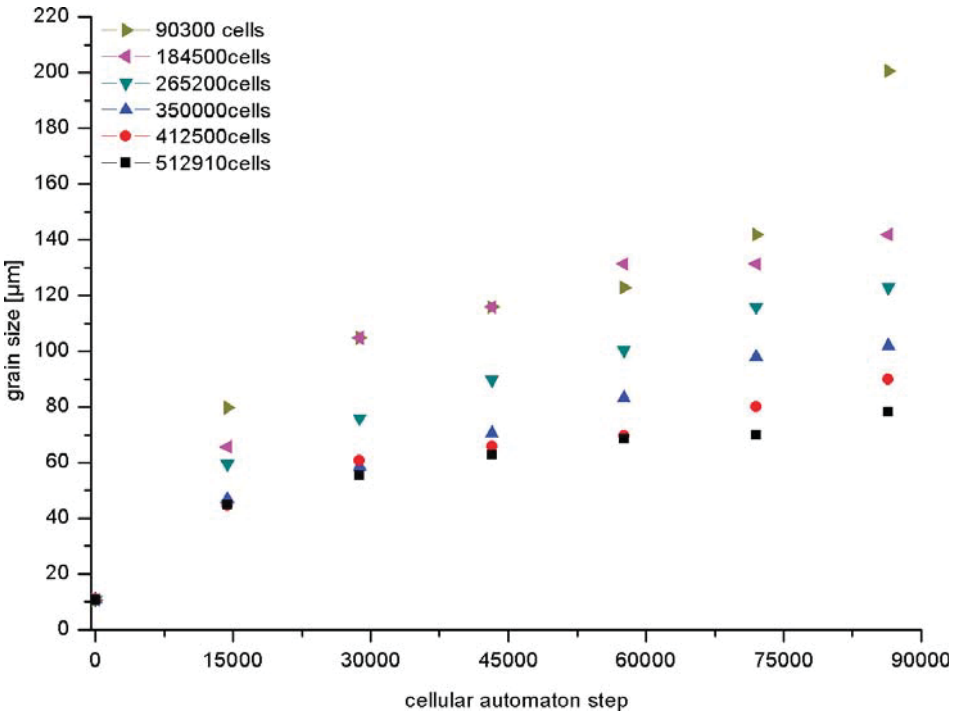

(a)

Figure 4.37: The resolution of microstructure influences the development of grain growth.

A high resolution of the microstructure leads to very long simulation times (table 4.22) but a low resolution of microstructure leads to an inaccurate simulation, especially for high transformation probabilities, i.e. high annealing temperatures.

Dimensions	Number of cells	$\Delta t_{simulation}$
$350x258$	90300	1
$500x369$	184500	4
$600x442$	265200	9
$700x500$	350000	20
$750x550$	412500	31
$834x615$	512910	48

Table 4.22: The influence of the resolution on the duration of the simulation

In order to simulate the development of annealing accurately, the dimension $834x615$ (= 512910 cells) was chosen to resolve the microstructure of further simulation steps. As a time scale, a cellular automaton step was defined to represent 0.5 s of annealing duration.

4.9.2 The Modeling Results for Normal Grain Growth

The grains in the starting microstructure were relatively uniform in size with an average value of about 10.6 μm, but there were clusters of fine grains in some regions, as shown in figure 4.38. The characteristics of grain growth depend strongly on the heat treatment temperature, shown by the modeling results in figures 4.39−4.45.

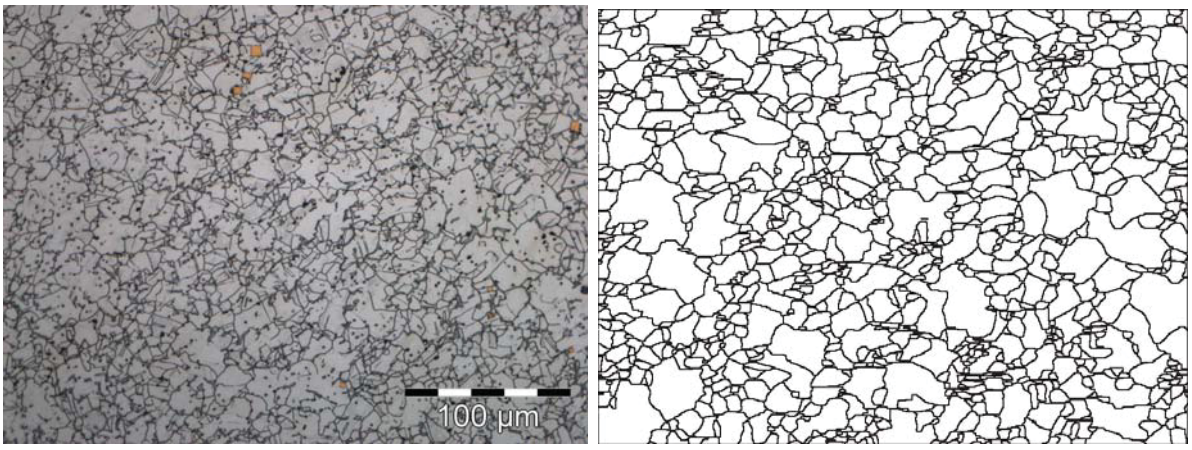

(a) optical microstructure (b) implemented microstructure

Figure 4.38: The implemented initial microstructure for the modeling of normal grain growth

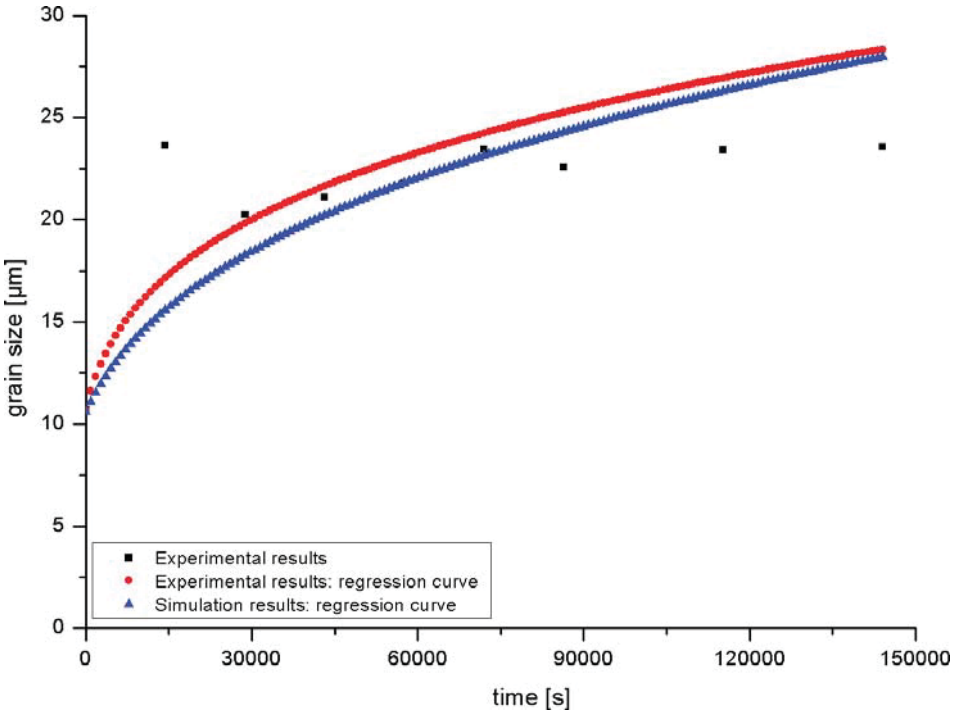

Figure 4.39: Comparison of experimental and simulated results for annealing at 900°C

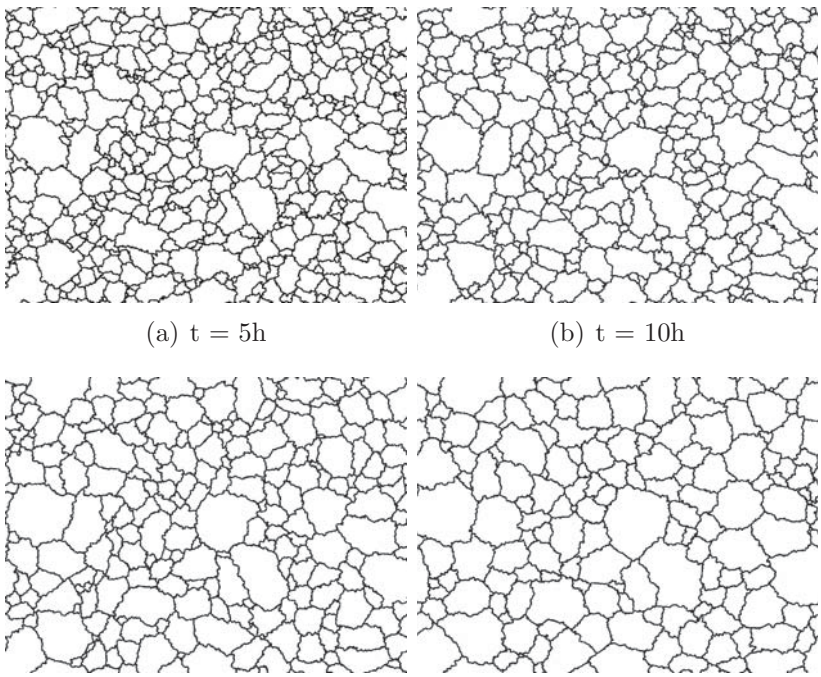

(a) t = 5h (b) t = 10h

(c) t = 20h (d) t = 40h

Figure 4.40: Simulated microstructure for the annealing process at 900°C

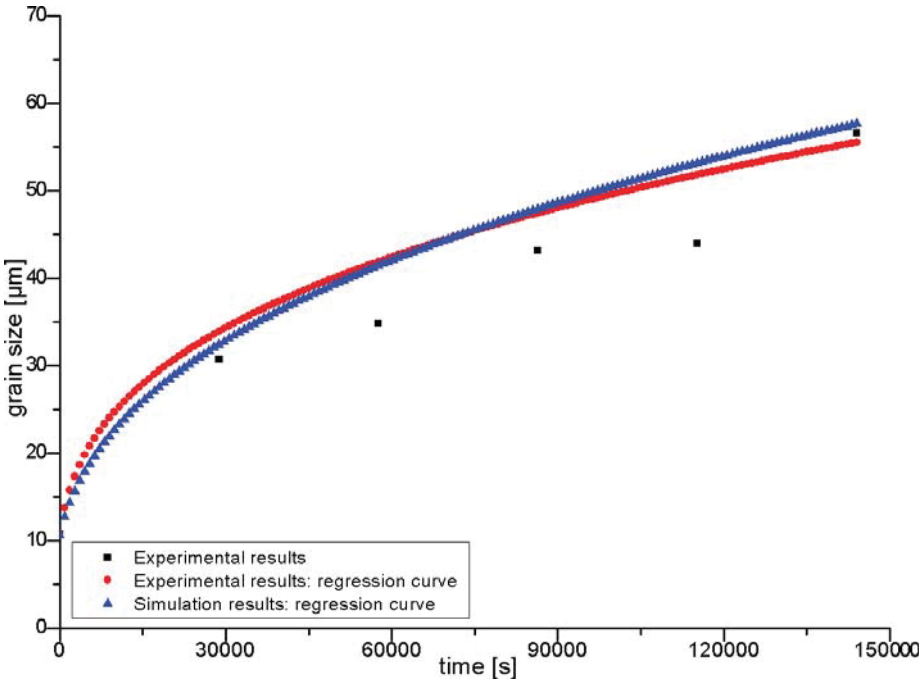

Figure 4.41: Comparison of experimental and simulated results for annealing at $1000°C$

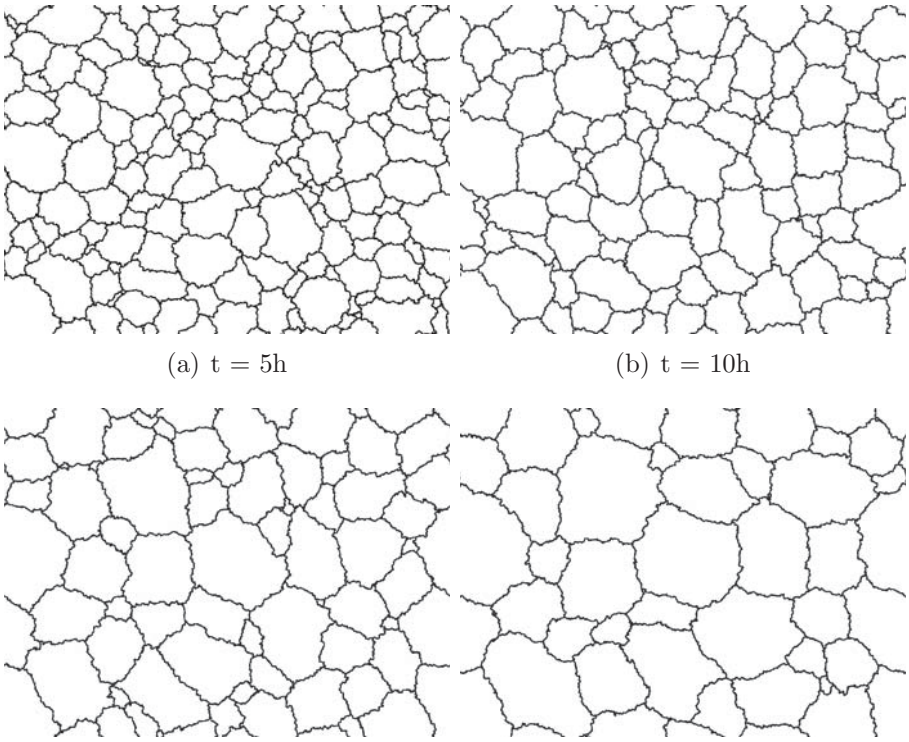

(a) t = 5h (b) t = 10h

(c) t = 20h (d) t = 40h

Figure 4.42: Simulated microstructure for the annealing process at $1000°C$

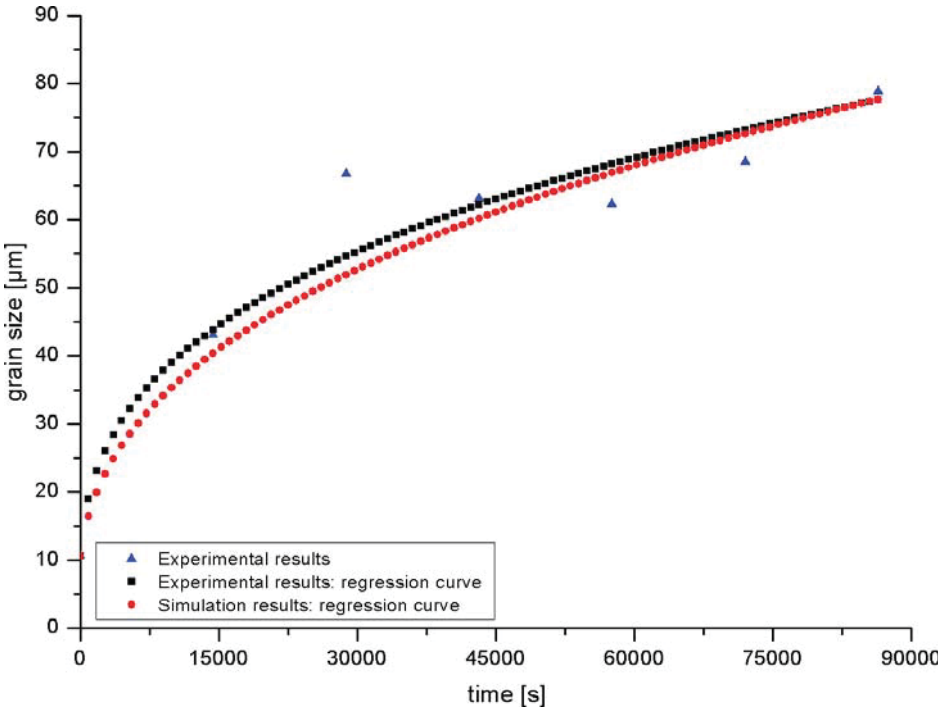

Figure 4.43: Comparison of experimental and simulated results for annealing at 1100°C

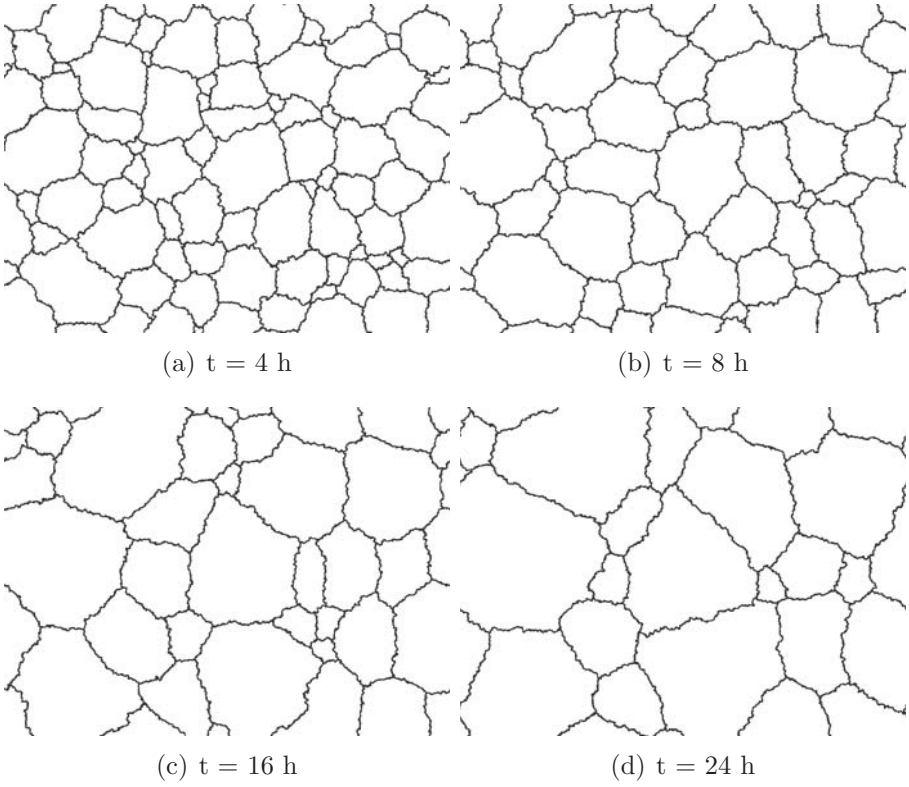

(a) t = 4 h (b) t = 8 h

(c) t = 16 h (d) t = 24 h

Figure 4.44: Simulated microstructure for the annealing process at 1100°C

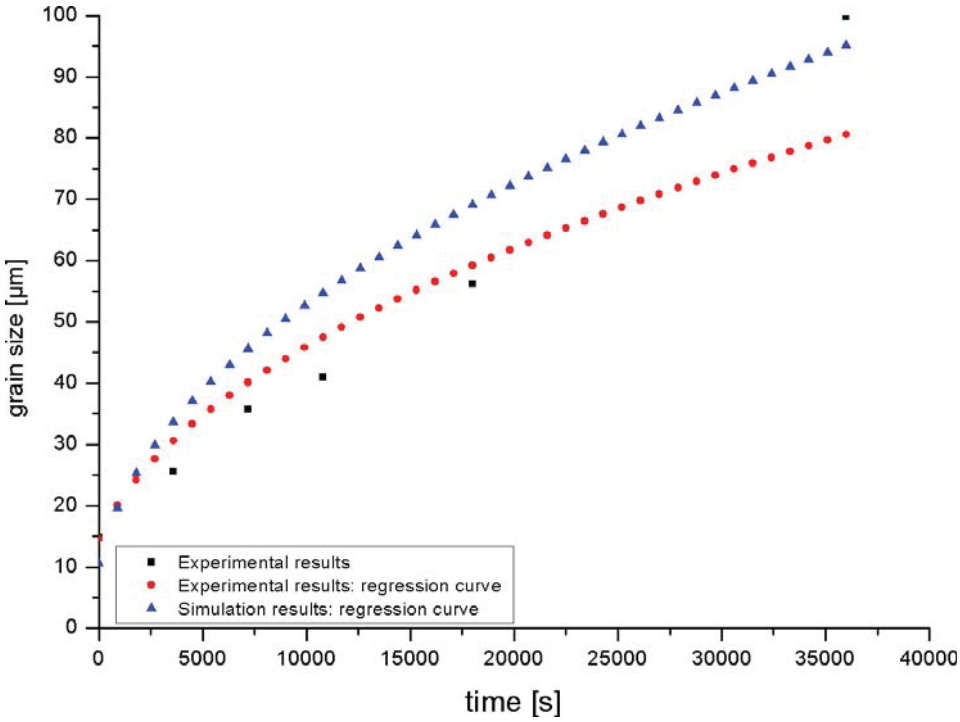

Figure 4.45: Comparison of experimental and simulated results for annealing at 1200°C

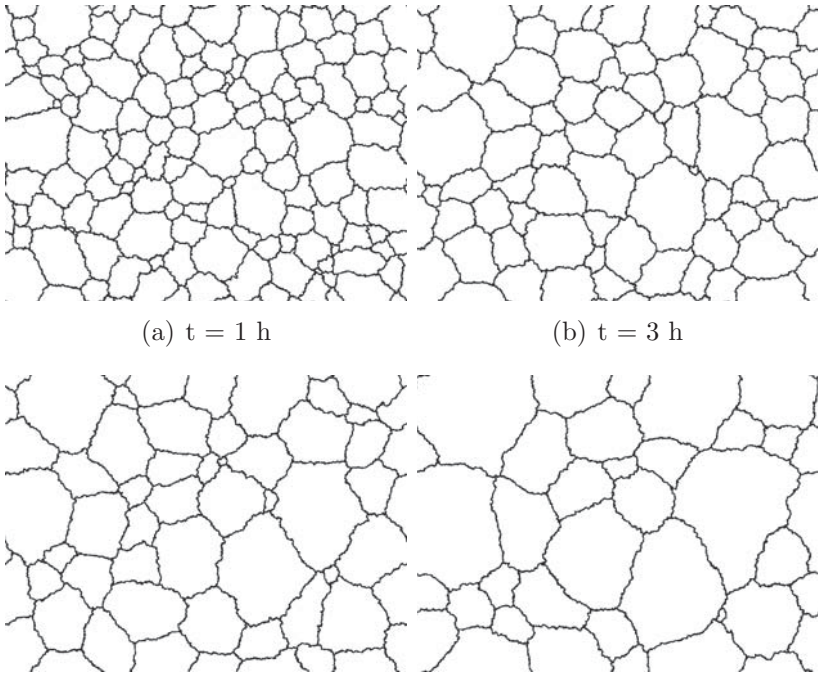

(a) t = 1 h (b) t = 3 h

(c) t = 5 h (d) t = 10 h

Figure 4.46: Simulated microstructure for the annealing process at 2000°C

The grain coarsening behavior as a function of temperature ($900°C$, $1000°C$, $1100°C$, $1200°C$) and the corresponding microstructure at different annealing times prove the value of useing modeling parameters.

Temperature is the most important parameter affecting the behavior of the grain coarsening process. The grain coarsening is a diffusion process, and in order for an atom to jump into a hole from lattice position, it must overcome the net attractive force of its surrounding neighbors. Thermal vibrations of the crystal lattice provide the atoms with enough energy to overcome this barrier. The basic process during the migration of grain boundary is the transfer of atoms to and from the grains which are adjacent to the grain boundary. The mechanism of grain boundary migration depends on several parameters including the boundary structure, temperature and point defects such as solutes and vacancies. The boundary structure and point defects are linked to the material's internal conditions while the temperature is related to the external condition. In general, the higher the temperature, the higher the frequency that the boundary energy barrier must overcome, and thus the higher the boundary velocity.

The chance that a given atom possesses an energy greater than Q_B is defined to be proportional to the function $e^{-\frac{Q_B}{RT}}$ or

$$P = A * e^{-\frac{Q_B}{RT}} \tag{4.1}$$

where P is the probability for an atom to jump, A is a constant, R the universal gas constant, Q_B is the activation energy for the movement of atoms across the boundary and T is the absolute temperature.The constant A depends on a number of factors, such as atom lattice structure, point defects and the rate of atom vibrations (figure 4.47).

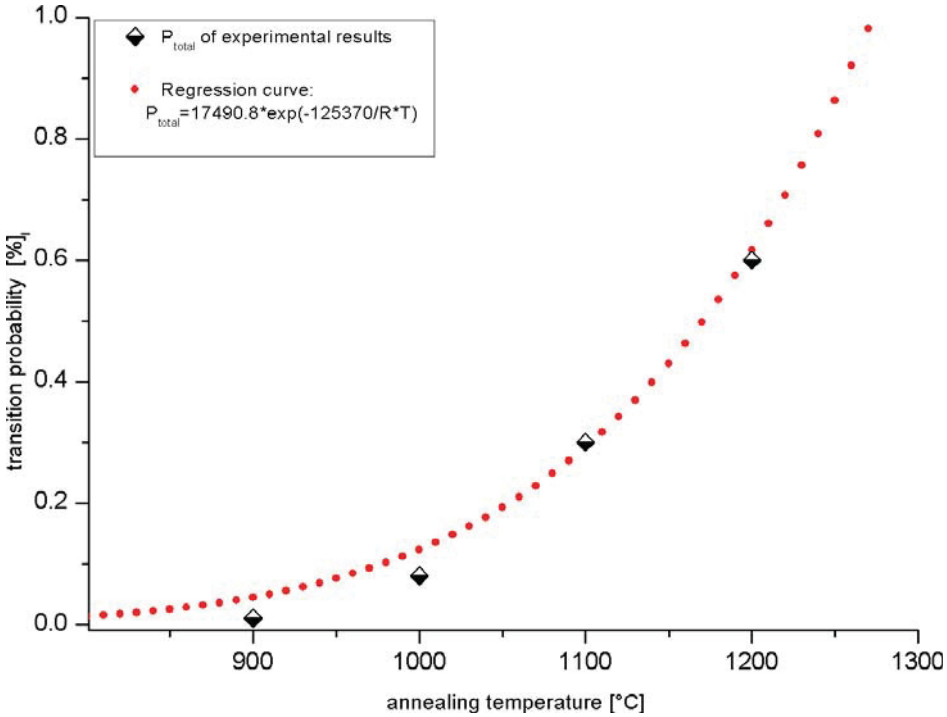

Figure 4.47: The transition probability vs. annealing temperature

5 Conclusion

The dependence of abnormal grain growth, also termed secondary recrystallization, on annealing temperature in the range between $900°C$ and $1200°C$ has been observed in austenitic stainlees steel 304L.

The one step annealing samples with an initial grain size of 15 μm show a higher grain growth rate than the two step annealed samples, thus the initial grain size and the temperature influence the grain growth kinetics. Abnormal grain growth starts at 1200C after 80 minutes, at 1100C after 8 hours, at 1000C after 12 hours and at 900C never, because the grain boundary pinning influence by the grain boundary carbide precipitations is too large and the temperature is too low.

The values of the regression for the experiment determined normal grain sizes of the one step annealing specimens after $d = [(A * exp^{\frac{-Q}{RT}})^m * t + do^m]^{(\frac{1}{m})}$ show that the grain growth exponent is addicted to the temperature and rises from 0.31 at 1000C to 0.43 at 1200C and the activation energy is 62314.6 J/Kmol. At abnormal grain growth n rises from 0.75 at 1000C to 0.89 at 1200C and the activation energy is 33682.7 J/Kmol. This decline of Q allows abnormal grains to grow faster.

Two step annealing specimens show a more gentle slope of the grain growth rate because the initial grain size for the second treatment step is higher than for the one step samples. Preheating for short times (10 to 40 minutes) at high temperatures like 1200C annihilates faceted grain boundaries. This annihilation allows for the second heat treatment long annealing times at 1000C up to 24 (32) hours.

A two dimensional Cellular Automata Model has been developed to describe the normal grain growth. The model reflects the fact that grain coarsening kinetics gradually increase with transition probability P. It is shown that grain coarsening kinetics increase with temperature, which is close to the experimental observation. This result paves the way for modelling both normal and abnormal grain coarsening quantitatively.

Research should be done on the application of the CA method to predict the microstructure evolution under complex conditions, i.e. abnormal grain growth. A 3D CA model could possibly provide more accurate information about grain size evolution.

List of Figures

List of Tables

Bibliography

[1] G. Gottstein: *Physikalische Grundlagen der Materialkunde*, vol. 2, Springer-Verlag, 2001.

[2] Wikipedia: *http://en.wikipedia.org* .

[3] P. Marschall: "Austenitic stainless steels Microstructure and mechanical properties", *Elsevier Applied Science Publisher Ltd* **431**, 1984.

[4] S. P. Products: *http://www.sppusa.com* .

[5] S. Jaiswal, D. Farrugia, Z. Husain, P. Ingham, J. Wilkinson and P. Morris: "Modelling of microstructure in rod rolling of alloy and stainless steels", *Final Report - European Commission* 1996.

[6] D. Lober: *http://www.metallograf.de* .

[7] M. E. Wahabi, J. Cabrera and J. Prado: "Hot working of two AISI 304 steels - a comparative study", *Materials Science and Engineering* **A 343**:116–125, 2003.

[8] H. Hong, B. Rho and S. Nam: "Correlation of the $M_{23}C_6$ precipitation morphology with grain boundary characteristics in austenitic stainless steel", *Materials Science and Engineering* **A 318**:285–295, 2001.

[9] H. Atkinson: "Theories of normal grain growth in pure single phase systems", *Acta metallurgica* **36**(3):469–491, 1988.

[10] R. Bürgel: *Handbuch Hochtemperatur-Werkstofftechnik: Grundlagen, Werkstoffbeanspruchungen, Hochtemperaturlegierungen-und beschichtungen*, vol. 3, Vieweg+Teubner, Dez. 2006.

[11] *ASM Handbook Volume 9 - Metallography and Microstructures*, ISBN 0-87170-706-3, 2004.

[12] G. Grest, D. Srolovitz and M. Anderson: "Computer simulation of grain growth-IV. Anisotropic grain boundary energy", *Acta metall.* **33**(5):509–520, 1985.

[13] D. QUIDORT and Y. J. M. BRECHET: "A Model of Isothermal and Non Isothermal Transformation Kinetics of Bainite in 0.5International" **42**:1010–1017, 2002.

[14] J. L. Walter and C. G. Dunn: "Impurity Atoms and Energy Relationship of Surfaces", *Acta metall.* **8**:497–503, 1960.

[15] R. Cahn: "Pysical Metallurgy, sec. rev. ed.", *American Elsevier Publishing Company* pp. 1149, 1181, 1186–1187, 1970.

[16] S. Lee, J. Choi and D. Y. Yoon: "The dependence of abnormal grain growth on initial grain size in 316 L stainless steel", *Zeitschrift für Metallkunde* **92**(7):655–662, 2001.

[17] H. Gleiter: "The Mechanism of Grain Boundary Migration", *Acta metall.* **17**:565–573, 1969.

[18] S. Lee, N. Hwang, D. Yoon and M. Henry: "Grain boundary faceting and abnormal grain growth in nickel", *Metallurgical and Materials Transactions A* **31A**(3):985–994, 2000.

[19] J. Koo and D. Yoon: "The Dependence of Normal and Abnormal Grain Growth in Silver on Annealing Temperature and Atmosphere", *Metallurgical and Metarials Transactions A* **32A**:469–475, 2001.

[20] J. Koo and D. Yoon: "Abnormal grain growth in bulk Cu-The dependence on initial grain size and annealing temperature", *Metallurgical and Metarials Transactions A* **32A**(8):1911–1926, 2001.

[21] J. Choi and D. Yoon: "The temperature dependence of abnormal grain growth and grain boundary faceting in 316 L stainless steel", *ISIJ International* **41**(5):478–483, 2001.

[22] H. Gleiter: "Theory of Grain Boundary Migration Rate", *Acta metall.* **17**:853–862, 1969.

[23] M. Candic: *PHD THESIS CANDIC*, vol. 1, CDL MMS, 2009 - at work.

[24] H. Schumann and H. Oettel: *Metallographie*, vol. 14, Wiley-VCH Verlag, 2005.

[25] Struers: *http://www.struers.com* .

[26] Struers: *Aplication Guide for Hot Mounting* .

[27] P. Technologies: *http://www.metallographic.com* .

[28] Olympus: *http://www.olympusmicroimaging.com* .

[29] R. Djaic and J. Jonas: "Static recrystallization of austenite between intervals of hot working", *Journal of the Iron and Steel Institute* pp. 256–261, 1972.

[30] H. Hu and B. Rath: "On the time exponent in isothermal grain growth", *Metallurgical Transactions* **01**:3181–3184, 1970.

6 Appendices

6.1 Appendix One Step Annealing

6.1.1 One Step Annealing Micrographs

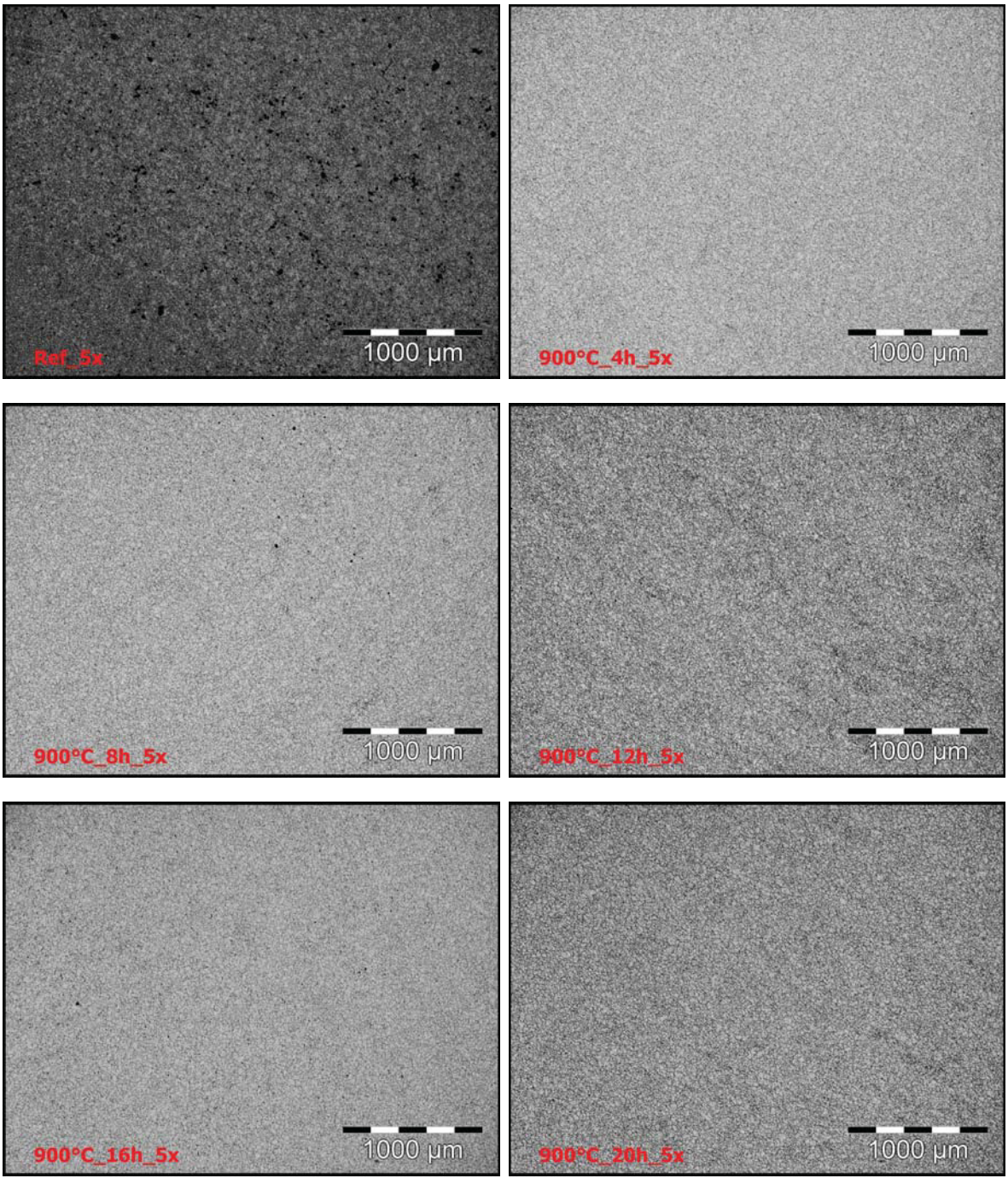

Figure 6.1: Micrographs one step annealing Part I

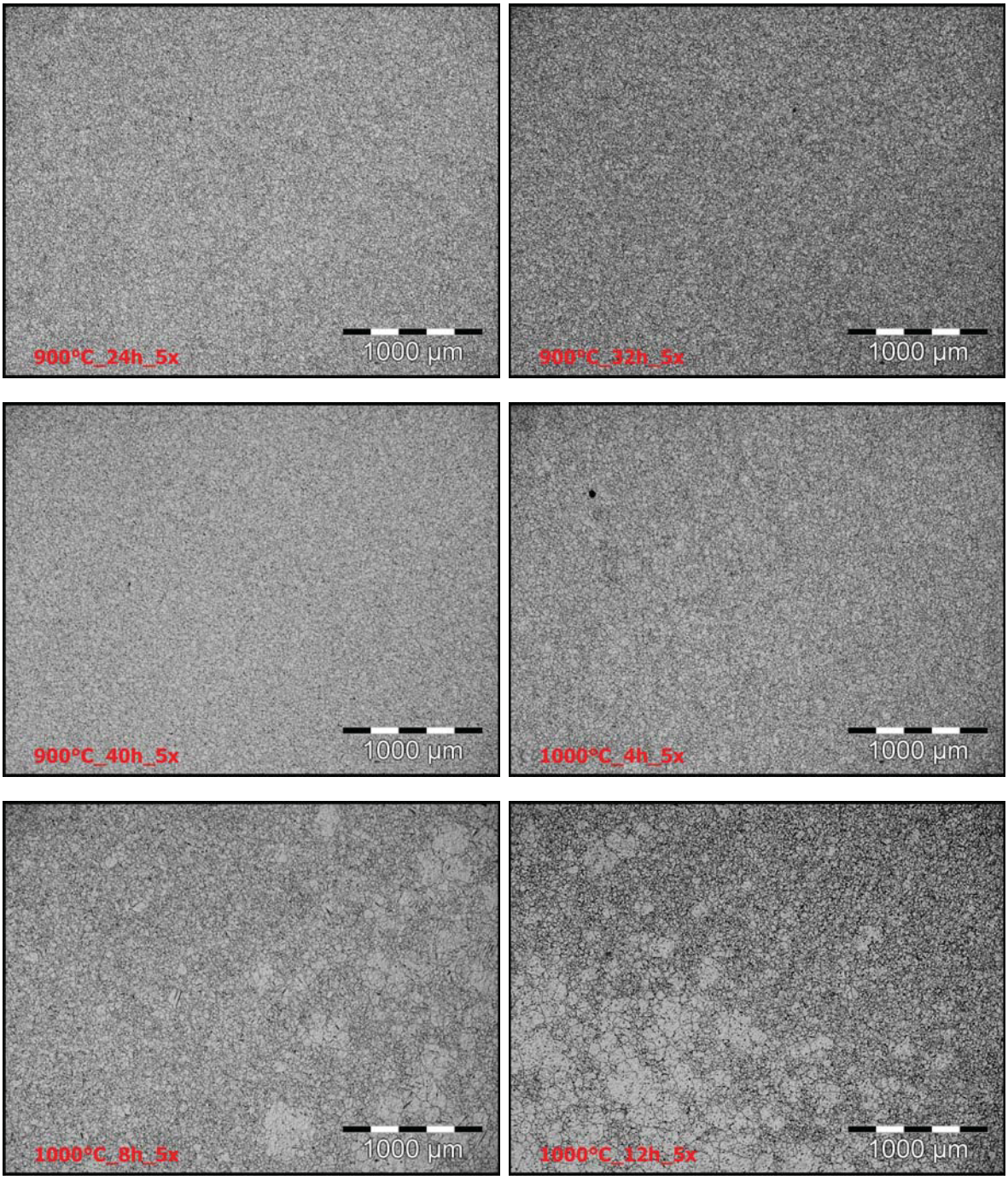

Figure 6.2: Micrographs one step annealing Part II

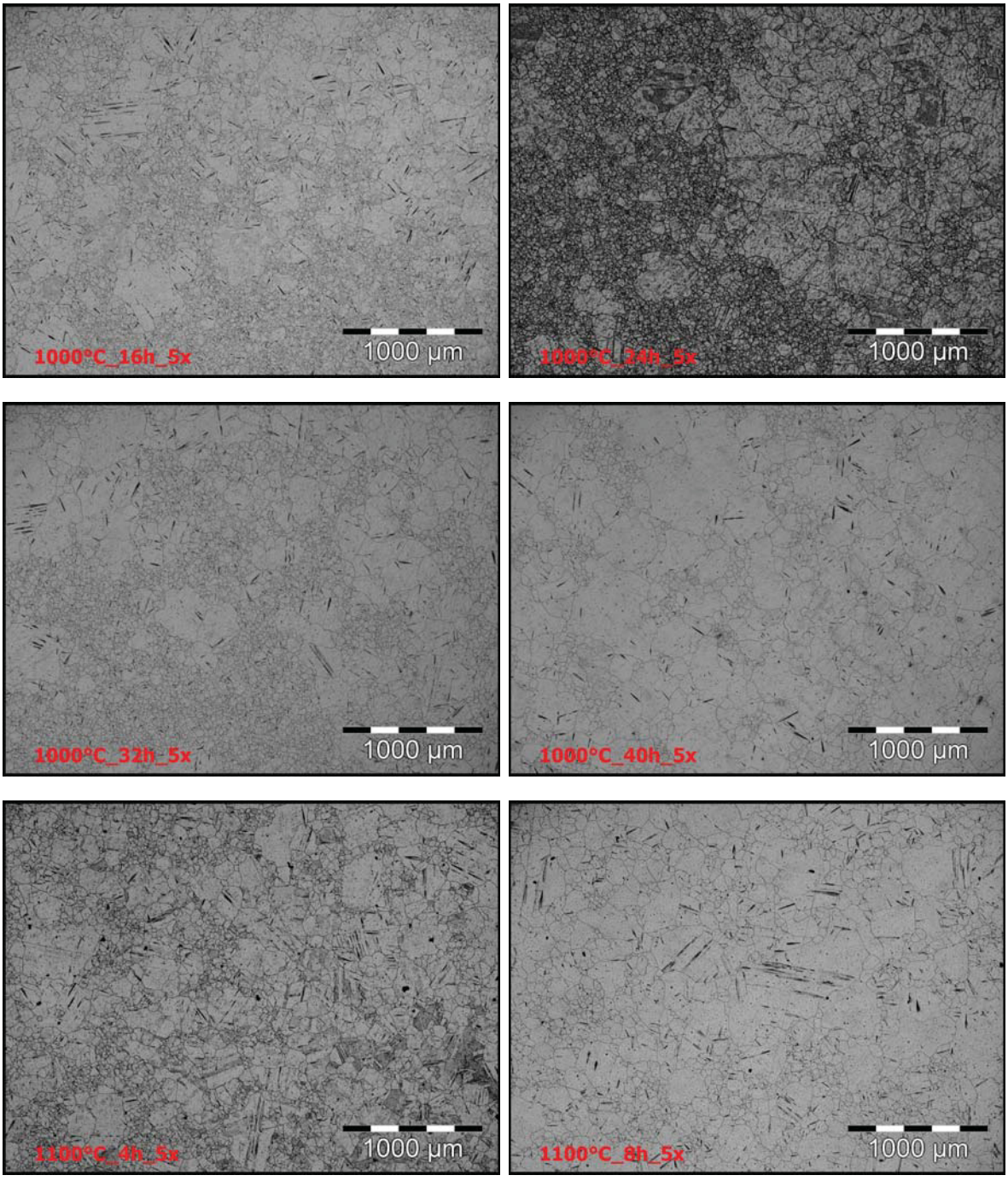

Figure 6.3: Micrographs one step annealing Part III

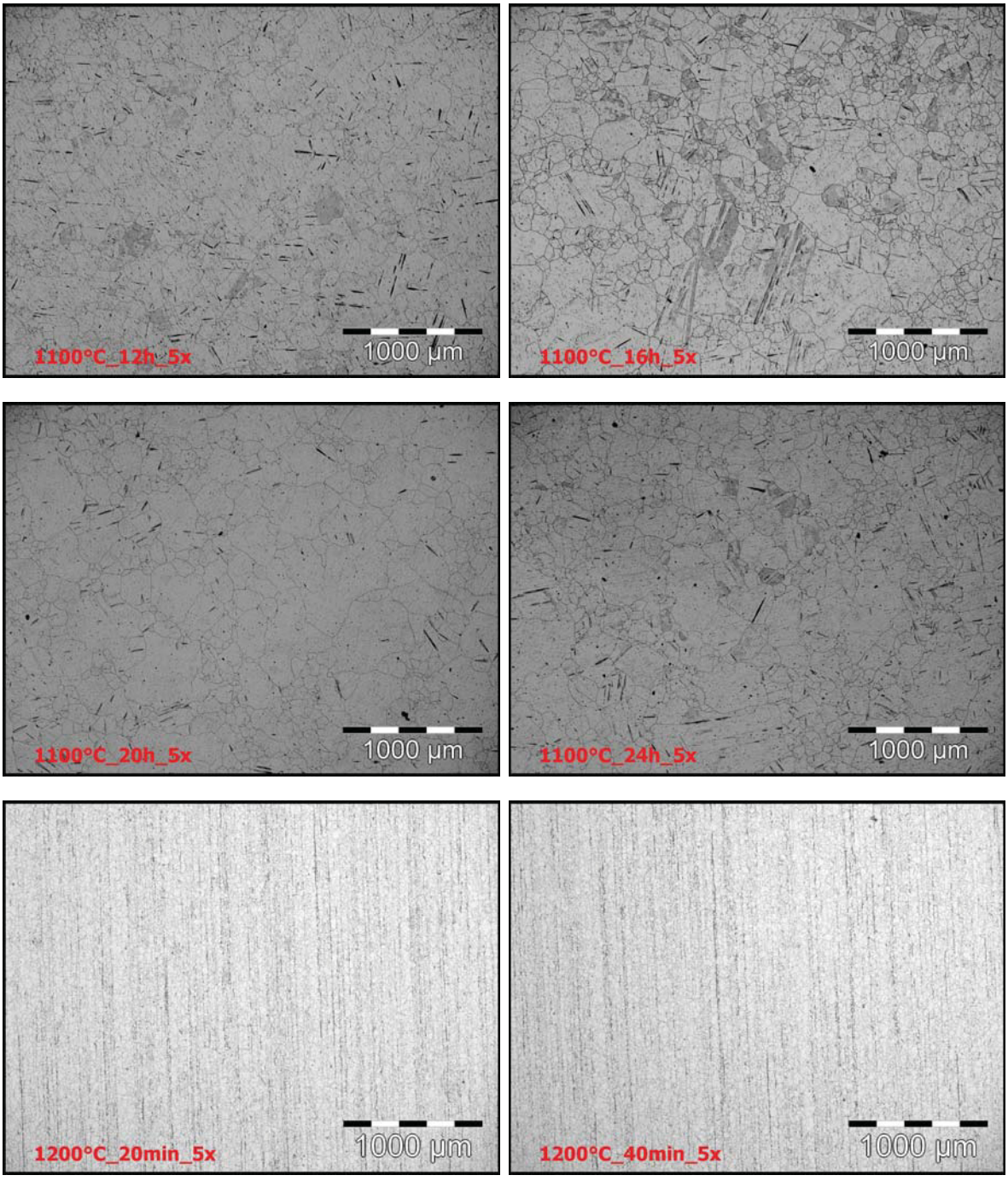

Figure 6.4: Micrographs one step annealing Part IV

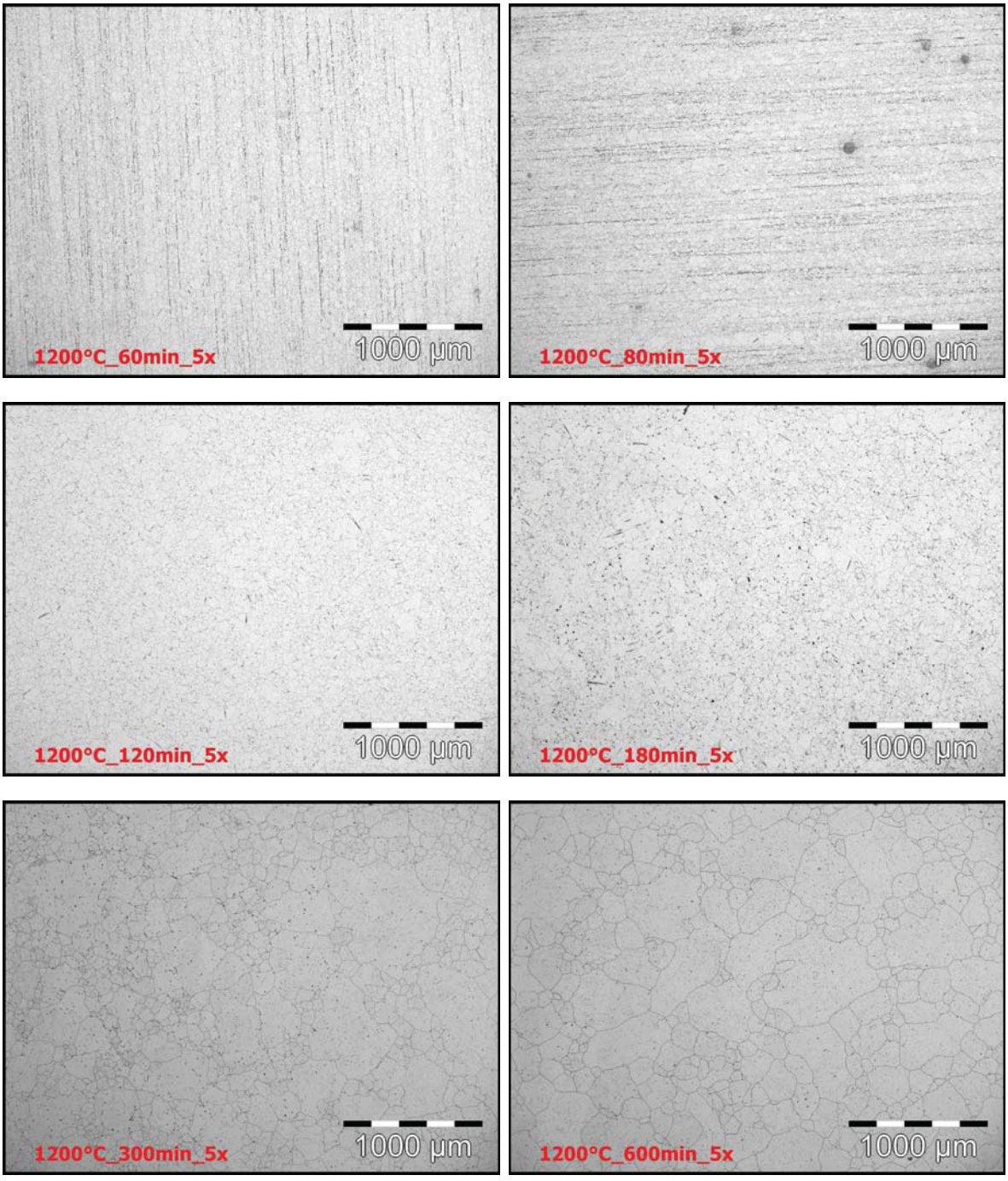

Figure 6.5: Micrographs one step annealing Part V

6.1.2 One Step Annealing Histograms

Class	*Lower class grain size [µm]*	*Upper class grain size [µm]*
1	0	15
2	15	25
3	25	35
4	35	45
5	45	55
6	55	65
7	65	75
8	75	85
9	85	95
10	95	1000

Table 6.1: Upper and lower grain size limit for each one step annealing histogram

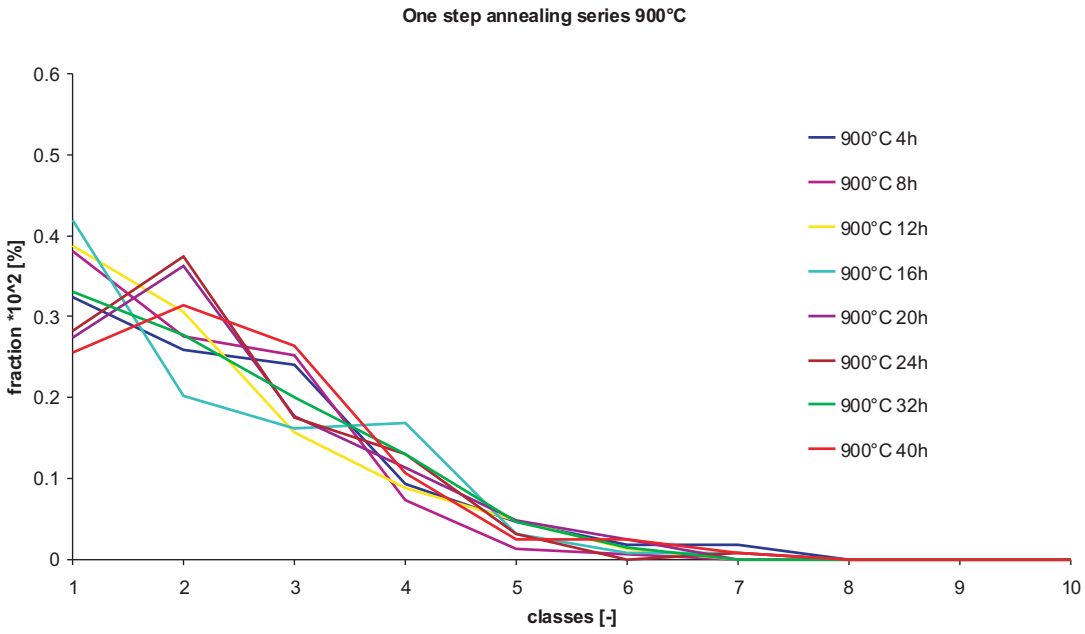

Figure 6.6: One step annealing histogram 900°C

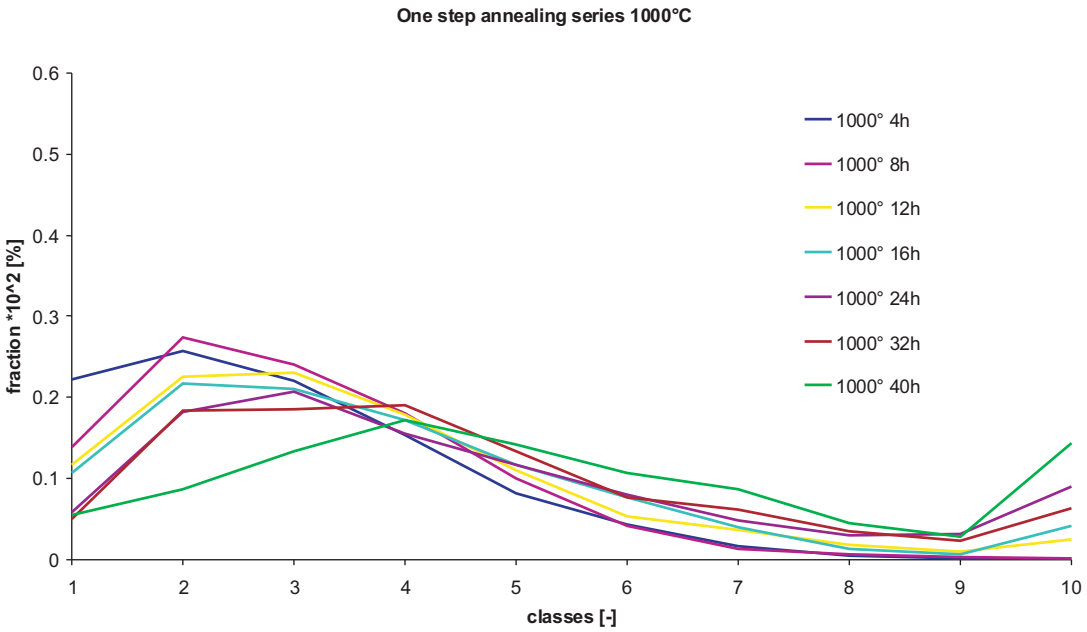

Figure 6.7: One step annealing histogram 1000°C

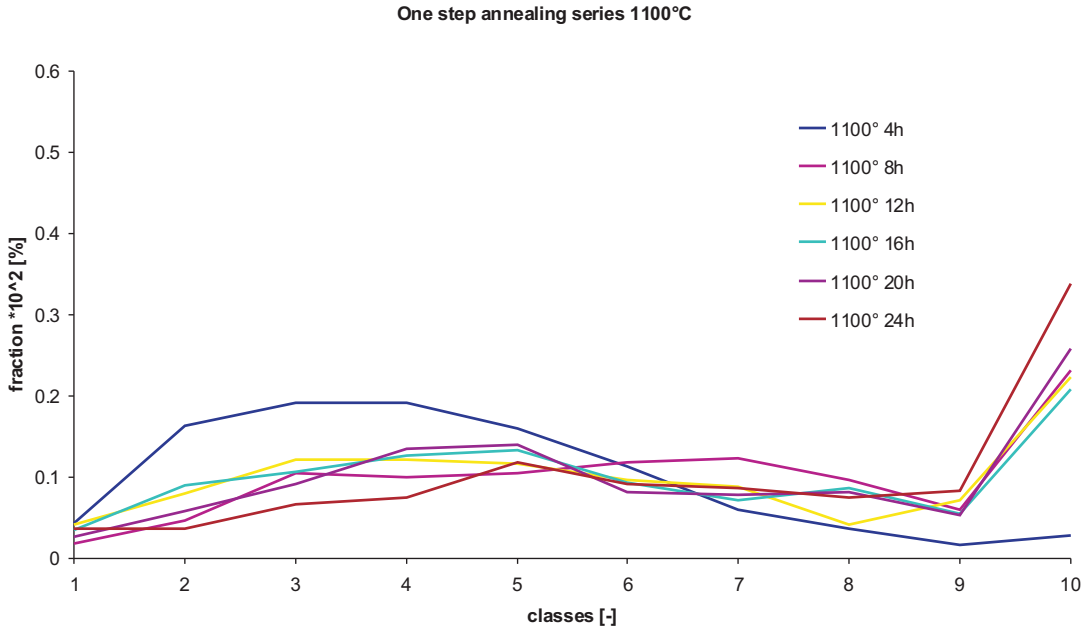

Figure 6.8: One step annealing histogram 1100°C

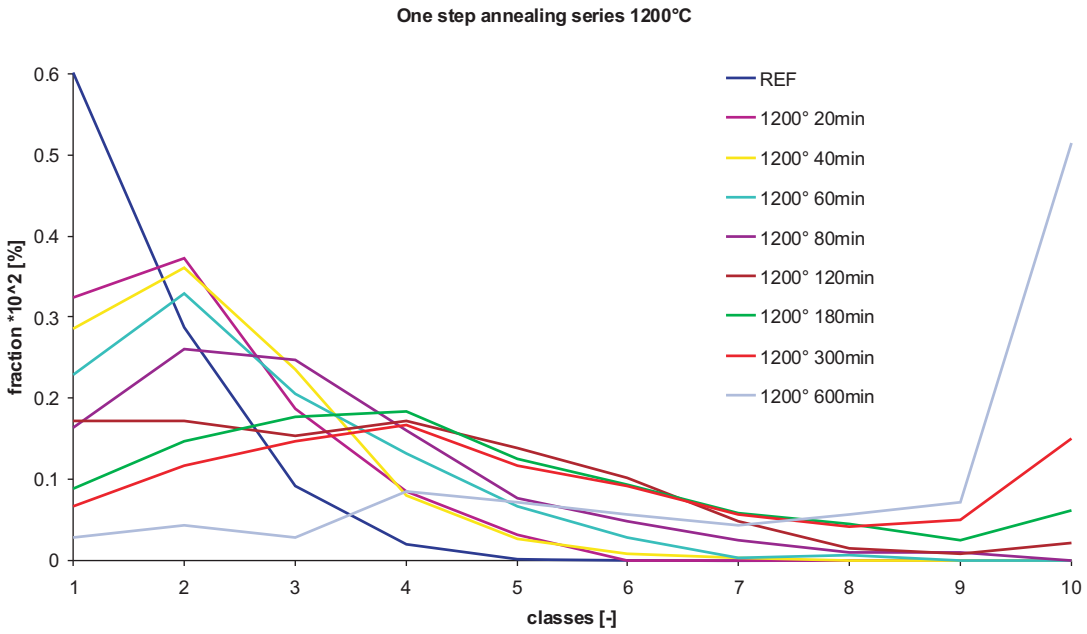

Figure 6.9: One step annealing histogram 1200°C

6.2 Appendix Two Step Annealing

6.2.1 Two Step Annealing Micrographs

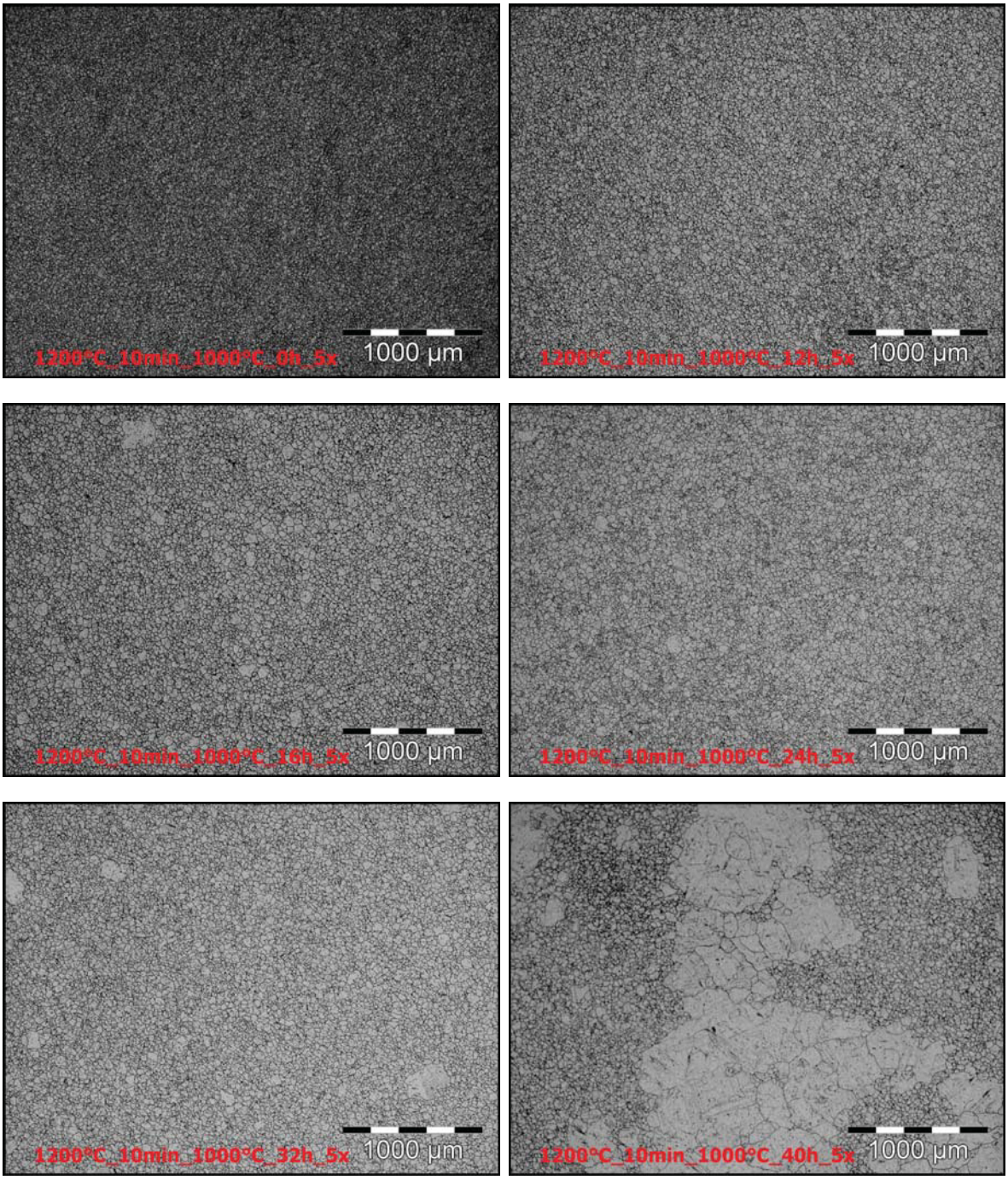

Figure 6.10: Micrographs two step annealing Part I

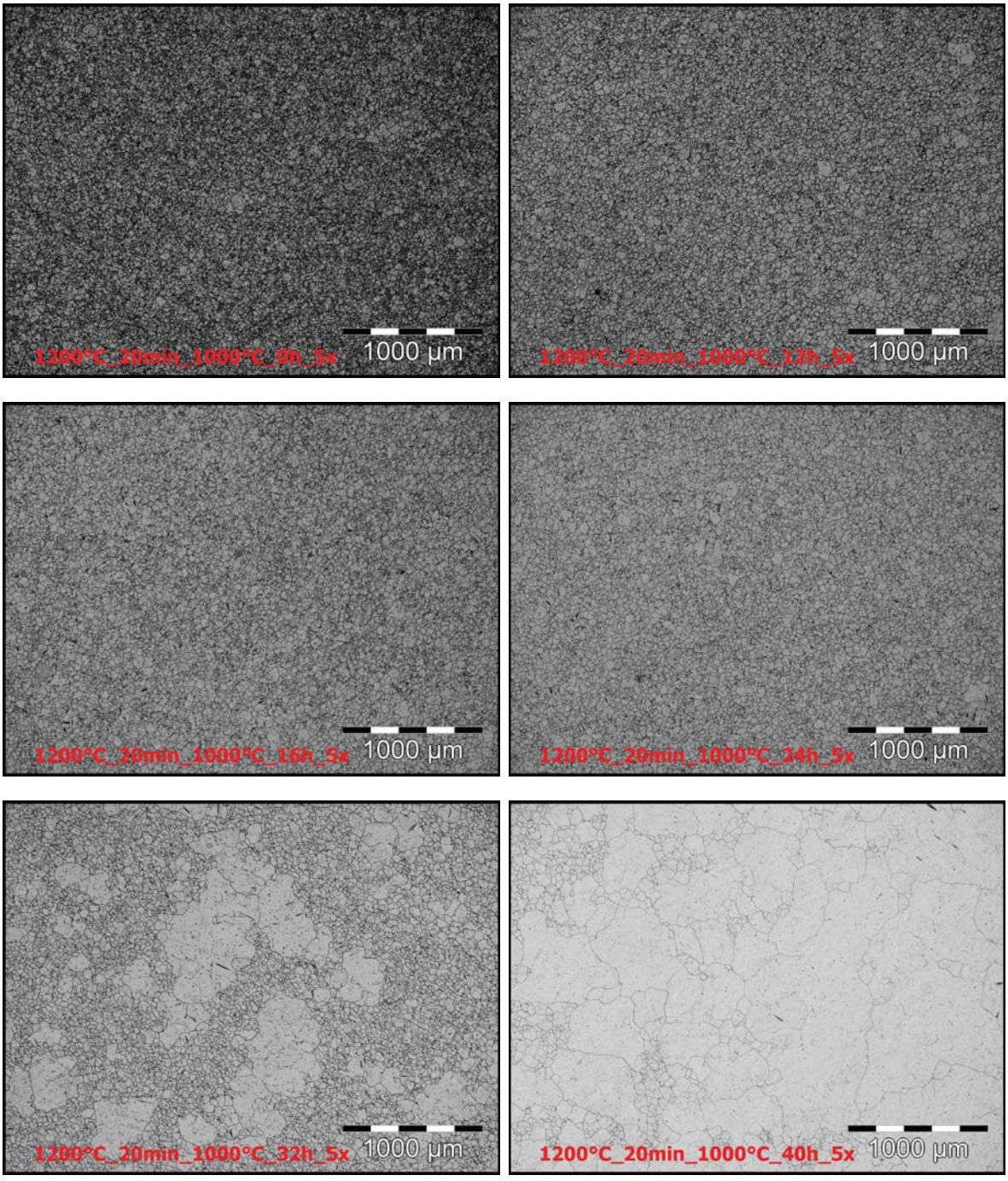

Figure 6.11: Micrographs two step annealing Part II

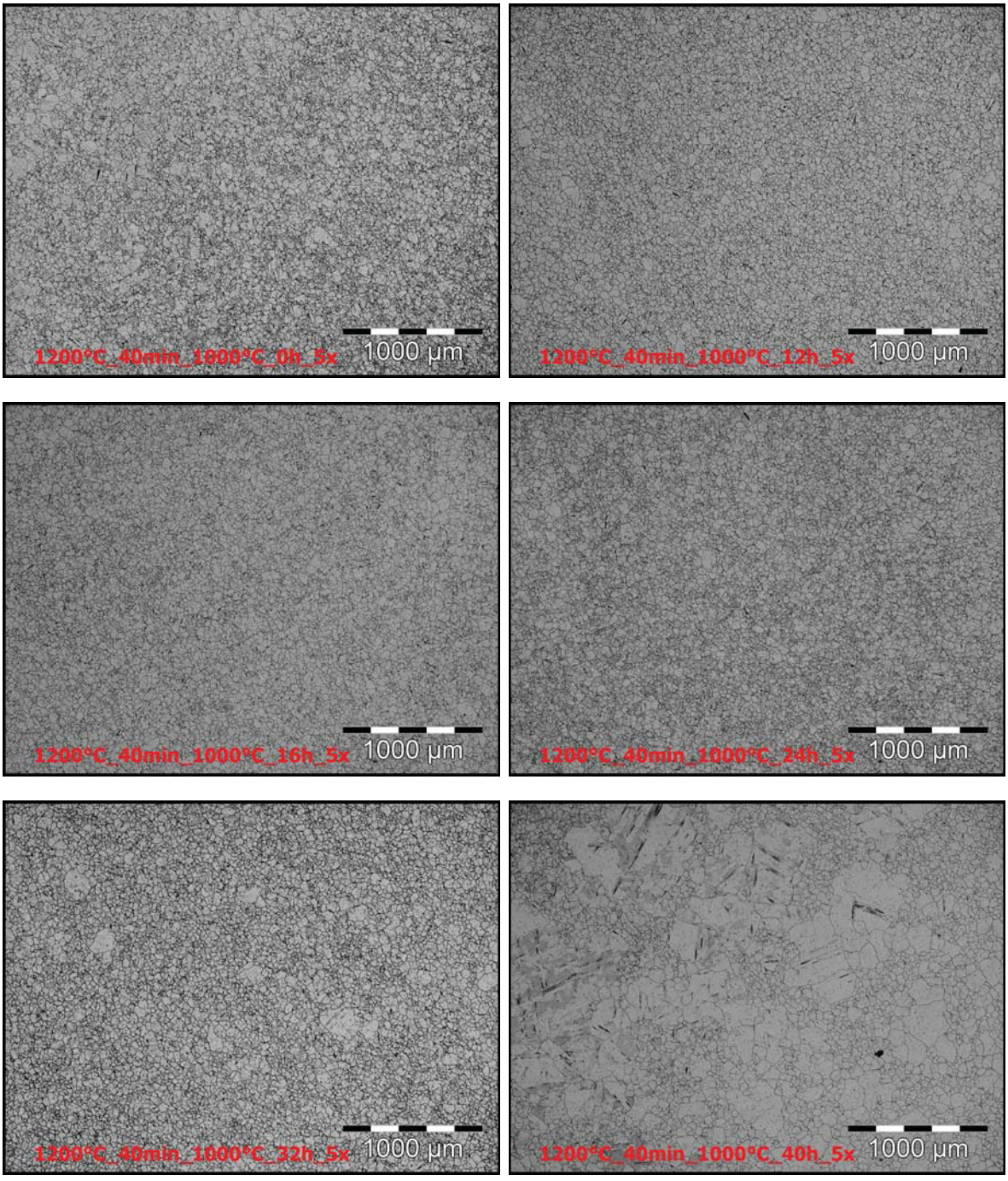

Figure 6.12: Micrographs two step annealing Part III

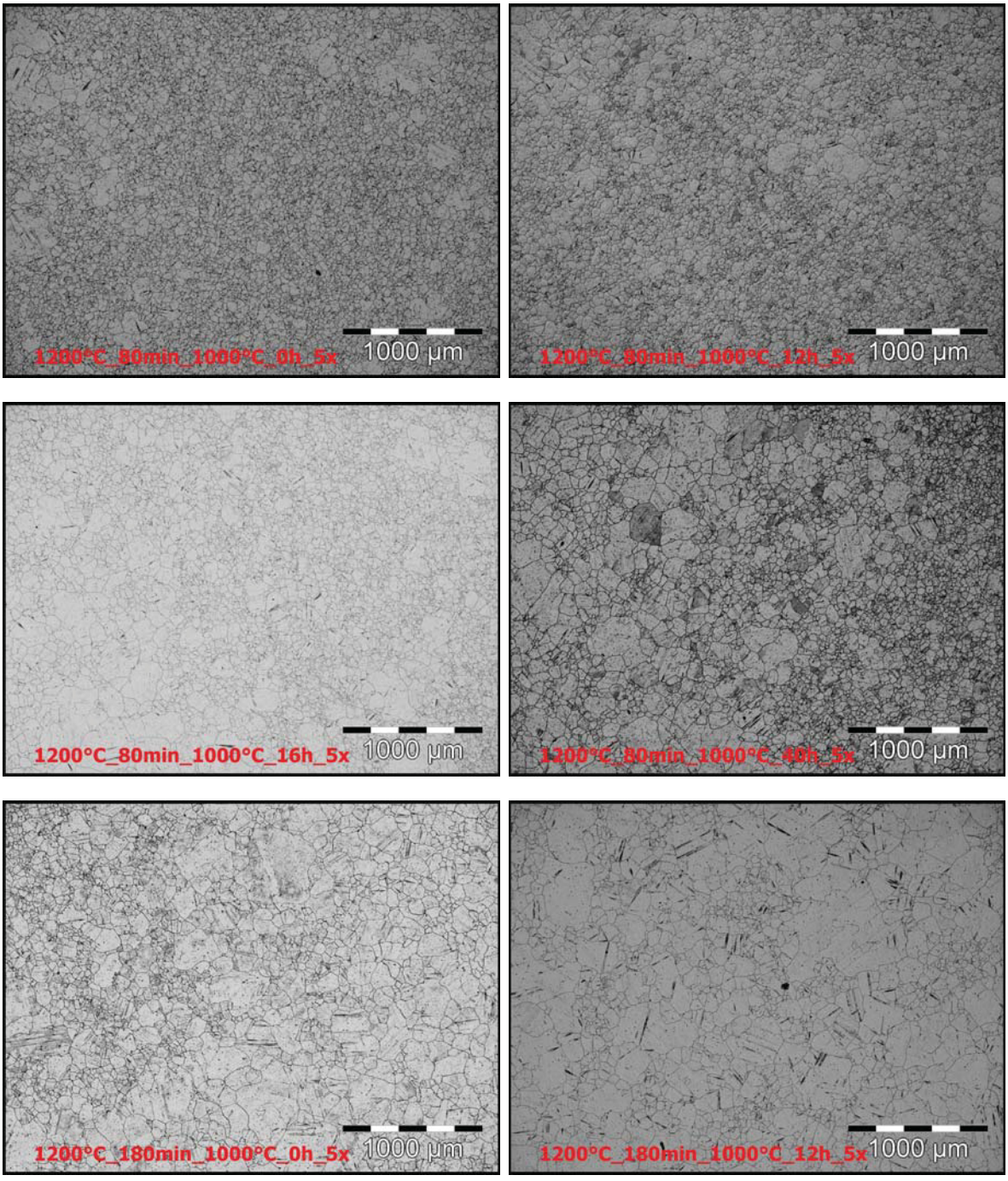

Figure 6.13: Micrographs two step annealing Part IV

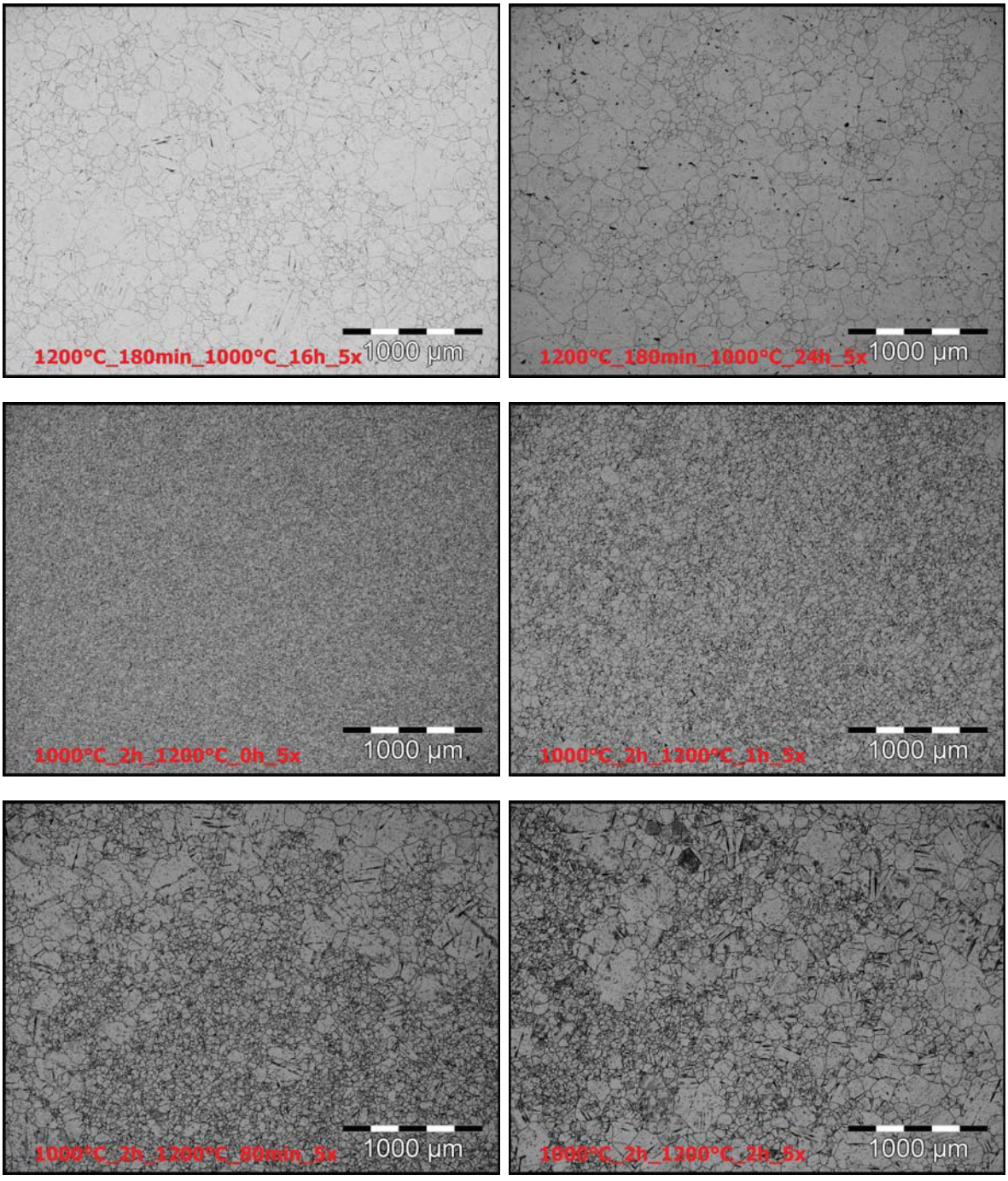

Figure 6.14: Micrographs two step annealing Part V

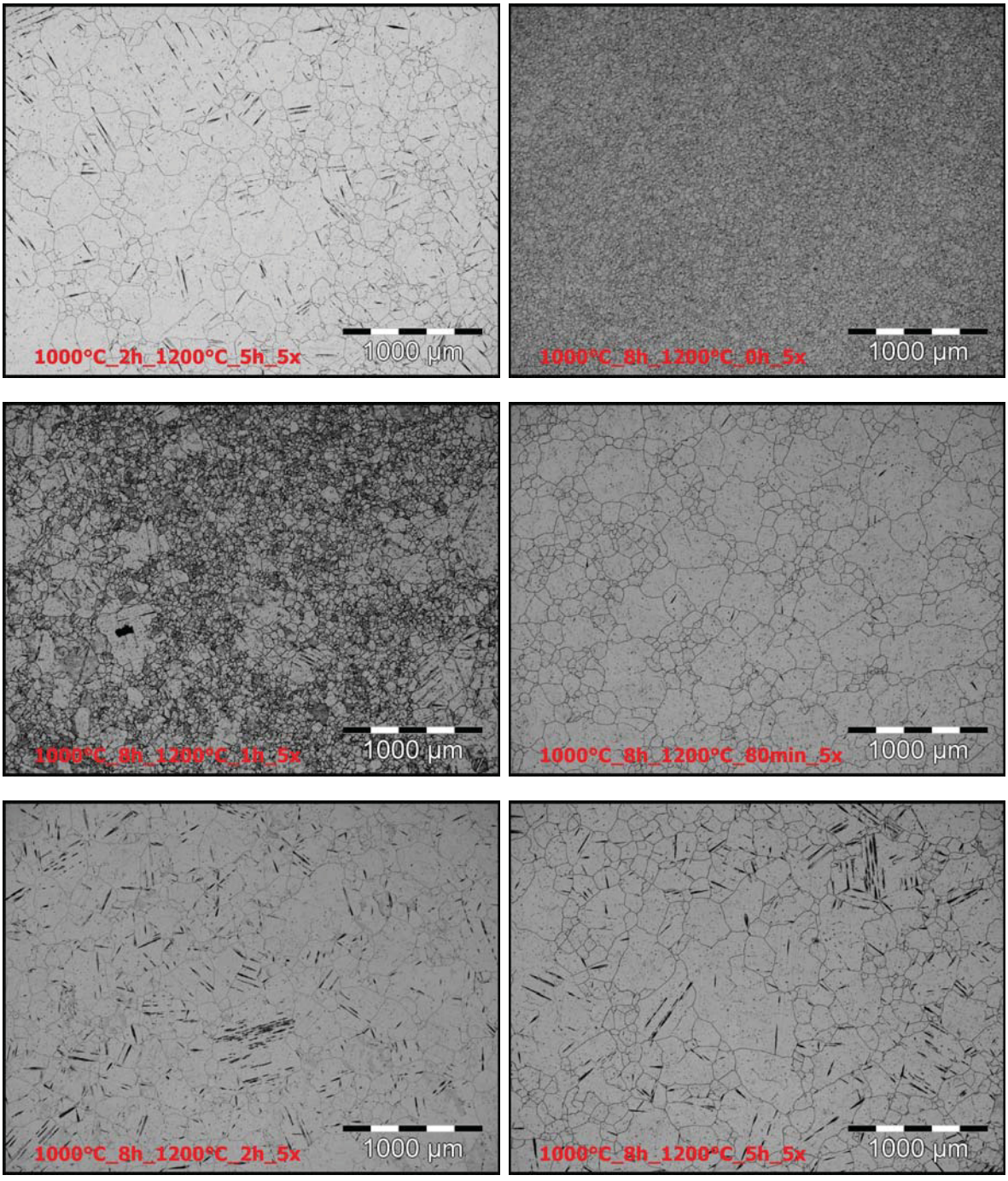

Figure 6.15: Micrographs two step annealing Part VI

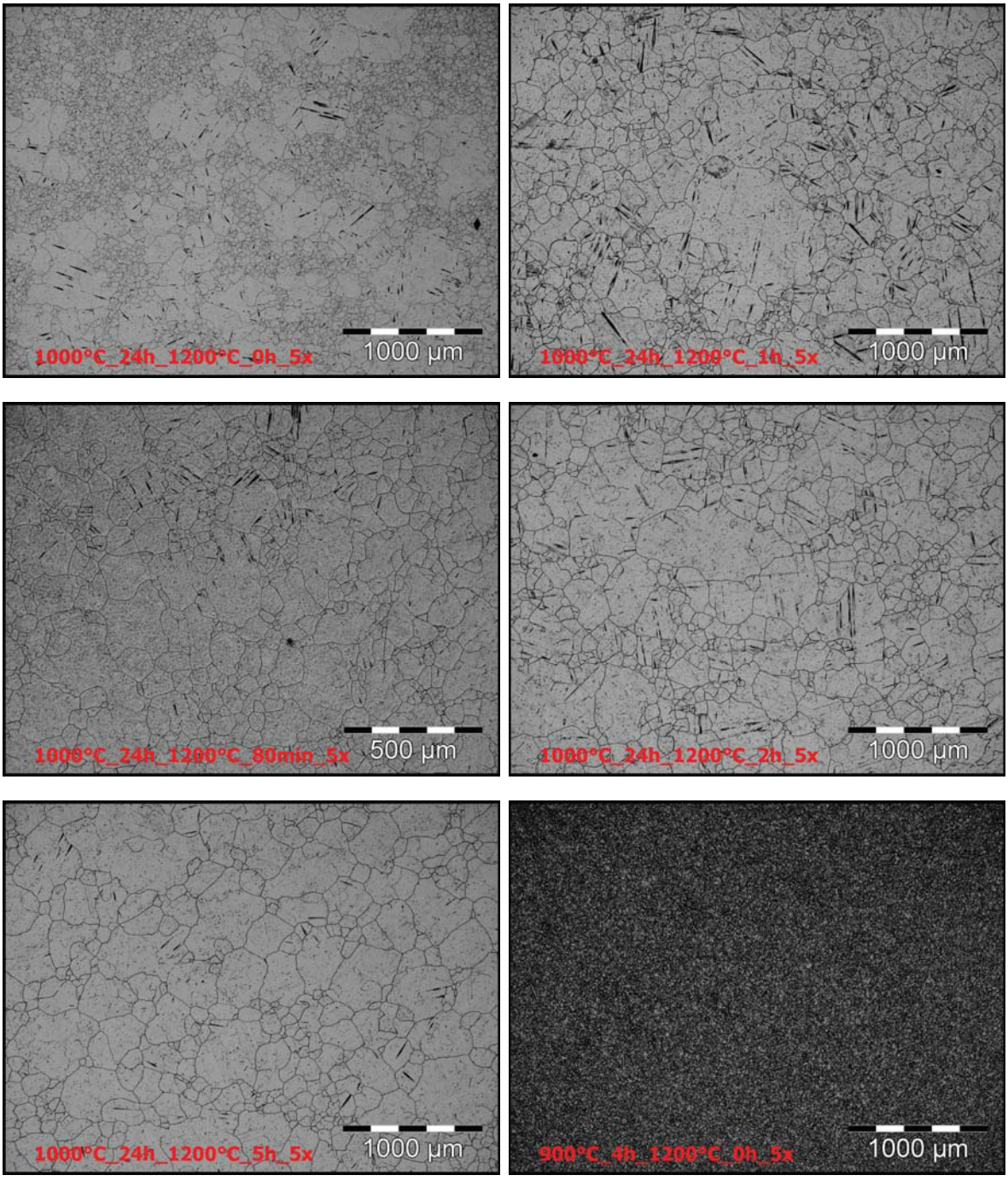

Figure 6.16: Micrographs two step annealing Part VII

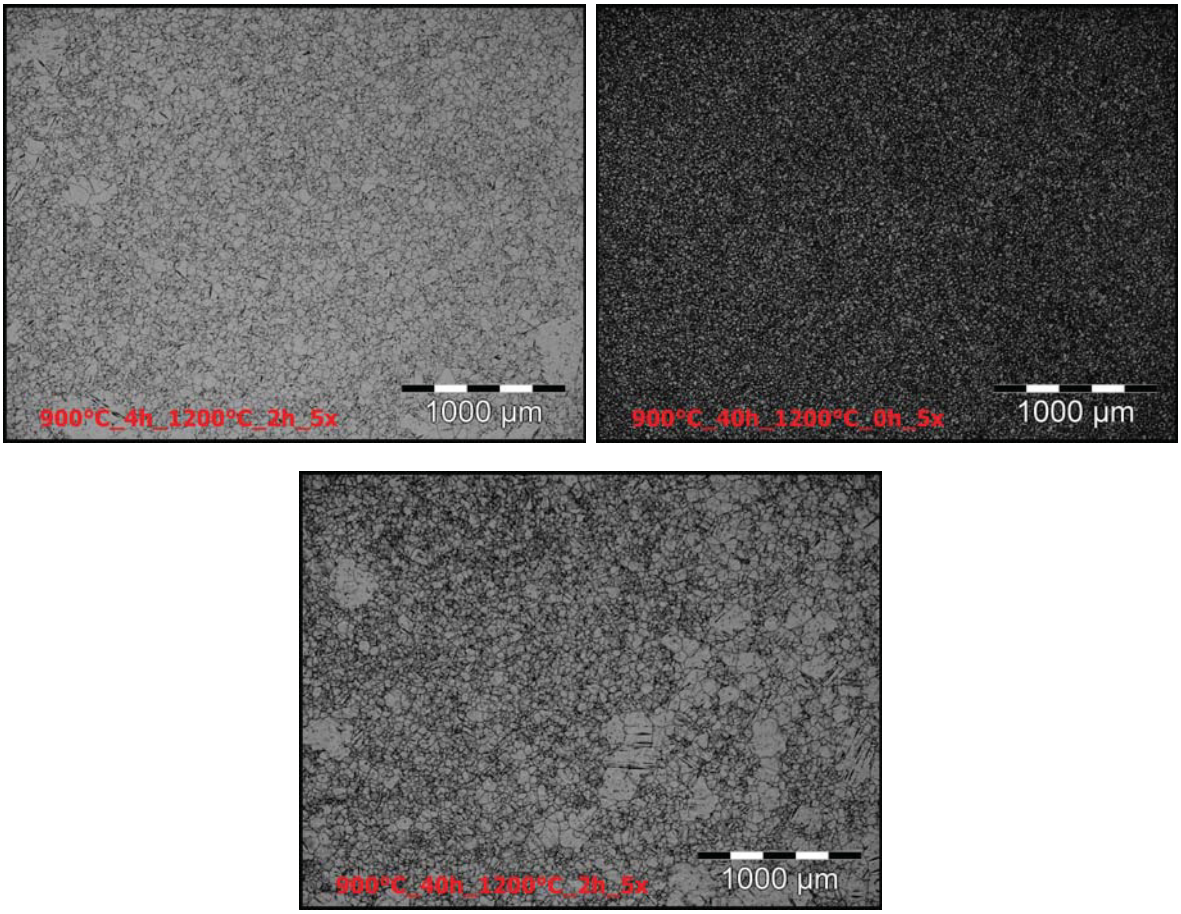

Figure 6.17: Micrographs two step annealing Part VIII

6.2.2 Two Step Annealing Histograms

Class	*Lower class grain size [µm]*	*Upper class grain size [µm]*
1	0	15
2	15	25
3	25	35
4	35	45
5	45	55
6	55	65
7	65	75
8	75	85
9	85	95
10	95	105
11	105	150
12	150	200
13	200	250
14	250	300
15	300	350
16	350	400
17	400	450
18	450	500
19	500	550
20	550	1000

Table 6.2: Upper and lower grain size limit for each two step annealing histogram

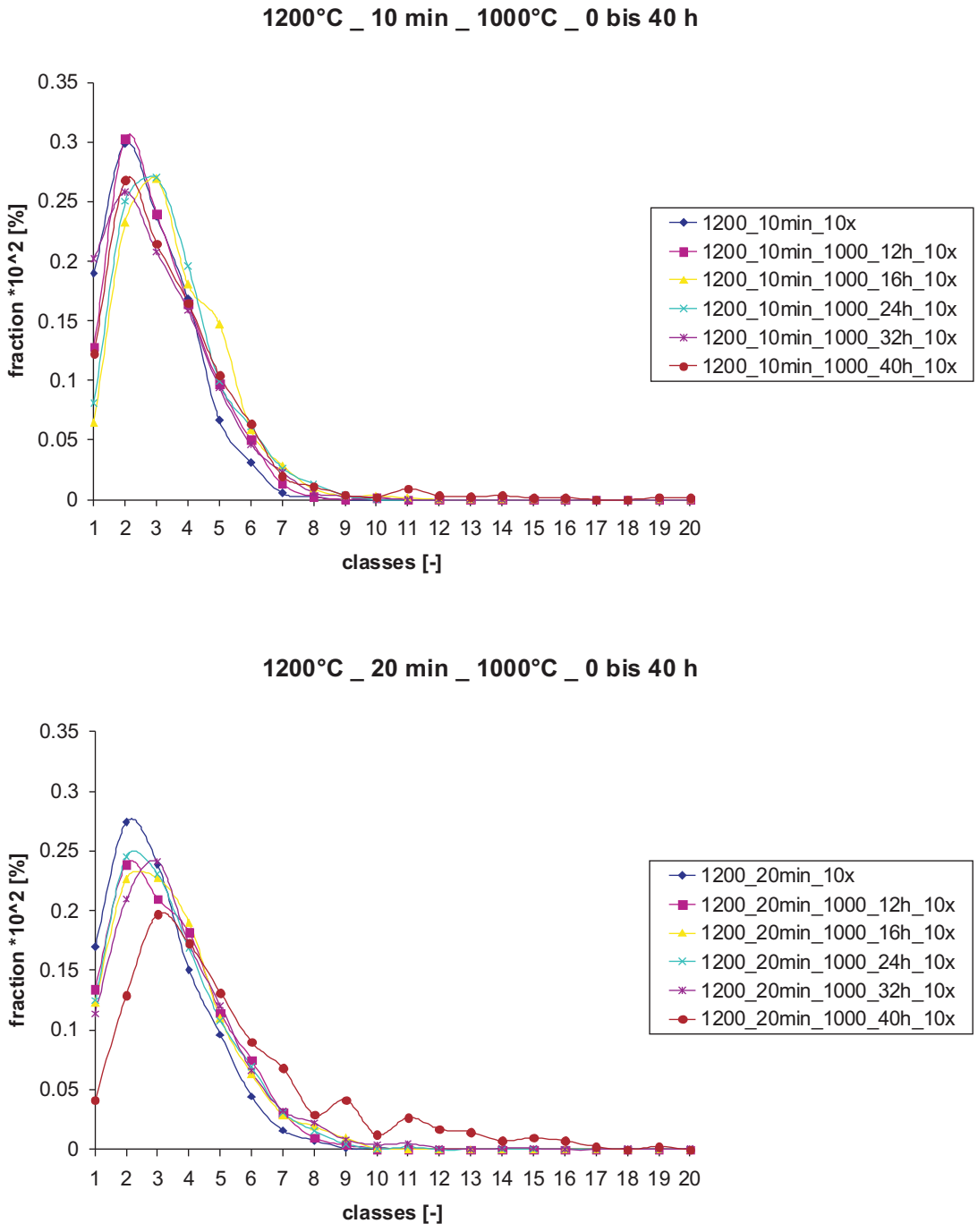

Figure 6.18: Two step annealing histograms 1200°C (10 and 20 minutes) and 1000°C

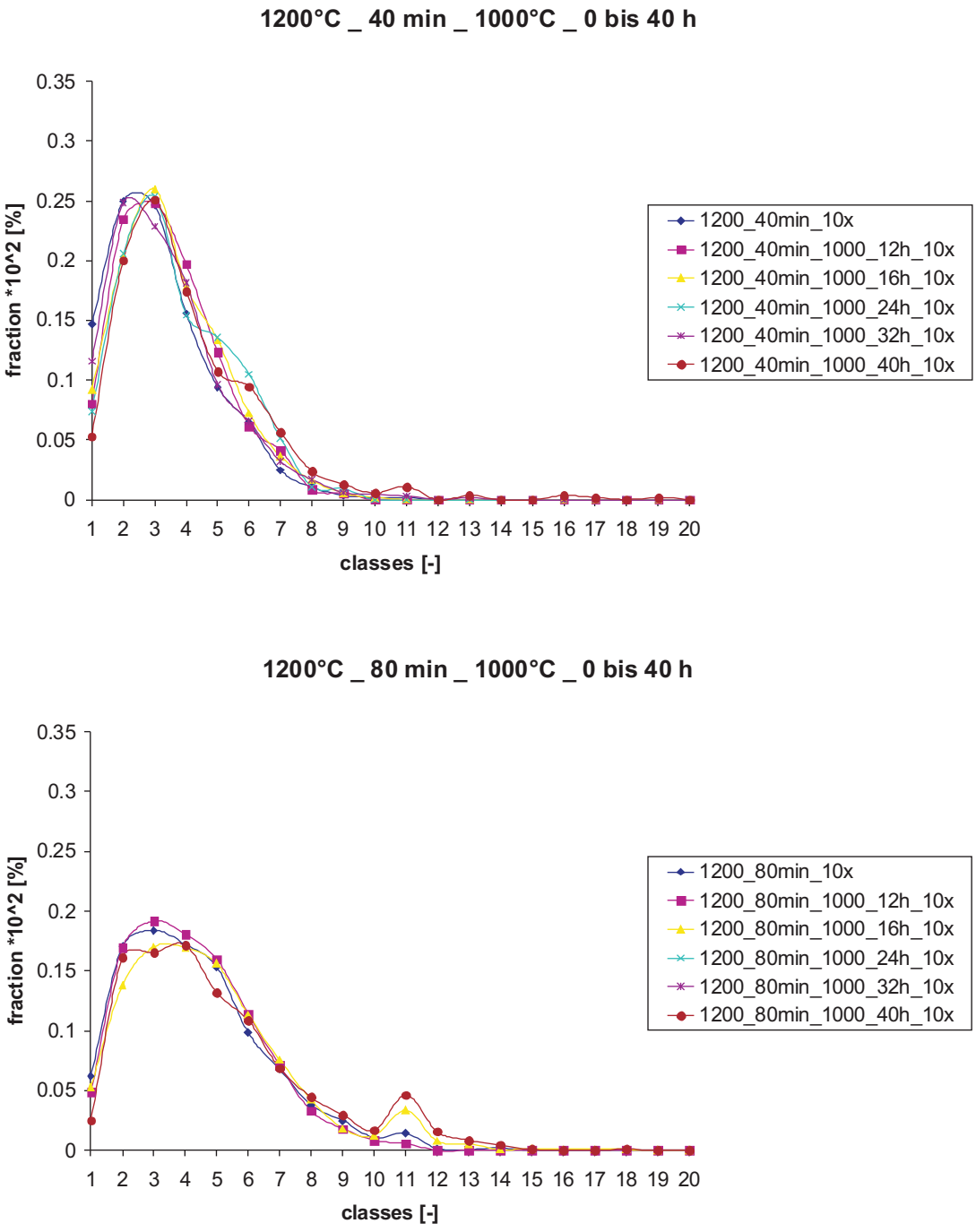

Figure 6.19: Two step annealing histograms 1200°C (40 and 80 minutes) and 1000°C

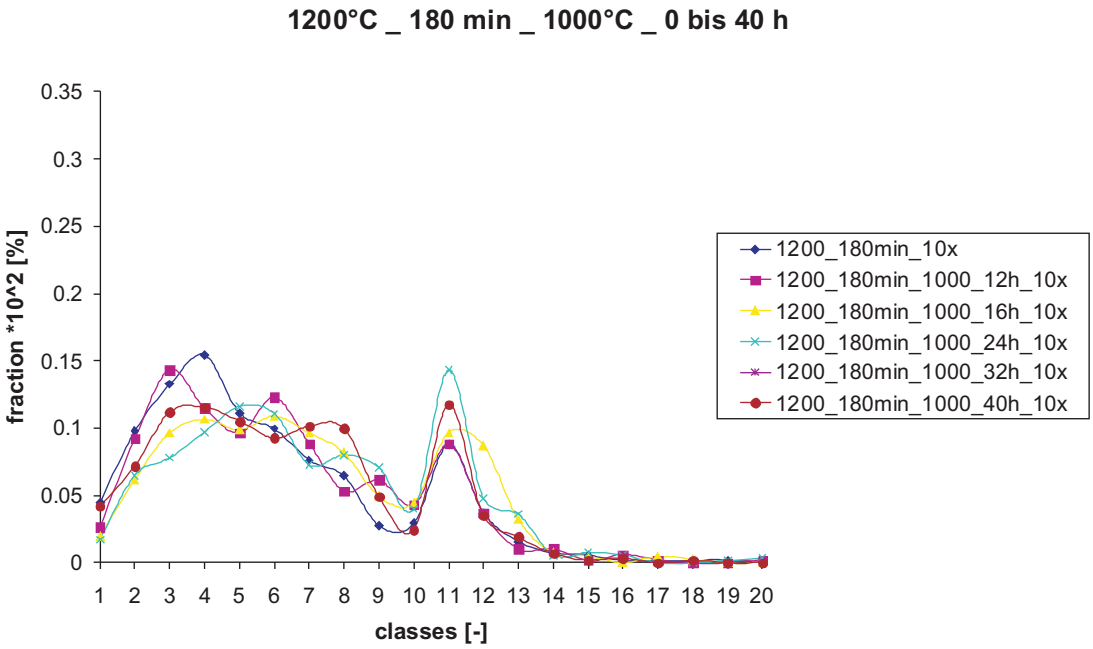

Figure 6.20: Two step annealing histogram 1200°C (180 minutes) and 1000°C

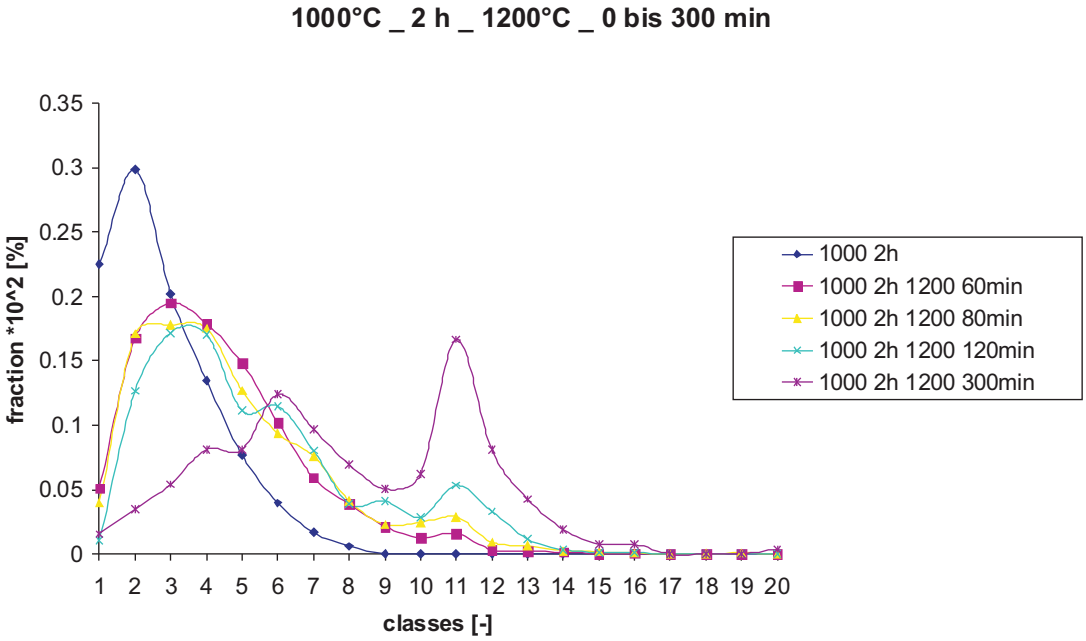

Figure 6.21: Two step annealing histogram 1000°C (2 hours) and 1200°C

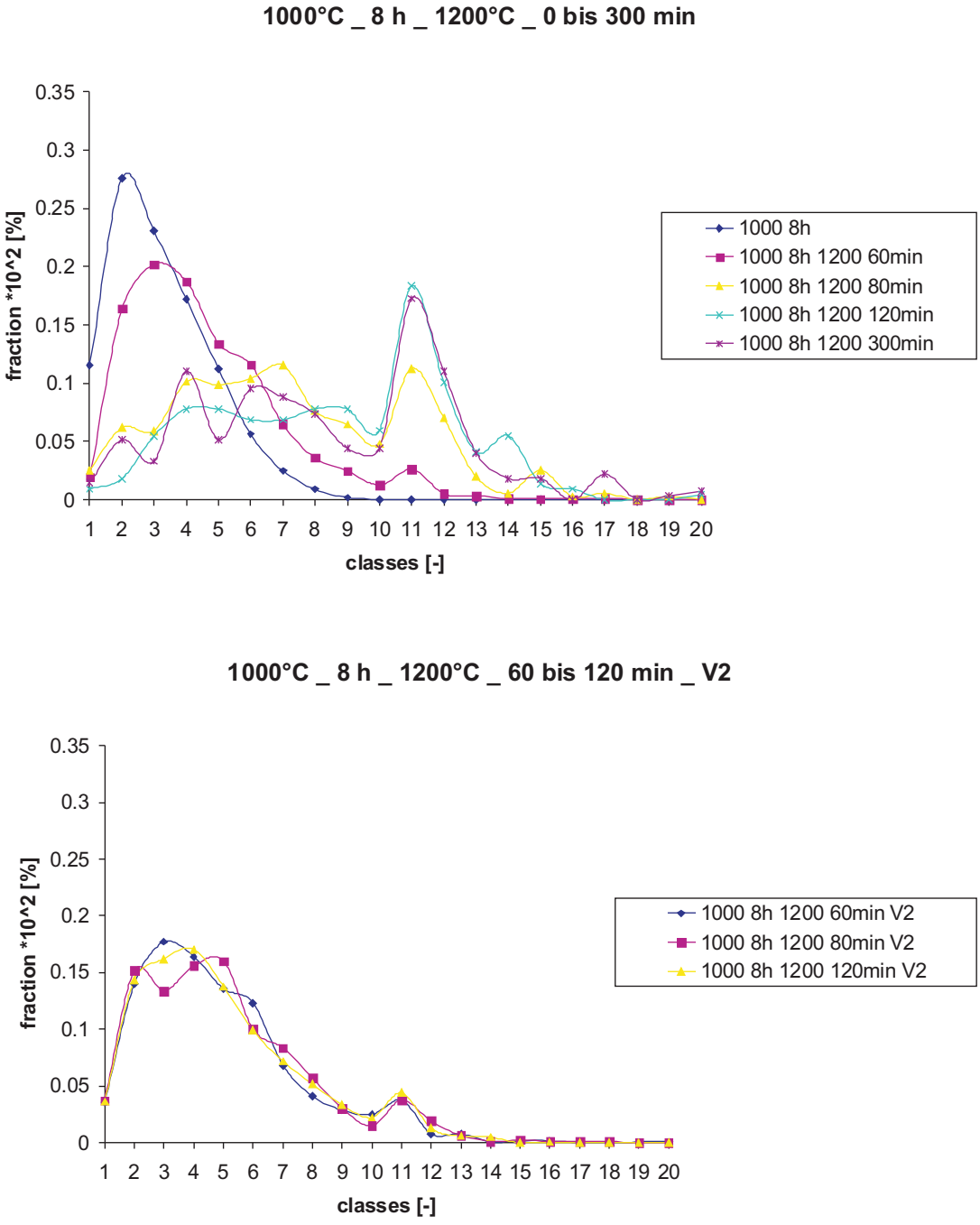

Figure 6.22: Two step annealing histograms 1000°C (8 hours) and 1200°C

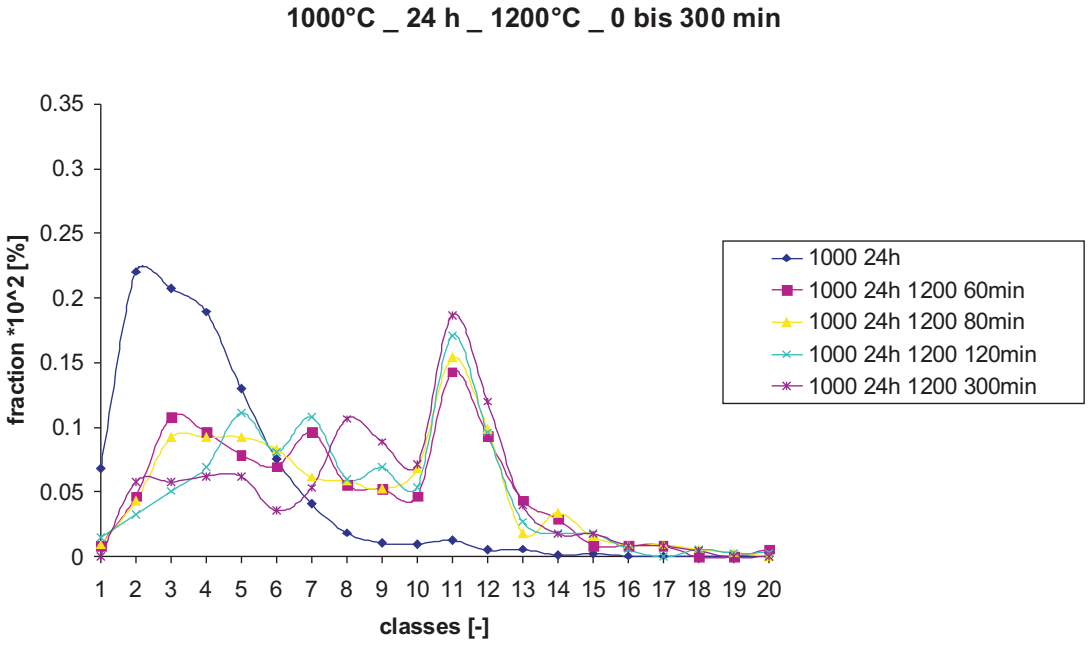

Figure 6.23: Two step annealing histogram 1000°C (8 and 24 hours)and 1200°C

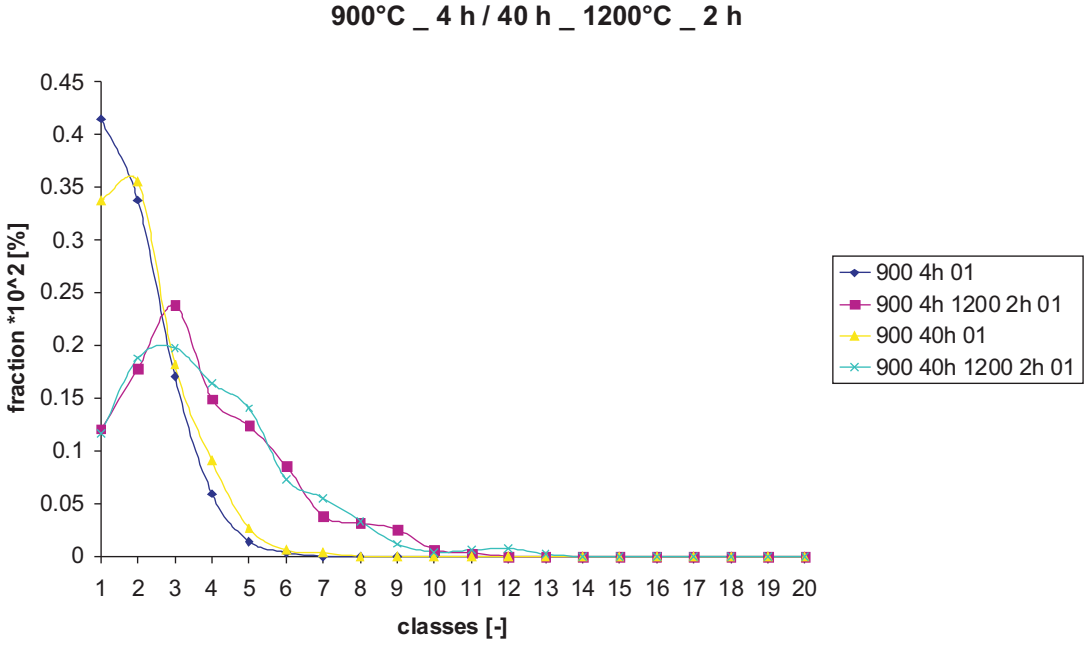

Figure 6.24: Two step annealing histogram 900°C (4 and 40 hours) and 1200°C